Bartosz Bursa

Rozprawa doktorska

# Spektroskopowe i termodynamiczne badania chromoforów porfirynopodobnych dla potencjalnych zastosowań w optoelektronice

Praca doktorska wykonana pod kierunkiem

prof. dr hab. Danuty Wróbel

w Zakładzie Fizyki Molekularnej

Instytut Fizyki

na Wydziale Fizyki Technicznej

Politechniki Poznańskiej

POZNAŃ 2016

Chciałbym serdecznie podziękować mojemu Promotorowi
Profesor doktor habilitowanej Danucie Wróbel
za codzienną życzliwość, dziesiątki cennych uwag i wskazówek
oraz za stworzenie mi szansy wszechstronnego rozwoju naukowego

Dziękuje również pracownikom i doktorantom tworzącym Zakład Fizyki Molekularnej
za miłą i owocną współpracę przy prowadzeniu badań

Niniejszą rozprawę doktorską dedykuję

**Moim Rodzicom**

**Mojej Żonie**

serdecznie dziękuje za wsparcie i pomoc,

dzięki którym wszystko było łatwiejsze i możliwe do zrealizowania

**Badania zostały sfinansowane:**

- ze środków Narodowego Centrum Nauki, projekt NCN 2011/03/N/ST4/0297


- w ramach projektu pt.: „Wsparcie stypendialne dla doktorantów na kierunkach uznanych za strategiczne z punktu widzenia rozwoju Wielkopolski”, Poddziałanie 8.2.2 Programu Operacyjnego Kapitał Ludzki, współfinansowanego przez Unię Europejską w ramach Europejskiego Funduszu Społecznego.


## SPIS SKRÓTÓW I SYMBOLI

| Oznaczenie | Opis skrótu/symbolu |
|---|---|
| CdSe/ZnS | selenek kadmu / siarczek cynku |
| Cl | chloroform |
| CuPc-octyl | miedź (II) 2,3,9,10,17,23,24 – oktakis (oktyloksy)-29H,31H ftalocyjanina |
| CuPc-tetr | miedź(II) 2,3,9,10,17,23,24 tetra-tetr-butyl-29H,31H ftalocyjanina |
| DMSO | dimetylosulfotlenek |
| DMF | dimetyloformamid |
| EPR | elektronowy rezonans paramagnetyczny |
| FT-IR | spektroskopia w podczerwieni z transformatą Furiera |
| FWHM | szerokość połówkowa |
| GaPc | gal (III) 2,3-tetrakis(4-benzyloksyfenoksy) ftalocyjanina |
| HOMO | najwyższy obsadzony orbital molekularny |
| InPc | ind (III) 2,3-tetrakis(4-benzyloksyfenoksy) ftalocyjanina |
| IR | promieniowanie w zakresie podczerwieni |
| IRRA | spektroskopia odbiciowa w zakresie podczerwieni |
| K1 | 10-(4,7-dimetoksynaftalen-1-yl)-5,15-bis(pentafluorofenyl) korol |
| K2 | 10-(2,7-dimetoksynaftaalen-1-yl)-5,15-bis(pentafluorofenyl) korol |
| K3 | 10-(7,8-dimetoksykumar-4-yl)-5,15-bis(pentafluorofenyl) korol |
| K4 | 10-(8-metoksychinolin-4-yl)-5,15-bis(pentafluorofenyl) korol |
| K5 | 5,10,15 tris (pentafluorofenyl) korol |
| K6 | 10-(4-nitrofenyl)-5,15-bis(pentafluorofenyl) korol |
| K7 | 10-(2,3,5,6-tetrafluoro-4-(4-formylofenyloksy)benzaldehyd)-5,15-bis(pentafluorofenyl) korol |
| K8 | 10-(2,3,5,6-tetrafluoro-4-(4-formylofenyloksy)benzaldehyd)-5,15-bis(pentafluorofenyl) korol – fuleren C60 |
| KBr | bromek potasu |
| LIOAS | laserowo indukowana spektroskopia foto-akustyczna |
| LUMO | najniższy obsadzony orbital molekularny |
| TL | toluen |

| | |
|---|---|
| TD-DFT | teoria zależnego od czasu funkcjonału gęstości |
| UV | promieniowanie w zakresie ultrafioletowym |
| Vis | promieniowanie w zakresie widzialnym |
| ZnPc-octyl | cynk (II) 2,3,9,10,17,23,24 – oktakis (oktyloksy)-29H,31H ftalocyjanina |
| ZnPc-tetr | cynk (II) 2,3,9,10,17,23,24 tetra-tetr-butyl-29H,31H ftalocyjanina |
| $\Phi_T$ | wydajność kwantowa populacji stanu trypletowego |
| $\Phi_F$ | wydajność kwantowa fluorescencji |
| $\Phi_{ET}$ | wydajność transferu energii |
| $\tau$ | czas zaniku fluorescencji |
| $\varepsilon$ | stała dielektryczna |

## SPIS TREŚCI

# STRESZCZENIE

Niniejsza rozprawa doktorska stanowiąca cykl artykułów naukowych poświęcona jest badaniom właściwości fotofizycznych i termodynamicznych metaloftalocyjanin, koroli oraz ich wybranych układów z fulerenem C60 lub półprzewodnikową kropką kwantową CdSe/ZnS. Badania przeprowadzono zarazem w roztworach organicznych (chloroform, toluen, dimetyloformamid, dimetylosulfotlenek) jak i warstwach molekularnych typu Langmuira i Langmuira-Blodgett. Artykuły naukowe składające się na pracę doktorską, obejmujące wyniki badań spektroskopowych w zakresie ultrafioletu, światła widzialnego i podczerwieni, potwierdziły silne oddziaływania między- i wewnątrz molekularne oraz redystrybucję gęstości elektronowej. Przeprowadzone badania spektroskopowe ewidentnie pokazały silny donorowo-akceptorowy charakter układów metaloftalocyjanina – kropka kwantowa (ZnPc-tetr – CdSe/ZnS) oraz diady korol-fuleren C60. Przeprowadzone badania umożliwiły również wyjaśnienie wpływu rozpuszczalnika na właściwości i parametry fotofizyczne badanych koroli, jak również wpływu grupy nitrylowej $NO_2$ na redystrybucję elektronów $\pi$ w stanie wzbudzonym. Badania spektroskopowe w świetle spolaryzowanym umożliwiły określenie orientacji molekuł chromoforu w warstwach Langmuira-Blodgett względem podłoża stałego. Przeprowadzone obliczenia komputerowe z wykorzystaniem teorii TD-DFT potwierdziły wyniki badań doświadczalnych, w szczególności położenia poziomów HOMO i LUMO uzyskane metodą woltoamperometrii cyklicznej.

Przeprowadzone w ramach pracy doktorskiej badania pozwoliły na wskazanie nowych możliwości wykorzystania badanych fotoaktywnych układów molekularnych w różnych obszarach optoelektroniki pokazując jednocześnie na możliwość wykorzystania tych układów w procesie konwersji energii światła widzialnego na energię elektryczną w ogniwach słonecznych.

# ABSTRACT

This dissertation constituting cycle of science articles is dedicated study photophysical and thermodynamic properties of metal phthtalocyanines and corroles and their selected system with fullerene C60 or a semiconductor quantum dot CdSe/ZnS. The research were performed both in organic solutions (chloroform, toluene, dimethylformamide, dimethylsulfoxide) and in a form of Langmuir and Langmuir-Blodgett molecular layers. Scientific articles comprising the doctoral dissertation include the results of spectroscopic investigations in the ultraviolet, visible and infrared range, confirmed the strong interaction between and within molecular structures and the redistribution of electron density. Spectroscopic studies clearly demonstrated a strong donor-acceptor nature of the metal phthalocyanines-quantum dot system (ZnPc-tetr – CdSe/ZnS) and corrole-fullerene C60 dyad. The research also allowed to explain the impact of solvent on the spectroscopic corroles properties and the effect of nitrile group $NO_2$ on the redistribution of the $\pi$ electrons in the excited state. Spectroscopic studies in polarized light study allowed to determine the orientation of chromophore molecules in the Langmuir-Blodgett layers with respect to solid substrates. Performed computer calculation using the theory of TD-DFT confirmed the experimental results, in particular the position of the HOMO and LUMO levels evaluated with the use of the cyclic voltammetry results.

Conducted as part of dissertation research allowed to identify new opportunities to use the examined photoactive molecular systems in different areas of optoelectronics, showing at the same time the possibility of using these systems in the process of converting the energy of visible light into electricity in solar cells.

# 1. WSTĘP

Rozwój urządzeń elektronicznych i technologii ich produkcji wymaga ciągłego poszukiwania nowych materiałów organicznych oraz organiczno-nieorganicznych o unikatowych właściwościach, niemożliwych do uzyskania przy użyciu technologii krzemowej. Elektronika organiczna jest nie tylko fascynującą dziedziną badań, lecz również rozwijającą się w zawrotnym tempie technologią, która towarzyszy nam każdego dnia. Już teraz konsumenci używają urządzeń takich jak chociażby telefony komórkowe, tablety, telewizory z wbudowanymi lekkimi, energooszczędnymi wyświetlaczami OLED, często nie zdając sobie sprawy z natury elektroniki organicznej. Pamiętać trzeba również, że potencjał materiałów organicznych to nie tylko ciągle miniaturyzowana, lekka i elastyczna elektronika. To również niedostępne dotychczas możliwości aplikacyjne w wielu innych dziedzinach życia, jak chociażby w medycynie. Zespoły specjalistów (chemików, fizyków i inżynierów) intensywnie badają układy złożone z molekuł, polimerów oraz innych związków na bazie węgla w aspekcie ich potencjalnej możliwości aplikacyjnych w przyrządach takich jak diody elektroluminenscyjne, ogniwa słoneczne, organiczne tranzystory czy też jako fotouczulacze w medycynie. Ta szeroka gama aplikacji związków organicznych wynika w dużej mierze z prostoty ich otrzymywania i formowania z nich cienkich, uporządkowanych dwuwymiarowych warstw przy użyciu powszechnie znanych technik wirowania (ang. *spin coating*), próżniowego naparowania termicznego, zanurzania (ang. *dip coating*), wylewania strefowego (ang. *zone casting*, *slot dye coating*), technik rozpryskowych (ang. *spray coating*) oraz techniki Lagmuira-Blodgett. Rozwój nowoczesnej gospodarki prowadzi nie tylko do zwiększonego zapotrzebowania na energię w procesach produkcyjnych, ale również do powstania ogromnej ilości zużytego sprzętu elektrycznego i elektronicznego oraz wyczerpania światowych zasobów galu i indu, których dostępność szacuje się na maksymalnie 20 lat. W tym kontekście, w dążeniu do osiągnięcia zrównoważonego rozwoju elektroniki nie bez znaczenia są ekologiczne walory materiałów organicznych takie jak niskoenergetyczne procesy syntezy oraz znikome koszty ich utylizacji.

Pierwszą z grup związków porfiryno-podobnych będących przedmiotem badań o potencjalnych zastosowaniach w optoelektronice są ftalocyjaniny (*Rysunek 1*). Termin „ftalocyjaniny" pochodzący do greckiego „naphta" – ropa oraz „cyanine" – ciemny niebieski,

został po raz pierwszy użyty przez profesora Reginalda Linstead z Imperial College of Science and Technology w 1933 roku jako nazwa nowej klasy związków organicznych[1]. Ftalocyjaniny, pochodne porfiryny, to grupa związków heterocyklicznych charakteryzujących się wysoką stabilnością chemiczną i termiczną. Od ich przypadkowego odkrycia przez Brauna i Tchernaca na początku ubiegłego wieku (1907 r.)[2] ftalocyjaniny są przedmiotem zainteresowania chemików oraz fizyków i stały się jednymi z najbardziej studiowanych grup materiałów funkcjonalnych. Ich użyteczne właściwości wynikają z efektywnego wewnątrz-molekularnego transferu elektronu oraz możliwości modyfikacji struktury molekularnej. Przyłączenie grup bocznych lub umieszczenie we wnętrzu makrocyklu jednego z 63 jonów metali lub jonu wodoru powoduje, że ftalocyjaniny tworzą dużą rodzinę związków organicznych o właściwościach katalitycznych, absorpcyjnych, przewodzących i fotoprzewodzących, dzięki czemu znalazły zastosowania w wielu aplikacjach.

Druga grupa związków to korole (*Rysunek 1*) będące syntetycznymi analogami porfiryn. Charakteryzują się trzema pozycjami węgla w pozycji meso oraz jednym bezpośrednim wiązaniem pomiędzy pierścieniami pirolowymi. Molekuły te, odkryte podczas nieudanej syntezy witaminy $B_{12}$ po raz pierwszy zostały opisane w 1965 roku przez Johnsona i Kay[3]. Mimo że korole znane są od ponad 50 lat, przez długi czas postęp w ich badaniach był bardzo ograniczony. Dopiero odkrycie nowych metod ich syntezy w 1999 roku przez dwie niezależne grupy przyspieszyło ich badania. Związki te posiadają charakterystyczne dla związków porfiryn widmo absorpcji w zakresie widzialnym z głównym maksimum absorpcji w tzw. paśmie Soreta. Unikatowe właściwości tych związków zawdzięczamy wiązaniu bezpośrednio pomiędzy pierścieniami pirolowymi, co prowadzi do redukcji symetrii z $D_{4h}$ lub $D_{2h}$ do $C_{2v}$[4]. Korole podobnie jak porfiryny są planarnymi molekułami, w których występuje sprzężony układ 10 elektronów $\pi$ spełniających teorie aromatyczności Hückla[5].

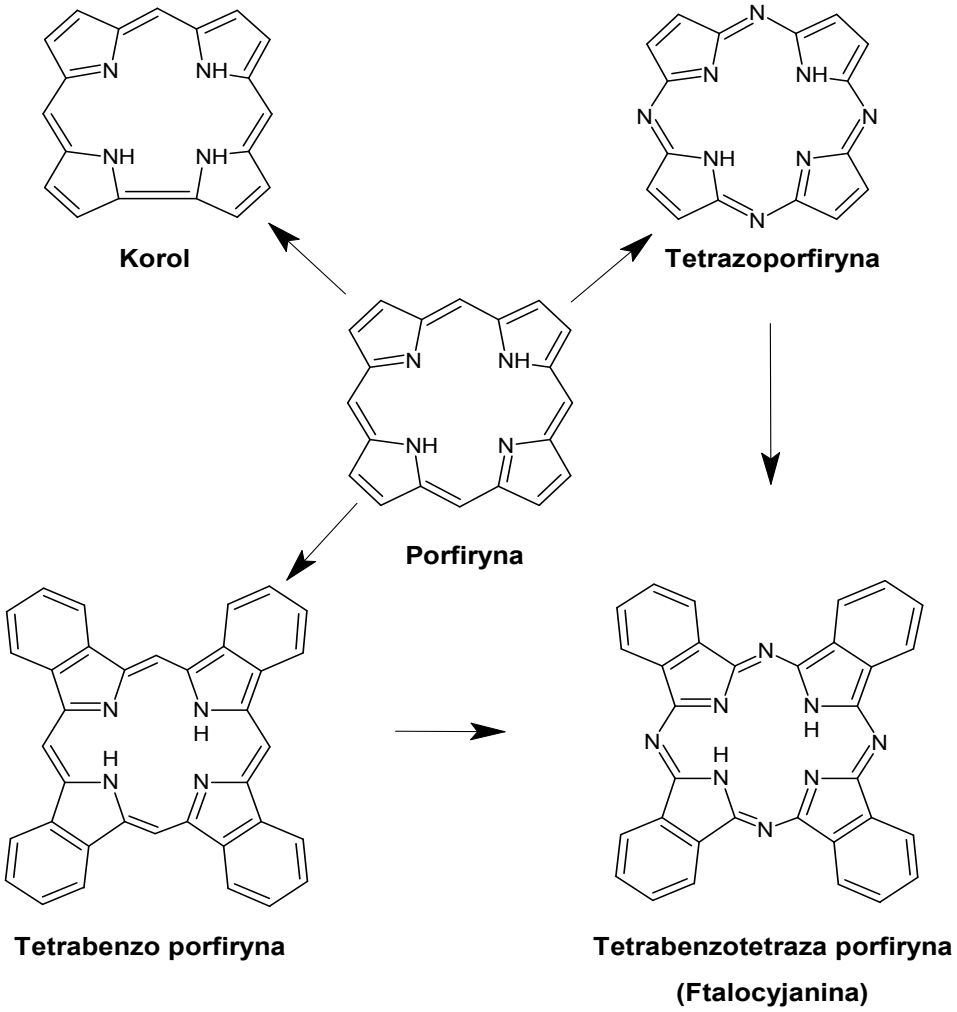


*Rysunek 1 Struktura molekularna oraz różnice pomiędzy molekułami z rodziny porfiryn, ftalocyjanin i koroli.*

Zasadniczym celem niniejszej rozprawy doktorskiej było zbadanie natury stanów wzbudzonych, procesu transferu elektronu oraz właściwości termodynamicznych wybranych barwników ftalocyjaninowych, korolowych oraz ich wybranych układów donorowo-akceptorowych z kropką kwantową lub fulerenem C60.

Dla przedmiotowych związków w fazie objętościowej, jak i układach cienkowarstwowych wytworzonych przy użyciu techniki Langmuira, Langmuira-Blodgett wykonano wiele badań spektroskopowych (m.in. absorpcja UV-Vis-IR, absorpcja metodą in-situ, emisja fluorescencji, kinetyka fluorescencji, spektroskopia Ramana) pozwalających na określenie właściwości stanów wzbudzonych oraz procesów aktywacji i dezaktywacji energii. Badania te pozwoliły m.in. na poznanie procesów tautomeryzacji, deprotonacji oraz

indukowanych efektów mezomerycznych, w tym ich wpływu na stany singletowe i trypletowe molekuł. Na podstawie przeprowadzonych badań określono również zdolność wybranych barwników do tworzenia struktur zagregowanych. Dodatkowo zarejestrowano widma elektronowego rezonansu paramagnetycznego oraz krzywe wolto-amperometryczne.

Uzupełnieniem wymienionych badań było przeprowadzenie szeregu symulacji komputerowych pozwalających określić zmiany rozkładu gęstości elektronowej w wyniku odziaływania molekuły z rozpuszczalnikiem lub w rezultacie dołączenia do jej struktury podstawników.

# 2. FORMA PRACY DOKTORSKIEJ ORAZ OPIS INDYWIDUALNEGO WKŁADU KANDYDATA

Na pracę doktorską ***Spektroskopowe i termodynamiczne badania chromoforów porfirynopodobnych dla potencjalnych zastosowań w optoelektronice*** składa się sześć oryginalnych artykułów opublikowanych w recenzowanych specjalistycznych czasopismach naukowych.

1. **B. Bursa**, D. Wróbel, A. Biadasz, K. Kędzierski, K. Lewandowska, A. Graja, M. Szybowicz, M. Durmuş, *Indium–chlorine and gallium–chlorine tetrasubstituted phthalocyanines in a bulk system, Langmuir monolayers and Langmuir–Blodgett nanolayers - spectroscopic investigations,* Spectrochimica Acta Part A: Molecular and Biomolecular Spectroscopy **128** (2014) 489-496, IF=2,653

2. **B. Bursa**, A. Biadasz, K. Kędzierski, D. Wróbel, *Quantum dot with zinc and copper substituted phthalocyanines. 1. Energy transfer in solution and in-situ light absorption in Langmuir monolayers*, Journal of Luminescence, **145** (2014) 779-786, IF=2,693

3. **B. Bursa**, B. Barszcz, W. Bednarski, J.P. Lewtak, D. Koszelewski, O. Vakuliuk, D.T. Gryko, D. Wróbel, *New meso-substituted corroles possessing pentafluorophenyl groups - Synthesis and spectroscopic characterization*, Phys. Chem. Chem. Phys. **17** (2015) 7411 – 7423, IF=4,493

4. **B. Bursa**, D. Wróbel, B. Barszcz, M. Kotkowiak, O. Vakuliuk, D.T. Gryko, Ł. Kolanowski, M. Baraniak, G. Lota, *The impact of solvents on the singlet and triplet states of selected fluorine corroles – absorption, fluorescence and optoacustic studies,* Phys. Chem. Chem. Phys. **18** (2016) 7216-7228, IF=4,493

5. K. Lewandowska, B. Barszcz, A. Graja, **B. Bursa**, A. Biadasz. D. Wróbel, W. Bednarski, S. Waplak, M. Grzybowski, D.T. Gryko, *Absorption and emission properties of the corrole-fullerene dyad*, Synthetic Metals, **166** (2013) 70-76, IF=2,229

6. **B. Bursa**, D. Wróbel, K. Lewandowska, A. Graja, M. Grzybowski, D.T. Gryko, *Spectral studies of molecular orientation in corrole-fullerene thin films*, Synthetic Metals, **176** (2013)18-25, IF=2,229

W publikacji 1 [**Bursa, SA 2014**] wkład kandydata polegał na nawiązaniu współpracy z prof. M. Durmuşem z Wydziału Chemii Instytutu Technologicznego w Gebze, dzięki którego uprzejmości otrzymał próbki. Kandydat zaplanował całość prac badawczych, koordynował pracę oraz przeprowadził większość prac eksperymentalnych, opracował dane pomiarowe oraz uczestniczył w analizie wyników. Kandydat wspólnie z promotorem prof. dr hab. Danutą Wróbel przygotował manuskrypt publikacji.

W publikacji 2 [**Bursa, JL 2014**] wkład kandydata polegał na wyselekcjonowaniu materiału badawczego, zaplanowaniu oraz przeprowadzeniu badań eksperymentalnych. Kandydat opracował wyniki badań oraz brał udział w ich analizie. Wraz z promotorem prof. dr hab. Danutą Wróbel przygotował manuskrypt publikacji.

W publikacjach 3 i 4 [**Bursa, PCCP 2015 oraz Bursa, PCCP 2016**] wkład kandydata polegał na zaplanowaniu prac badawczych, koordynowaniu przeprowadzonych badań eksperymentalnych i symulacyjnych. Kandydat przeprowadził również większość pracy eksperymentalnej, opracował dane eksperymentalne oraz uczestniczył w analizie wyników. Kandydat wspólnie z promotorem prof. dr hab. Danutą Wróbel opracował manuskrypt.

W publikacji 5 [**Bursa, SM 2013**] kandydat przeprowadził większość pracy eksperymentalnej, opracował wyniki badań oraz uczestniczył w analizie wyników. Kandydat wspólnie z promotorem prof. dr hab. Danutą Wróbel napisał manuskrypt.

W publikacji 6 [**Lewandowska, SM 2013**] kandydat miał istotny wkład w przeprowadzone badania eksperymentalne, przeprowadził pomiary stacjonarnej spektroskopii absorpcyjnej, emisji oraz kinetyki fluorescencji. Kandydat brał czynny udział w analizie, dyskusji otrzymanych wyników oraz w opracowaniu manuskryptu publikacji.

# 3. BADANE MATERIAŁY ORAZ ZASTOSOWANE TECHNIKI POMIAROWE

Badania przeprowadzone w ramach pracy doktorskiej wykonano w laboratoriach Wydziału Fizyki Technicznej Politechniki Poznańskiej oraz w Instytucie Fizyki Molekularnej Polskiej Akademii Nauk w Poznaniu. W pracy skoncentrowano się przede wszystkim na badaniach dwóch grup barwników organicznych.

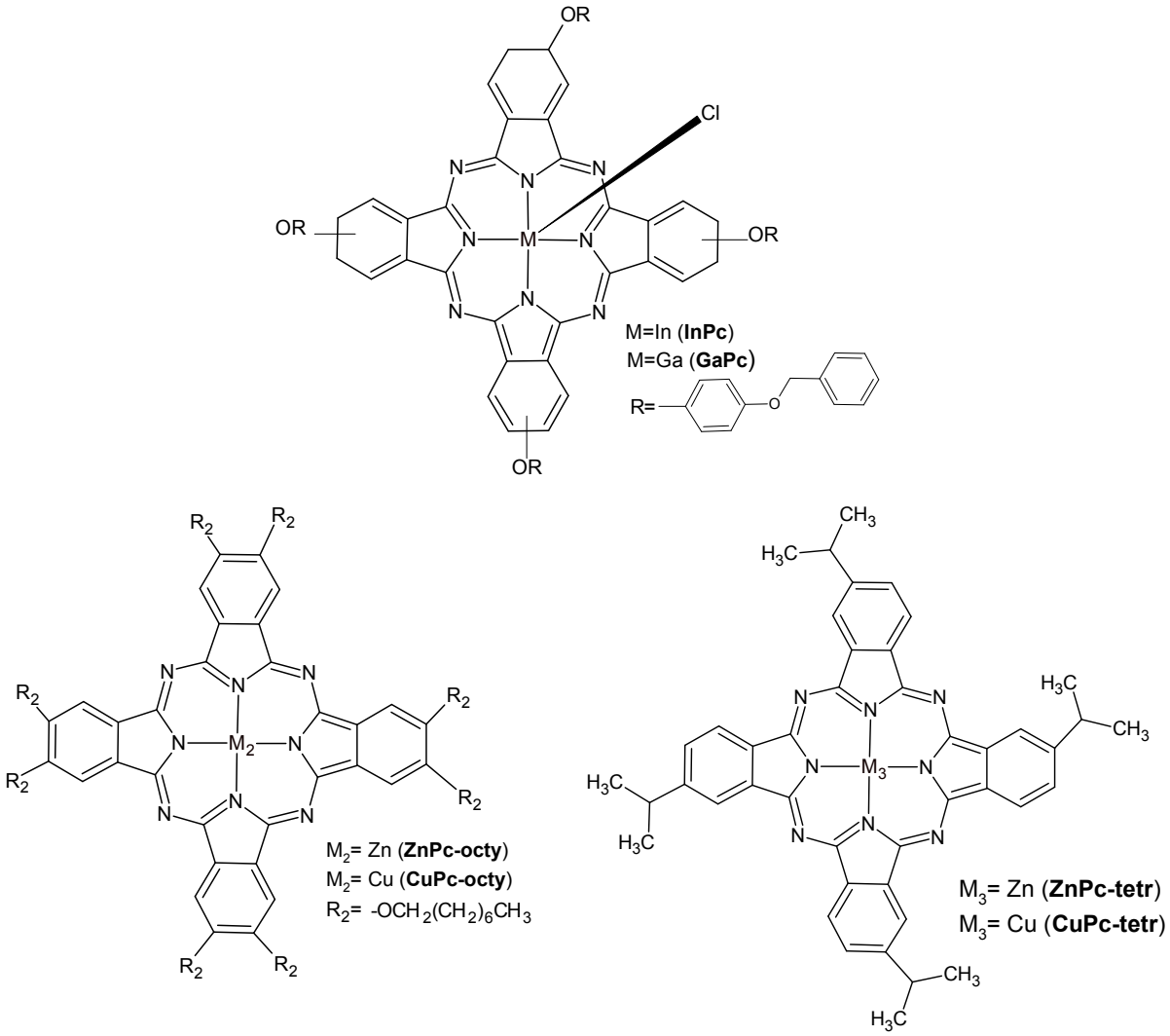


*Rysunek 2 Struktura molekularna badanych układów z rodziny ftalocyjanin*.

Pierwszą grupę stanowił szereg wybranych barwników metaloftalocyjaninowych (ftalocyjaniny miedziowe, ftalocyjaniny cynkowe, ftalocyjanina indowa, ftalocyjanina galowa) oraz ich wybrane układy z kropkami kwantowymi CdSe/ZnS. Drugą grupą badanych związków

organicznych były związki koroli oraz ich kowalencyjnych układów z fulerenami, które zostały zsyntezowane przez grupę prof. Daniela Gryko z Instytutu Chemii Organicznej Polskiej Akademii Nauk w Warszawie.

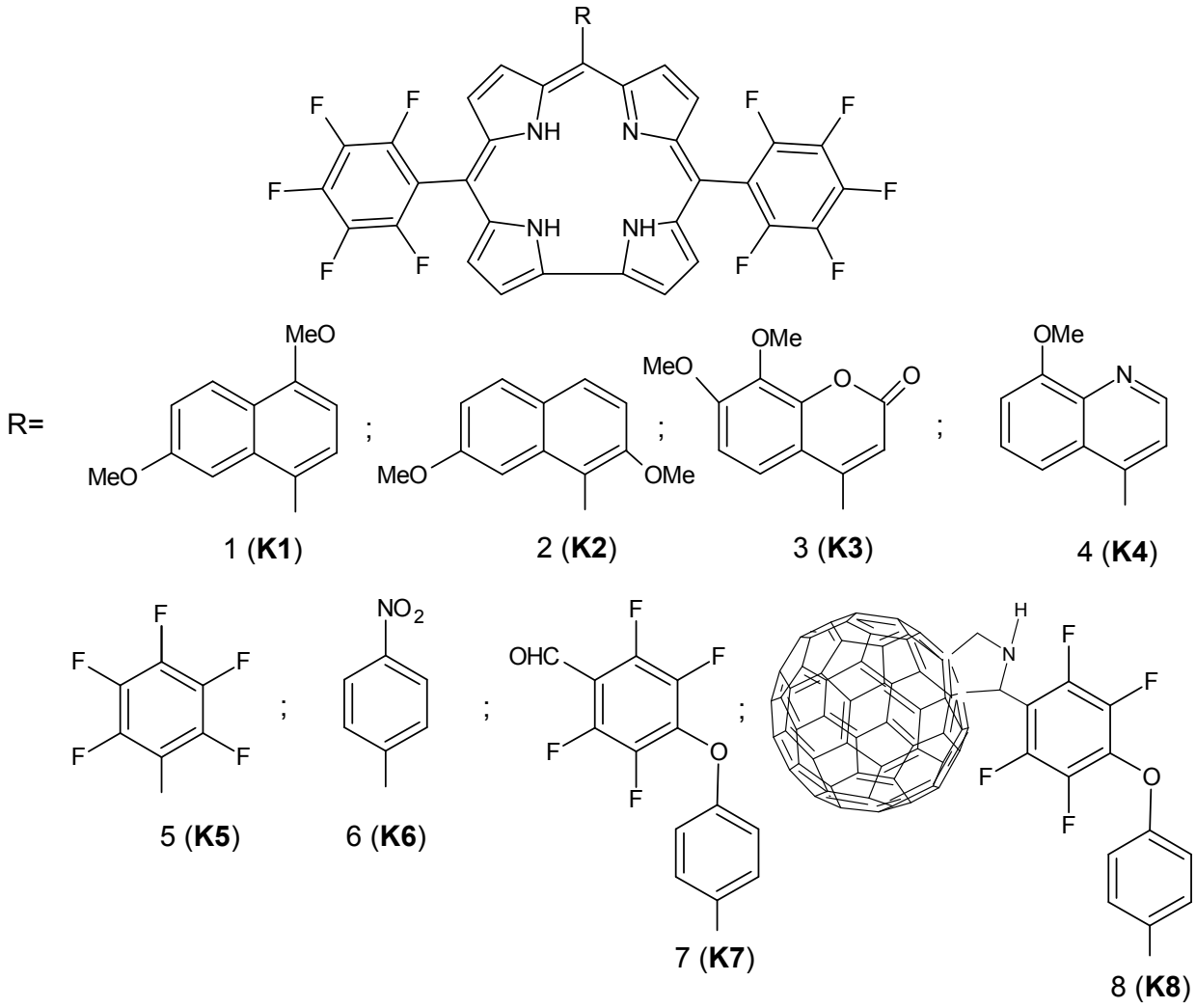


*Rysunek 3 Struktura molekularna badanych układów z rodziny koroli.*

Badania przeprowadzono zarówno dla układów w fazie objętościowej jak i dla układów cienkowarstwowych (warstw Langmuira, Langmuira-Blodgett). W celu scharakteryzowania i uzyskania informacji na temat właściwości fizycznych i fotofizycznych otrzymanych materiałów wykorzystano następujące techniki badawcze: stacjonarną spektroskopię absorpcyjną, stacjonarną spektroskopie absorpcyjną metodą in-situ, fluorescencyjną, spektroskopię Ramana, spektroskopię elektronowego rezonansu paramagnetycznego (EPR), spektroskopię absorpcji i odbicia w zakresie IR, laserowo indukowaną spektroskopię laserową

(LIOAS), woltoamperometrię cykliczną, techniki cienkowarstwowe Langmuira i Langmuira-Blodgett oraz symulacje komputerowe przy użyciu programu Gaussian. Symulacje komputerowe oraz badania eksperymentalne przy użyciu elektronowego rezonansu paramagnetycznego oraz spektroskopii odbiciowej IR wykonane zostały w Instytucie Fizyki Molekularnej PAN w Poznaniu w ramach współpracy naukowej. Pomiary woltoamperometryczne dzięki uprzejmości dr. hab. Grzegorza Loty wykonane zostały na Wydziale Technologii Chemicznej Politechniki Poznańskiej.

# 4. KRÓTKI OPIS BADAŃ

## a) Ftalocyjaniny i ich wybrane mieszaniny z kropkami kwantowymi

Ftalocyjaniny stanowiły pierwszą grupę związków pochodnych porfiryn, które były przedmiotem badań w pracy doktorskiej. Przeprowadzone, w obrębie tych związków badania obejmowały metaloftalocyjaniny galowe i indowe, które udostępnione zostały przez profesora Mahmuta Durmuşa z Uniwersytetu Technicznego w Gebze (Turcja) w ramach nawiązanej współpracy naukowej. Druga grupa związków to mieszaniny komercyjnie dostępnych metaloftalocyjanin cynkowych i miedziowych podstawionych różnymi grupami bocznymi z kropkami kwantowymi CdSe/ZnS.

Publikacja 1 [**Bursa, SA 2014**] obejmuje badania spektroskopowe wybranych ftalocyjanin, które miały na celu analizę wpływu jonu metalu (In, Ga) w głównym makrocyklu na właściwości optyczne otrzymanej metaloftalocyjaniny w fazie objętościowej oraz na podłożu stałym. Na potrzeby badań spektroskopowych (pomiary absorpcji w zakresie UV-Vis), przeprowadzonych dla fazy objętościowej przygotowano roztwory **InPc** i **GaPc** w chloroformie. Chloroform został wybrany, ponieważ dzięki bardzo słabej mieszalności z wodą i niskiej temperaturze wrzenia (61,2 $^{o}$C) doskonale nadaje się jako rozpuszczalnik do nanoszenia rozpuszczonego w nim barwnika na subfazę wodną w przypadku tworzenia monomolekularnych warstw Langmuira. Przeprowadzone badania spektroskopowe dla barwników **InPc** i **GaPc** o różnym stężeniu w fazie objętościowej pozwoliły określić korelacje pomiędzy stężeniem danego barwnika a występowaniem struktur zagregowanych. Widma absorpcji badanych związków w zakresie UV-Vis zarejestrowane zostały również dla warstw Langmuira w funkcji napięcia powierzchniowego. Na podstawie przeprowadzonych badań obejmujących pomiary absorpcji dla fazy objętościowej i dwuwymiarowych warstw Langmuira określono wpływ jonu metalu na tendencję do tworzenia struktur zagregowanych (H,J) badanego barwnika. Badania spektroskopowe w zakresie UV-Vis uzupełnione zostały o badania struktury oscylacyjnej badanych układów przy użyciu techniki FT-IR i spektroskopii Ramana. Pomiary FT-IR przeprowadzone zostały dla próbek w matrycy KBr oraz dla wytworzonych warstw Langmuira-Blodgett na podłożu złota (Au). Szczegółowy opis przeprowadzonych badań oraz otrzymanych wyników znajduje się w publikacji 1 [**Bursa, SA 2014**].

Układy wykazujące przeniesienie energii (ang. *energy transfer*) pomiędzy donorem a akceptorem są szczególnie interesujące i ważne dla zastosowań optoelektronicznych. To też badania będące przedmiotem pracy 2 [**Bursa, JL 2014**] obejmowały również układy organiczno-półprzewodnikowe na bazie chromofor-kropka kwantowa. Dla wybranych komercyjnych ftalocyjanin cynkowych i miedziowych podstawionych bocznymi grupami tetrabutylowymi (**ZnPc-tetr**, **Cu-tetr**) oraz grupami octyloksy (**ZnPc-octy**, **CuPc-octy**) przygotowano ich mieszaniny z kropkami kwantowymi CdSe/ZnS w chloroformie. W ramach pracy pokazano, że mieszaniny półprzewodnikowych kropek kwantowych z metaloftalocyjaninami mogą tworzyć wydajne układy donorowo-akceptorowe ($\Phi_{ET}$=90%). Ponadto, co ciekawe, pokazano, że kropki kwantowe w dwuwymiarowych warstwach Langmuira mogą znacznie ograniczać tworzenie się agregatów molekularnych. Szczegółowy opis przeprowadzonych badań oraz otrzymanych wyników znajduje się w publikacji 2 [**Bursa, JL 2014**].

### b) Korole i ich kowalencyjne diady z fulerenem C60

Dzięki uprzejmości grupy prof. Daniela Gryko otrzymano szereg barwników porfirynopodobnych z grupy koroli, z których wyróżnić można dwie grupy; jedną stanowiły korole a drugą ich układy kowalencyjne z fulerenem C60.

Praca 3 [**Bursa, PCCP 2015]** obejmuje badania właściwości fotofizycznych kilku barwników z rodziny koroli (*Rysunek 3*) (**K1-K6**). W pierwszej części pracy przygotowano roztwory chromoforów rozproszonych w niskopolarnym chloroformie (ε=4,60) dla trzech stężeń $10^{-4}$, $10^{-5}$ i $10^{-6}$ M, których widma absorpcji w zakresie UV-Vis zarejestrowano przy użyciu spektrofotometru absorpcyjnego Cary 4000. Zarejestrowane widma absorpcji nie wykazały wpływu stężenia barwnika w roztworze na kształt rejestrowanych widm absorpcji. Badania absorpcji uzupełniono badaniami emisji i kinetyki fluorescencji. Na ich podstawie wyznaczono szereg parametrów fotofizycznych takich jak: wydajność emisji fluorescencji ($\Phi_F$), szerokość połówkowa dla wybranych maksimów absorpcji (FWHM), czasy życia fluorescencji ($\tau$) oraz wzajemne stosunki natężeń w maksimum absorpcji dwóch form tautomerycznych ($T_1/T_2$). Następnie pokazano, że do opisania pochodzenia przejść absorpcyjnych zarejestrowanych dla badanych koroli można wykorzystać czteroorbitalny model Goutermana[6] opracowany dla porfiryn. W tym celu pozyskane dane eksperymentalne porównano z wynikami

teoretycznymi przewidywanymi w modelu Goutermana i na tej podstawie przypisano przejścia absorpcyjne odpowiednim formom tautomerycznym badanych koroli. Badania przejść promienistych uzupełniono o badania elektronowego rezonansu paramagnetycznego (EPR), które przeprowadzono dla roztworów barwników o stężeniu $10^{-5}$ M. Widma EPR pozwoliły na oszacowanie koncentracji rodnikowych form badanych barwników w roztworze przed i po wzbudzeniu próbki światłem lasera o długości fali 405 nm. Badania eksperymentalne uzupełnione zostały o obliczenia numeryczne przeprowadzone z wykorzystaniem programu Gaussian w oparciu o technikę TD-DFT ( ang. *Time-Dependent Density Functional Theory*), na podstawie których m.in. wyznaczono położenia energetyczne poziomów HOMO, LUMO oraz przedstawiono dla nich graficzną interpretacje obsadzenia poszczególnych orbitali molekularnych. Szczegółowy opis przeprowadzonych badań oraz otrzymanych wyników znajduje się w publikacji 3 [**Bursa, PCCP 2015**].

Następnym celem prowadzonych badań było sprawdzenie wpływu polarności rozpuszczalnika na właściwości fotofizyczne wybranych koroli, w szczególności wpływu na tworzenie form zagregowanych oraz form tautomerycznych. W ramach pracy 4 [ **Bursa, PCCP 2016 ]** skupiono uwagę na dwóch korolach **K5** i **K6** (*Rysunek 3*), których roztwory o stężeniu $10^{-4}$, $10^{-5}$ i $10^{-6}$M przygotowano w rozpuszczalnikach niepolarnych toluenie (Tl, ε=2,38 ), chloroformie (Cl, ε=4,6) oraz polarnych dimetyloformamidzie (DMF, ε=37), dimetylosulfotlenku (DMSO, ε=46,70). Dla tak przygotowanych roztworów zarejestrowane widma absorpcji w zakresie UV-Vis oraz emisji fluorescencji dostarczyły wielu intersujących informacji o naturze procesów zachodzących w badanych próbkach pod wpływem wybranych rozpuszczalników w tym efektów mezomerycznych i procesów deprotonacji. W dalszych badaniach, w celu wyznaczenia kinetyki powstawania poszczególnych form tautomerycznych, przeprowadzono badania spektroskopowe obejmujące pomiary absorpcji i fluorescencji w zakresie UV-Vis roztworów **K5** i **K6** w toluenie (c=$10^{-5}$ M) w funkcji stężenia drugiego bardziej polarnego rozpuszczalnika DMF; badania w DMSO nie zostały podjęte ze względu na tendencję do tworzenia struktur zagregowanych barwnika dla stężeń większych niż $10^{-4}$ M. Przeprowadzone podstawowe badania spektroskopowe (pomiary absorpcji, emisji fluorescencji, kinetyki fluorescencji) uzupełniono o obliczenia numeryczne oparte o technikę TD-DFT. Obliczenia numeryczne potwierdziły obserwowany w rozpuszczalnikach polarnych (w przypadku korolu **K6)** efekt mezomeryczny związany z obecnością grupy $NO_2$. W celu potwierdzenia uzyskanych metodą TD-DFT wyników dotyczących energii poziomów HOMO i LUMO badanych układów dla roztworów **K5** i **K6** przeprowadzono badania

woltoamperometri cyklicznej, które dostarczyły informacji zbieżnych z obliczeniami komputerowymi oraz potwierdziły ujemny charakter obserwowanego wcześniej w przypadku **K6** efektu mezomerycznego. Przeprowadzone w pracy 4 [**Bursa, PCCP 2016 ]** laserowo indukowane badania foto-akustyczne (LIOAS) dostarczyły informacji dotyczących parametrów termicznej dezaktywacji, które pozwoliły określić wydajności obsadzenia stanu trypletowego oraz kwantowej wydajności generowania tlenu singletowego ($\Phi_{\Delta}$). Szczegółowy opis przeprowadzonych badań oraz otrzymanych wyników znajduje się w publikacji 4 [**Bursa, PCCP 2016**].

Kolejnym etapem pracy doktorskiej było przeprowadzenie badań wpływu kowalencyjnie związanego fulerenu C60 (**K8**) (*Rysunek 3*) na właściwości spektroskopowe i termodynamiczne wybranego korolu (**K7**) [**Lewandowska, SM 2013] i** [**Bursa, SM 2013]**. Widma emisji i kinetyki zaniku fluorescencji zarejestrowane dla roztworu korolu **K7** i diady **K8**, ewidentnie pokazały donorowo-akceptorowy charakter układu kowalencyjnie sprzężonego korolu z fulerenem C60 (**K8**). Donorowo-akceptorowa natura chromoforu **K8** potwierdzona została również przy użyciu zawartych w pracy 5 [**Lewandowska, SM 2013]** obliczeń numerycznych TD-DFT oraz badań przy użyciu rezonansu paramagnetycznego (EPR). W celu uzyskania informacji o energii oscylacyjnej wiązań badanych układów wykonano badania absorpcji w podczerwieni w matrycy KBr i obicia-absorpcji w zakresie podczerwieni (IRRA) dla warstw Langmuira-Blodgett w świetle spolaryzowanym i niespolaryzowanym [**Bursa, SM 2013].** Badania warstw Langmuira-Blodgett na podłożu Au i kwarcu poprzedzono badaniami właściwości optycznych i termodynamicznych warstw Langmuira wybranych chromoforów i diad **K7** i **K8** na subfazie wodnej [**Bursa, SM 2013].** Aby potwierdzić/wykluczyć możliwości postawania zagregowanych struktur wybranych koroli, uzyskane przy różnych ciśnieniach powierzchniowych widma absorpcji metodą in-situ z warstw Langmuira, porównano z widmami **K7** i **K8** rozproszonymi w fazie objętościowej dla szerokiego zakresu stężeń $10^{-4}$ – $10^{-6}$ M (w Cl, TL, DMSO). Wyznaczając kąt pomiędzy moment przejścia a normalną do powierzchni w oparciu o wyniki IRRA i metodę zaproponowaną przez Arnold i współpracowników[7] oszacowano ułożenie molekuł w warstwie LB. Rezultaty uzyskane w oparciu o model Arnolda[7] porównano z wynikami uzyskanymi z badań dichroizmu liniowego z wykorzystaniem modelu Yoneyama[8]. Szczegółowy opis przeprowadzonych badań oraz otrzymanych wyników znajduje się w publikacjach 5 i 6 [**Lewandowska, SM 2013]**, [**Bursa, PCCP 2016**].

# 5. PODSUMOWANIE ORAZ WNIOSKI

W ramach pracy doktorskiej przedstawiono i przedyskutowano wyniki badań eksperymentalnych i symulacji komputerowych obejmujących badania właściwości spektroskopowych i termodynamicznych wybranych związków porfiryno-podobnych takich jak ftalocyjaniny i korole oraz ich wybrane układy typu chromofor-fulleren C60, chromofor-kropka kwantowa o właściwościach donorowo-akceptorowych. W badaniach zastosowano metody stacjonarnej spektroskopii absorpcyjnej, stacjonarnej spektroskopii absorpcyjnej metodą in-situ, fluorescencyjnej, spektroskopii Ramana, spektroskopii elektronowego rezonansu paramagnetycznego, spektroskopii absorpcyjne i odbicia w zakresie IR, laserowo-indukowanej spektroskopii optoakustycznej, techniki Langmuria i Langmuira-Blodgett, woltoamperometrii cyklicznej oraz wykonano symulacje wykorzystując program Gaussian.

**a) Ftalocyjaniny i ich wybrane mieszaniny z kropkami kwantowymi**

- Na podstawie analizy widm absorpcji ftalocyjanininy indowej (**InPc**) 2,3 tetrakis(4-benzyloksyphenoksylowej) oraz ftalocyjaniny galowej (**GaPc**) 2,3 tetrakis(4-benzyloksyfenoksylowej) wykazano, że molekuły **GaPc,** w przeciwieństwie do **InPc**, mają tendencję do agregowania w roztworach przy stężeniach powyżej $10^{-5}$M. Oba barwniki wykazują tendencję do tworzenia struktur agregacyjnych w warstwach Langmuira, przy czym typ agregatu zależy istotnie od jonu metalu wbudowanego do wnętrza makrocyklu. Makrocykl zawierający jon indu tworzy agregaty pochyłe (ang. *oblique*), a zawierający jon galu tworzy agregaty typu H. Jon metalu In lub Ga w głównym makrocyklu badanych ftalocyjanin nie wpływa na jego orientację molekularną względem podłoża Au w przypadku warstw Langmuira-Blodgett[9].
- Pokazano, że istnieje bardzo silne oddziaływanie o charakterze donorowo-akceptorowym między molekułami ftalocyjaniny cynkowej (**ZnPc-tetr)** a kropką kwantową CdSe/ZnS w wyniku którego obserwuje się silne wygaszenie emisji fluorescencji chromoforu oraz ograniczenie powstawania form zagregowanych barwnika w warstwach Langmuira[10].

**b) Korole i ich układy kowalencyjne z fulerenem C60**

- Widma absorpcji zarejestrowane dla badanych koroli pokazały, że barwniki rozpuszczone w chloroformie nie tworzą form zagregowanych w szerokim zakresie stężeń $10^{-4}$-$10^{-6}$ M [11].
- Badania wykonane przy użyciu elektronowego rezonansu paramagnetycznego wykazały, że niesparowane elektrony zlokalizowane są na głównym makrocyklu a nie na podstawniku zarówno przed i po zaabsorbowaniu energii promieniowania[11].
- Grupa nitrylowa $NO_2$ w podstawniku (**K6**) wpływa silnie na dystrybucje elektronów π w stanie wzbudzonym, o czym świadczy zarejestrowany efekt mezomeryczny prowadzący do spadku wydajności emisji fluorescencji poniżej limitu detekcji. Występowanie efektu mezomerycznego potwierdziły zarówno badania eksperymentalne jak i obliczenia numeryczne. Wykazano, że deprotonacja jest procesem dominującym w przypadku korolu 5,10,15 tris (pentafluorofenylowego) (**K5**) w rozpuszczalnikach silnie polarnych (DMF, DMSO). Wyniki otrzymane z obliczeń numerycznych i wolto-amperometrii cyklicznej pokazały silną korelacje w położeniach poziomów HOMO i LUMO badanych barwników. Ponadto, przeprowadzone badania przy użyciu techniki LIOAS wskazały na możliwość wykorzystania korolu 5.10,15 tris (pentafluorofenylowego) również w fototerapii dynamicznej[12].
- Na podstawie badania emisji i kinetyki zaniku fluorescencji jak i elektronowego rezonansu paramagnetycznego potwierdzono donorowo-akceptorowy charakter kowalencyjnych układów typu korol-fuleren C60 (**K8**)[13].
- Spolaryzowane widma absorbcji w zakresie UV-Vis oraz absorbcji odbiciowej w zakresie podczerwieni wykazały, że obecność sferycznej molekuły fulerenu C60 wpływa na orientację głównego makrocyklu korolu względem powierzchni podłoża w dwuwymiarowych warstwach Langmuira-Blodgett[14].

Podsumowując, przeprowadzone badania wykazały, że w przypadku barwników o obniżonej symetrii takich jak korole w zależności od polarności rozpuszczalnika mamy do czynienia z wieloma procesami konkurencyjnymi m.in. tautomeryzacją, deprotonacją, a zmiana polarności rozpuszczalnika jest stosunkowo łatwym narzędziem pozwalającym sterować właściwościami spektroskopowymi tych barwników.

Dla badanych układów wyznaczono szereg parametrów spektroskopowych, co pozwala na ilościową ocenę przydatności badanych związków w optoelektronice i dziedzinach pokrewnych. Na szczególną uwagę zasługują układy donorowo-akceptorowe korol-fuleren C60 (**K8**) oraz ftalocyjanina z grupą tetrbutylową (**ZnPc-tetr**) z kropką kwantową (**CdSe/ZnS**).

# 6. DOROBEK NAUKOWY KANDYDATA

**DOROBEK PUBLIKACYJNY:**

1. **B. Bursa**, D. Wróbel, A. Biadasz, K. Kędzierski, K. Lewandowska, A. Graja, M. Szybowicz, M. Durmuş, *Indium–chlorine and gallium–chlorine tetrasubstituted phthalocyanines in a bulk system, Langmuir monolayers and Langmuir–Blodgett nanolayers - spectroscopic investigations,* Spectrochimica Acta Part A: Molecular and Biomolecular Spectroscopy **128**, (2014) 489-496, IF=2,653

2. **B. Bursa**, A. Biadasz, K. Kędzierski, D. Wróbel, *Quantum dot with zinc and copper substituted phthalocyanines. 1. Energy transfer in solution and in-situ light absorption in Langmuir monolayers*, Journal of Luminescence, **145** (2014) 779-786, IF=2,693

3. **B. Bursa**, B. Barszcz, W. Bednarski, J.P. Lewtak, D. Koszelewski, O. Vakuliuk, D.T. Gryko, D. Wróbel, *New meso-substituted corroles possessing pentafluorophenyl groups - Synthesis and spectroscopic characterization*, Phys. Chem. Chem. Phys. **17** (2015) 7411 – 7423, IF=4,493

4. **B. Bursa**, D. Wróbel, B. Barszcz, M. Kotkowiak, O. Vakuliuk, D.T. Gryko, Ł. Kolanowski, M. Baraniak, G. Lota, *The impact of solvents on the singlet and triplet states of selected fluorine corroles – absorption, fluorescence and optoacustic studies,* Phys. Chem. Chem. Phys. **18** (2016) 7216-7228, IF=4,493

5. K. Lewandowska, B. Barszcz, A. Graja, **B. Bursa**, A. Biadasz. D. Wróbel, W. Bednarski, S. Waplak, M. Grzybowski, D.T. Gryko, *Absorption and emission properties of the corrole-fullerene dyad*, Synthetic Metals, **166** (2013) 70-76, IF=2,229

6. **B. Bursa**, D. Wróbel, K. Lewandowska, A. Graja, M. Grzybowski, D.T. Gryko, *Spectral studies of molecular orientation in corrole-fullerene thin films*, Synthetic Metals, **176** (2013)18-25, IF=2,229

7. K. Kędzierski, B. Barszcz, M. Kotkowiak, **B. Bursa**, J. Goc, H. Dinçer, D. Wróbel, *Photophysics of an unsymmetrical Zn(II) phthalocyanine substituted with terminal alkynyl group,* J. Lumin., **180** (2016), 132-139 IF= 2,693

8. D. Kasprowicz, M. Brik, K. Jaroszewski, T. Pedziński, **B. Bursa**, P. Głuchowski, A. Majchrowski, E. Michalski, *Spectroscopic properties of Bi2ZnOB2O6 single crystals doped with Pr3+ ions: absorption and luminescence investigations*, Optical Materials, **47** (2015) 428-434, IF=2,044

9. D. Wróbel, A. Biadasz, **B. Bursa**, *Triplet thermal relaxation study as a probe of weak interdimer of porphyrin derivatives*, Int. J. of Thermophys., **33** (2012) 716–732, IF=0,623

10. K. Lewandowska, B. Barszcz, A. Graja, B. Biadasz, **B. Bursa**, D. Wróbel, *Molecular orientation in self-assembled layers of two functionalized fullerenes – role of bromine atom at the end of akryl chain*, Synthetic Metals, **162** (2012) 2134-2137, IF=2,256

11. A. Biadasz, **B. Bursa**, B. Barszcz, A. Bogucki, B. Laskowska, A. Graja, D. Wróbel, *Thermodynamics and in-situ absorption of Langmuir monolayers of selected copper phthalocyanine substituted with different peripheral groups*, Dyes and Pigments, **89** (2011) 86-92, IF=3,255

12. B. Barszcz, A. Bogucki, A. Biadasz, **B. Bursa**, D. Wróbel, A. Graja, *Molecular orientation and spectral investigations of Langmuir-Blodgett films of selected copper phthalocyanines*, Journal of Photochemistry and Photobiology A: Chemistry, **218** (2011) 48–57, IF=2,475

13. B. Olejarz, **B. Bursa**, I. Szyperska, R.-M. Ion, A. Dudkowiak, *Spectral properties and deactivation processes of anionic porphyrin coupled with TiO2 nanostructure*, Int. J. Thermophys., **31** (2010) 163-171, IF=0,623

**PROJEKTY BADAWCZE:**

1. **Kierownik projektu badawczego** „Badania nad zastosowaniem układów donorowo-akceptorowych na bazie nanostruktura półprzewodnikowa – chromofor w układach fotowoltaicznych typu DSSC" o numerze 2011/03/N/ST4/02957 finansowanego przez NCN.
2. **Kierownik projektu badawczego** „Wpływ asymetrii barwnika ftalocyjaninowego na zdolność konwersji promieniowania słonecznego na energię elektryczną w ogniwach fotowoltaicznych" o numerze 06/62/DSMK/0196.
3. **Kierownik projektu badawczego** „Właściwości plazmoniczne nanostrukturalnych filmów srebrnych (kontynuacja)" o numerze DS 62-191 DS-MK/2013.
4. **Kierownik projektu badawczego** „Właściwości plazmoniczne nanostrukturalnych filmów srebrnych" o numerze DS 62-183/12 DS-MK/2012.
5. **Wykonawca projektu badawczego** „Prace badawczo rozwojowe nad uzyskaniem pierwszego na świecie ultra cienkiego ogniwa fotowoltaicznego na bazie perowskitów nadrukowanego metodą „electronic inkjet" na podkład elastyczny", projekt nr POIR.01.01.01-00-0090/15.
6. **Wykonawca projektu badawczego** „Wpływ struktury cynku na właściwości optyczne i parametry pracy modelowego ogniwa fotowoltaicznego opartego o perowskity" o numerze 06/62/DSMK/0194.
7. **Wykonawca projektu badawczego** „Wpływ nanocząstek metalicznych na właściwości optyczne i elektryczne ogniw fotowoltaicznych" o numerze 06/62/DSMK/0192.
8. **Wykonawca projektu badawczego** „Supramolekularne układy fulleren-tiofen w dwuwymiarowych warstwach Langmuira" o numerze DS. 62-180/11.
9. **Wykonawca projektu badawczego** nr N N202 260 234, 2008-2011 finansowanego z MNiSW.
10. **Wykonawca projektu B+R** z firmą Saule sp. z o.o. od 2015.
11. **Wykonawca projektu B+R** z firmą LenaLighting S.A od roku 201.4
12. **Wykonawca projektu B+R** z firmą Colagen Active Science w roku 2014.
13. **Wykonawca projektu B+R** z firmą 3MK w roku 2013.

**STYPENDIA:**

1. 2013 – Stypendium Wielkopolskiego Urzędu Pracy w ramach projektu „Wsparcie stypendialne dla doktorantów na kierunkach uznanych za strategiczne z punktu widzenia rozwoju Wielkopolski".
2. 2013 – Stypendium Rektora Politechniki Poznańskiej oraz stypendium z dotacji projakościowej dla najlepszych doktorantów.
3. 2012 – Stypendium Wielkopolskiego Urzędu Pracy w ramach projektu „Wsparcie stypendialne dla doktorantów na kierunkach uznanych za strategiczne z punktu widzenia rozwoju Wielkopolski".
4. 2012 – Stypendium Rektora Politechniki Poznańskiej oraz stypendium z dotacji projakościowej dla najlepszych doktorantów.
5. 2012 – Stypendium w ramach projektu „Era Inżyniera" „Rozbudowa Potencjału Rozwojowego Politechniki Poznańskiej" - dofinansowanie stażu naukowego na Uniwersytecie Aalto w Finlandii.
6. 2011 – Stypendium Rektora Politechniki Poznańskiej dla najlepszych doktorantów.
7. 2011 – 3 miesięczne stypendium w ramach programu „Era Inżyniera".

**STAŻE NAUKOWE**

1. III-X 2007- Brandenburgische Technische Universitat Cottbus (Niemcy).
2. IV-VII 2012 - Aalto University Espoo (Finlandia).

**ORGANIZACJA KONFERENCJI**

1. Członek komitetu organizacyjnego konferencji „Zjazd Fizyków Polskich", Poznań, Czerwiec 2013".
2. Przewodniczący komitetu organizacyjnego „5$^{th}$ International Interdisciplinary Technical Conference of Young Scientists InterTech 2012", Poznań, Maj 2012.
3. Przewodniczący komitetu organizacyjnego „4th International Interdisciplinary Technical Conference of Young Scientists InterTech 2011", Poznań, Maj 2011.

## ORGANIZACJE I KOŁA NAUKOWE

1. Założyciel i opiekun koła naukowego NanoiżynieriI Molekularnej na Wydziale Fizyki Technicznej Politechniki Poznańskiej w latach 2012-2015.
2. Członek Polskiego Towarzystwa Fizycznego (od roku 2012 Skarbnik Oddziału Poznańskiego).

## KONFERENCJE NAUKOWE

W okresie od 2008 do 2016 kandydat był autorem/współautorem 39 komunikatów na konferencjach krajowych i międzynarodowych. Z najważniejszych wymienić można:

1. **B. Bursa,** B. Barszcz, A. Bogucki, W. Bednarski, D. Wróbel, J.P. Lewtak, D. Koszalewski, O. Vakuliuk, D.T. Gryko, *Układy donorowo-akceptorowe na bazie korol-fuleren C70 do zastosowań w fotowoltaice,* Nauka i Przemysł, Lublin, Czerwiec 2014.
2. **B. Bursa**, B. Barszcz, W. Bednarski, D. Wróbel, *Donor-acceptor systems based on a quantum dot-chromophore for applications in hybrid photovoltaic cells*, HOPV14, Lausanne, Maj 2014.
3. **B. Bursa**, T. Buchwald, M. Bińczyk, M. Szybowicz, M. Kamiński, *Wpływ temperatury na orientację ftalocyjaniny galowej zaadsorbowanej na powierzchni nanostruktur srebra*, Kryształy Molekularne 2012, Gdańsk-Sobieszewo, Wrzesień 2012.
4. **B. Bursa**, T. Buchwald, M. Szybowicz, M. Kamiński, M. Huuppola, J. Kelly, *Orientation and SERS effect of gallium phthalocyaninses absorbed on Ag nanoprism,* CNBM, Poznań, Maj 2012.
5. **B. Bursa**, A. Biadasz, M. Szybowicz, M. Durmuş, K. Lewandowska, D. Wróbel, *Wybrane barwniki ftalocyjaninowe dla zastosowań w elektronice molekularnej*, WCZT, Poznań, Listopad 2012.
6. **B. Bursa**, A. Biadasz, D. Wróbel, *Układy donorowo-akceptorowe dla zastosowań w ogniwach fotowoltaicznych trzeciej generacji*, i Ogólnopolska Konferencje Naukowa Studentów i Doktorantów, Kryształki Molekularne, Wrocław, Wrzesień 2011.
7. **B. Bursa**, D. Wróbel, A. Biadasz, W*eak interdimer formation in selected phthalocyanines and porphyrin-polymer systems*, 40th Winter School on wave and Quantum Acoustics, 16th winter workshop on Photoacoustic and Thermal Wave Methods, Szczyrk, Luty 2011.
8. **B. Bursa**, A. Biadasz, D. Wróbel, *Układy donorowo-akceptorowe dla zastosowań w*

*fotowoltaice na bazie kropka kwantowa – chromofor,* IV Krajowa Konferencja Nanotechnologii – NANO, Poznań, Czerwiec 2011.

9. **B. Bursa**, A. Biadasz, D. Wróbel, *Układy donorowo-akceptorowe dla zastosowań w fotowoltaice na bazie kropka kwantowa – chromofor*, BioMediTech - I Ogólnopolskie Studenckie Seminarium Naukowo-Technologiczne, Poznań, Kwiecień 2010.

# 7. BIBLIOGRAFIA


1 T. A, *Phthalocyanine research and applications*, II Edition, CRC Press, 1990.

2 A. Braun and J. Tcherniac, *J. Ber. Dusch. Chem. Ges.*, 1907, **40**, 2709.

3 A. W. Johnson and I. T. Kay, *J. Chem. Soc.*, 1965, 1620–1629.

4 R. K. Hocking, S. D. George, Z. Gross, F. A. Walker, K. O. Hodgson, B. Hedman, E. I. Solomon, *Inorg. Chem.*, 2009, **48**, 1678–1688.

5 J. H. Palmer, M. W. Day, A. D. Wilson, L. M. Henling, Z. Gross, H. B. Gray, *J. Am. Chem. Soc.*, 2008, **130**, 7786–7787.

6 M. Gouterman, G. H. Wagnière, L. C. Snyder, *J. Mol. Spectrosc.*, 1963, **11**, 108–127.

7 R. Arnold, A. Terfort and C. Wöll, *Langmuir*, 2001, **17**, 4980–4989.

8 M. Yoneyama, M. Sugi, M. Saito, K. Ikegami, S. Kuroda, S. Iizima, *Jpn. J. Appl. Phys.*, 1986, **25**, 961–965.

9 B. Bursa, D. Wróbel, A. Biadasz, K. Kędzierski, K. Lewandowska, A. Graja, M. Szybowicz, M. Durmuş, *Spectrochim. Acta - Part A Mol. Biomol. Spectrosc.*, 2014, **128**, 489–496.

10 B. Bursa, A. Biadasz, K. Kędzierski, D. Wróbel, *J. Lumin.*, 2014, **145**, 779–786.

11 B. Bursa, B. Barszcz, W. Bednarski, J. P. Lewtak, D. Koszelewski, O. Vakuliuk, D. T. Gryko, D. Wróbel, *Phys. Chem. Chem. Phys.*, 2015, **17**, 7411–23.

12 B. Bursa, D. Wróbel, B. Barszcz, M. Kotkowiak, O. Vakuliuk, D. T. Grytko, Ł. Kolanowski, M. Baraniak, G. Lota, *Phys. Chem. Chem. Phys.*, 2016, **18**, 7216–7228.

13 K. Lewandowska, B. Barszcz, A. Graja, B. Bursa, A. Biadasz, D. Wróbel, W. Bednarski, S. Waplak, M. Grzybowski, D. T. Gryko, *Synth. Met.*, 2013, **166**, 70–76

14 B. Bursa, D. Wrobel, K. Lewandowska, A. Graja, M. Grzybowski, D. T. Gryko, *Synth. Met.*, 2013, **176**, 18–25.

## 8. SPIS ZAŁĄCZNIKÓW

Załącznik nr 1- Oświadczenie współautora: prof. Mahmut Durmuş

Załącznik nr 2 - Oświadczenie współautorów: prof. dr hab. Daniel Gryko, dr Olena Vakuliuk, dr Dominik Koszalewski, dr Jan Paweł Lewtak

Załącznik nr 3 - Oświadczenie współautora: prof. dr hab. Stefan Waplak

Załącznik nr 4 - Oświadczenie współautora: dr hab. Waldemar Bednarski

Załącznik nr 5 - Oświadczenie współautorów: dr hab. inż. Grzegorz Lota, dr inż. Marek Baraniak, mgr inż. Łukasz Kolanowski

Załącznik nr 6 - Oświadczenie współautora: dr inż. Andrzej Biadasz

Załącznik nr 7 – Oświadczenie współautora: dr inż. Bolesław Barszcz

Załącznik nr 8 - Oświadczenie współautora: dr inż. Marek Grzybowski

Załącznik nr 9 - Oświadczenie współautora: dr inż. Kornelia Lewandowska

Załącznik nr 10 - Oświadczenie współautora: mgr inż. Kamil Kędzierski

Załącznik nr 11 - Oświadczenie współautora: mgr inż. Michał Kotkowiak

# 9. PRZEDRUKI ARTYKUŁÓW WCHODZĄCYCH W SKŁAD PRACY DOKTORSKIEJ

Artykuły umieszczono w następującej kolejności:

1. **[Bursa, SA 2014] B. Bursa**, D. Wróbel, A. Biadasz, K. Kędzierski, K. Lewandowska, A. Graja*, Indium–chlorine and gallium–chlorine tetrasubstituted phthalocyanines in a bulk system, Langmuir monolayers and Langmuir–Blodgett nanolayers–Spectroscopic investigations,* Spectrochimica Acta Part A: Molecular and Biomolecular Spectroscopy **128** (2014) 489-496

2. **[Bursa, JL 2014] B. Bursa**, A. Biadasz, K. Kędzierski, D. Wróbel, *Quantum dot with zinc and copper substituted phthalocyanines. 1. Energy transfer in solution and in-situ light absorption in Langmuir monolayers*, Journal of Luminescence, **145** (2014) 779-786

3. **[Bursa, PCCP 2015] B. Bursa**, B. Barszcz, W. Bednarski, J.P. Lewtak D. Koszelewski, O. Valulyuk, D.T. Gryko, D. Wróbel, *New meso-substituted corroles possessing pentafluorophenyl groups - Synthesis and spectroscopic characterization*, Phys. Chem. Chem. Phys. **17** (2015) 7411 – 7423

4. **[Bursa, PCCP 2016] B. Bursa**, D. Wróbel, B. Barszcz, M. Kotkowiak, O. Valulyuk, D. Gryko, Ł. Kolanowski, M. Baraniak, G. Lota, *Solvent impact on the singlet and triplet states of selected fluorine corroles – absorption, fluorescence and aptoacustic studies,* Phys. Chem. Chem. Phys. **18** (2016) 7216-7228

5. **[Lewandowska, SM 2013]** K. Lewandowska, B. Barszcz, A. Graja, **B. Bursa**, A. Biadasz. D. Wróbel, W. Bednarski, S. Waplak, M. Grzybowski, D.T. Gryko, *Absorption and emission properties of the corrole-fullerene dyad*, Synthetic Metals, **166** (2013) 70-76

6. **[Bursa, SM 2013] B. Bursa**, D. Wróbel, K. Lewandowska, A. Graja, M. Grzybowski, D.T. Gryko, *Spectral studies of molecular orientation in corrole-fullerene thin films*, Synthetic Metals, **176** (2013) 18-25

**Praca nr 1**

**[Bursa, SA 2014]** B. Bursa, D. Wróbel, A. Biadasz, K. Kędzierski, K. Lewandowska, A. Graja*, Indium–chlorine and gallium–chlorine tetrasubstituted phthalocyanines in a bulk system, Langmuir monolayers and Langmuir–Blodgett nanolayers–Spectroscopic investigations,* Spectrochimica Acta Part A: Molecular and Biomolecular Spectroscopy **128** (2014) 489-496

Spectrochimica Acta Part A: Molecular and Biomolecular Spectroscopy 128 (2014) 489–496

Contents lists available at ScienceDirect

Spectrochimica Acta Part A: Molecular and Biomolecular Spectroscopy

journal homepage: www.elsevier.com/locate/saa

# Indium–chlorine and gallium–chlorine tetrasubstituted phthalocyanines in a bulk system, Langmuir monolayers and Langmuir–Blodgett nanolayers – Spectroscopic investigations

B. Bursa [a], D. Wróbel [a,*], A. Biadasz [a], K. Kędzierski [a], K. Lewandowska [b], A. Graja [b], M. Szybowicz [c], M. Durmuş [d]

[a] Faculty of Technical Physics, Institute of Physics, Poznan University of Technology, 60-965 Poznań, Poland
[b] Institute of Molecular Physics, Polish Academy of Sciences, 60-179 Poznań, Poland
[c] Faculty of Technical Physics, Chair of Optical Spectroscopy, Poznan University of Technology, 60-965 Poznań, Poland
[d] Gebze Institute of Technology, Department of Chemistry, Gebze 41400, Turkey

## HIGHLIGHTS

- Electronic, FTIR, Raman spectra of In-ClTPc and Ga-ClTPc in chloroform and *in situ* light absorption of Langmuir monolayers.
- In-ClTPc forms the oblige cooplanar aggregate while Ga-ClTPc creates the H-type aggregate.
- The dyes in Langmuir–Blidgett layers are oriented nearly vertically in relation to the gold substrate.

## GRAPHICAL ABSTRACT

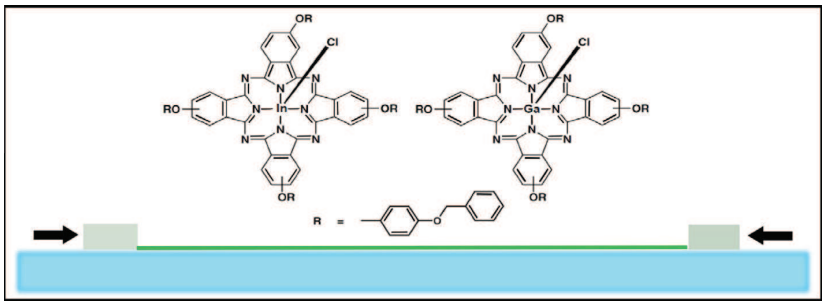


## ARTICLE INFO

*Article history:*
Received 21 October 2013
Received in revised form 18 February 2014
Accepted 23 February 2014
Available online 12 March 2014

*Keywords:*
Metallic phthalocyanine
*In situ* light absorption measurements
UV–Vis–NIR–IR–Raman spectra
Langmuir, Langmuir–Blodgett layer
Molecular aggregation

## ABSTRACT

The paper deals with spectroscopic characterization of metallic phthalocyanines (Pc's) (indium and gallium) complexed with chlorine and substituted with four benzyloxyphenoxy peripheral groups in bulk systems, 2D Langmuir monolayers and Langmuir–Blodgett nanolayers. An influence of the molecular structure of dyes (the presence of metal and of substitutes attached to the phthalocyanine macroring) on the *in situ* measurements of light absorption is reported. Molecular arrangement of the phthalocyanine molecular skeleton in the Langmuir monolayers on water substrate and in the Langmuir–Blodgett nanolayers is evaluated. A comparison of the light absorption spectra of the phthalocyanine monolayers with the spectra of the dyes in solution supports the existence of dye aggregates in the monolayer. It was shown that the type of dye aggregates (oblique and H types) depends markedly on the dye molecular structures. The NIR-IR, IR reflection–absorption and Raman spectra are also monitored for Langmuir–Blodgett nanolayers in non-polarized and polarized light. It was shown that the dye molecules in the Langmuir–Blodgett layers are oriented nearly vertically with respect to a gold substrate.



## Introduction

Since the past decades phthalocyanines have been a subject of numerous papers because of their unique spectroscopic, photoelectric and magnetic properties [1]. Pc's are usually characterized

*Abbreviations:* Pc, phthalocyanine; Ga-ClTPc, gallium–chlorine benzyloxyphenoxy phthalocyanine; In-ClTPc, indium–chlorine benzyloxyphenoxy phthalocyanine; L, Langmuir; LB, Langmuir–Blodgett; DMSO, dimethyl sulfoxide; HWFM, half width at full maximum; IR, infrared; IRRA, infrared reflection-absorption.

* Corresponding author. Tel.: +48 616653179; fax: +48 616653178.
*E-mail address:* danuta.wrobel@put.poznan.pl (D. Wróbel).

http://dx.doi.org/10.1016/j.saa.2014.02.178
1386-1425/

by large absorption coefficients and some of them are known as thermally stable molecular materials. They are still a subject of many studies due to their potential applications in science and technological fields due to their particular properties. Phthalocyanines are able to create coordination bonding, molecular aggregates, organic polymers and low-dimensional semiconductors and so on [1,2]. Moreover, because of their well known photoactivity more and more attention is put in investigations directed towards conversion of light energy to electric energy, photodynamic therapy, modeling of artificial photosynthesis, photocatalysis and tailoring sensors [1–7].

Characterization of nanolayers (mono- and multilayers) is extremely important when organic materials are supposed to be used as electronic elements in molecular electronic and optoelectronic devices in which they are in a close contact with metal or semiconductive electrodes. Therefore, it is interesting to follow their properties and processes occurring in ultra-thin films with densely packed dye molecules. In thin films their thickness can be controlled in the order of nanometers and their studies can give information on organic material-interface and organic molecule interactions. Moreover, the molecular arrangement in ultra-thin films can be also kept under observation. As a lot of phthalocyanine dyes are rather insoluble in organic solvents, substitution of dyes with peripheral groups allows to intensify their solubility. In this paper Pc derivatives – indium-chlorine phthalocyanine and gallium–chlorine phthalocyanine substituted with benzyloxyphenoxy peripheral groups are dissolved in chloroform because of their perfect solubility in this solvent. Besides fast evaporation of chloroform is also essential while forming dye Langmuir (L) layers. Moreover, some phthalocyanines show a trend towards aggregated structure creation when molecules are in highly concentrated solutions or densely packed in thin films [2,8].

Bulk systems and thin solid films can be characterized by the use of different spectroscopic and microscopic methods [9–16]. In this paper we take full advantage of Langmuir technique supported by the *in situ* measurements of light absorption. We also decided to benefit from IR transmission spectra of the samples in a bulk system and reflection–absorption spectroscopy of Langmuir–Blodgett (LB) layers in polarized light and also from Raman spectroscopy. With the use of these experimental methods we can get information on interaction of molecules with their vicinity (subphase and neighbor molecules). The L and L–B layer properties of In-ClTPc and Ga-ClTPc substituted with benzyloxyphenoxy peripheral group are presented. However, the *in situ* investigations were also done by us in [8] and also presented in [9] but for different porphyrin/phthalocyanine dyes.

In our previous paper [8] we reported the results of the *in situ* measurements of light absorption of L monolayers of copper Pc's substituted with tetra-tert-butyl and octakis(octyloxy) groups. In this paper we present the influence of metal ion (In or Ga) with covalently attached chlorine in the main π-electron macroring on some spectroscopic properties of the dyes in solution, monolayers and multilayers. Thus, firstly we extend our UV–Vis investigations done in organic solvents [10] with the use of the UV–Vis *in situ* measurements of light absorption for Langmuir monolayers. Secondly, we perform IR transmission spectra in KBr and polarized reflection–absorption spectra of LB layers on a gold plate as well as Raman spectra of the dye powder and LB systems. The molecular arrangement of the dyes in the L monolayers and L–B nanolayers is also evaluated.

## Materials and methods

In these studies we present investigations of two metallic phthalocyanine dyes: 2,3-tetrakis(4-benzyloxyphenoxyphthalocyaninato)indium(III) (named herein **1**) and 2,3-tetrakis(4-benzyloxyphenoxyphthalocyaninato)gallium(III) (named herein **2**) in KBr, powder and in a form of Langmuir monolayers and Langmuir–Blodgett nanolayers. The detailed description of chemical synthesis of the dyes is presented in [10–17]. The molecular structures of the dyes under investigations are shown in Scheme 1.

A Varian spectrophotometer Cary 4000 is applied for recording of the electronic spectra in the range 300–800 nm. Absorption spectra of the dyes in chloroform are done for the $10^{-6}$, $10^{-5}$ and $10^{-4}$ M samples.

We have also done the *in situ* measurements of light absorption of the dye L layer to get information about closely packed dyes in a compressed ultra-thin layer. The samples are dissolved in chloroform in view of their perfect solubility in this solvent and sufficiently fast evaporation to receive good L and LB layers. The L monolayers and the LB layers of the samples are created with a KSV 2000 minitrough (KSV Instruments Ltd.) equipped with a temperature control system. The Langmuir trough area is $364 \times 75$ mm$^2$. Temperature of subphase is achieved and kept constant (20 °C) with a cooling circulator. Deionized water (electrical resistivity 18.2 MΩ cm – Mili-Q Milipore Corp. water purification system) as the subphase is used. The sample dissolved in chloroform ($10^{-4}$ M) is carefully spread on the subphase and chloroform evaporation takes 15 min. A floating film of the L layer is compressed symmetrically from both sides with motion barrier speed of 5 mm/min. The LB layers (5 layers on each side) are deposited on a gold plate (average transfer ratio = 0.92).

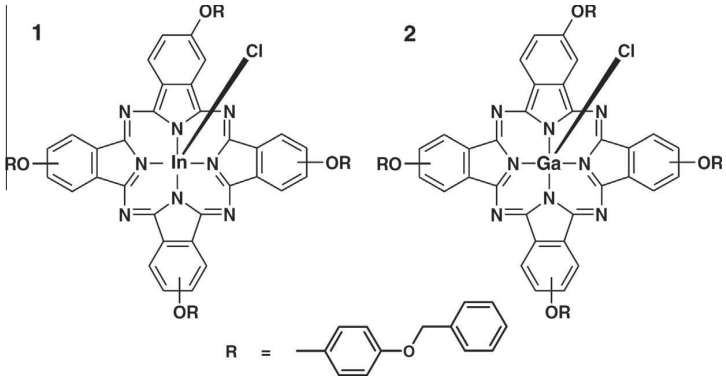


**Scheme 1.** Molecular structure of dyes **1** (2,3-tetrakis(4-benzyloxyphenoxyphthalocyaninato)indium(III)) and **2** (2,3-tetrakis(4-benzyloxyphenoxyphthalocyaninato) gallium(III)).

The *in situ* measurements of absorption spectra of the L layers are recorded in the region 300–850 nm with an Ocean Optics spectrometer QE65000, which was localized in proximity to a quartz window of the KSV instrument.

IR transmission spectra of the samples dispersed in KBr are recorded with the use of FT-IR Bruker Equinox 55 spectrometer in the range 400–3500 $cm^{-1}$ at room temperature. IRRA spectroscopy is applied for vibrational analysis of the LB films, in particular for evaluation of molecule orientation in the layer. In this experiment the sample is placed on a gold mirror so that absorption of a sample reduced reflectance, and a sort of transmission spectrum of the sample results. The IRRA spectra are done in the unpolarized and polarized light, with the electric vector of the light wave parallel (*p*-polarization) and perpendicular (*s*-polarization) to the plane of incidence. The spectra are obtained at the angle of incidence 80°. Both IR and IRRA spectra are recorded with the use of the same FT IR Bruker Equinox 55 spectrometer in the range 400–3500 $cm^{-1}$.

As it was mentioned in our previous papers [18,19] orientation of organic molecules grafted on a metal surface can be determined with the use of IRRA spectroscopy. We apply the simplified method proposed by Arnold et al. [20] to evaluate orientation of molecules. Since the intensity of a band is proportional to the absolute value of the transition dipole moment $M$ of the band, the ratio $(M_i/M_j)^2$ of two bands can be supposed to be the ratio of the band intensities $I_i^{bulk}/I_j^{bulk}$ of the bulk spectrum. This simple method is also described in details in [21]. A tilt angle Ω determined as the angle between the transition moment $M_i$ and normal to the samples surface can be estimated using the following equation:

$$\tan^2 \Omega = \frac{I_i^{bulk} I_j^{LB}}{I_j^{bulk} I_i^{LB}}, \quad (1)$$

where $I_i^{bulk}$ and $I_j^{bulk}$ are intensities of the measured (i) and reference (j) bands, respectively, recorded in KBr pellets and $I_i^{LB}$ and $I_j^{LB}$ are intensities of the adequate bands of the dye LB films.

Raman scattering spectra of the dyes are performed with the use of an inVia Renishaw micro-Raman system. As an excitation light the blue line of an argon laser operating at 488 nm is used (with the use of 488 nm excitation we can minimize sample fluorescence). In this experiment the laser beam is tightly focused on a sample surface with the use of a Leica 50× long working distance (LWD) microscope objective. An excitation beam power is fixed at 5 mW to prevent any damage of a sample. The Raman spectra are recorded in the spectral range 1100–1800 $cm^{-1}$ with the spectral resolution ±1 $cm^{-1}$ and spatial resolution of about 1 μm. The position of the microscope objective with respect to a thin layer is controlled piezoelectrically. The reference position (level 0) is assumed for a laser spot focusing on a sample surface. The Raman method used in the experiment is described in details in [22].

## Results and discussion

### *Electronic absorption of samples in solution – aggregation ability of the dyes in chloroform*

Electronic absorption studies are done for recognization of our samples to get knowledge on interaction between the dye molecules and their ability to form aggregated structures in chloroform. Absorption measurements of the dyes in selected non-polar and polar solvents were done by one of us and the results are presented in [10]; the dye concentration experiments were done in dimethyl sulfoxide (DMSO – $\varepsilon = 46.70$) and the results showed monomeric species as expected for dyes in polar solvent. However, in this paper we use chloroform as a solvent because of two reasons: (i) chloroform is much less polar ($\varepsilon = 4.80$) than DMSO and thus dye ability to form aggregates is expected to be much stronger than that in DMSO, and (ii) in monolayer creation the fast evaporation is required for making a good L layer. The concentration examinations done with the electronic absorption measurements of the samples in solution demonstrate ability of the samples to create aggregated structures – the $10^{-6}$ M sample is used to minimize the presence of aggregates and serves as a standard sample. The electronic absorption spectra of the dyes in chloroform (dye concentrations: $10^{-6}$, $10^{-5}$ and $10^{-4}$ M) are presented in Fig. 1A and B and they show the existence of aggregates in highly concentrated solution (very well seen in the sample **2**). A starting point for a discussion of the origin of absorption bands Gouterman's four-orbital model will be shortly presented [23]. Gouterman proposed

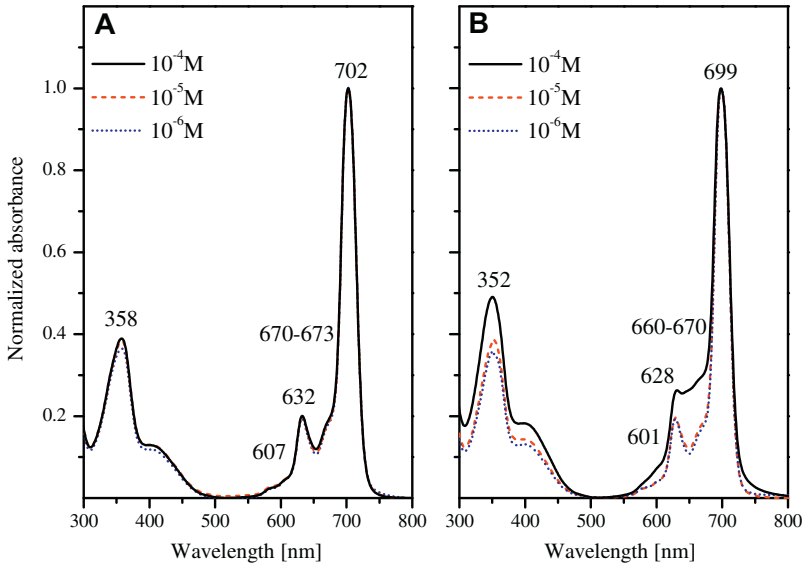


**Fig. 1.** Absorption spectra of **1** (A) and **2** (B) in chloroform normalized to unity at the main Q band; dye concentrations: $10^{-4}$, $10^{-5}$ and $10^{-6}$ M.

an idea that the porphyrin (and thus also phthalocyanine) spectra results from $\pi$–$\pi^*$ transition from the two highest occupied molecular orbitals (HOMO) to the first lowest unoccupied molecular orbital (LUMO). The absorption bands of phthalocyanines contain weak Soret bands (known also as $B_Y$, Bx bands) and stronger bands (known also as $Q_X$ and $Q_Y$ bands); (the symbols x and y refer to $N_{II}$–$N_{IV}$ and $N_{II}$–$N_{IV}$ axis, respectively). The Q bands correspond to the Q00 and Q01 components of the Q transition. Effect of dimerization on the HOMO and LUMO in terms of the four-orbital model is presented and interaction in the $\pi$–$\pi$ dimers is widely discussed in [24]. In our absorption experiments two sets of the bands are well recognized: in the Soret region 300–500 nm (the origin of the B-bands is discussed in details in [10,24,25] and the low energy Q bands which are located at 702 and 632 nm with a 670–673 nm hump (sample **1**) and 699 and 628 nm with a shoulder at 660–670 nm (sample **2**). The band/hump clearly seen between both maxima is usually attributed to an aggregate [26]. The intensities of the bands increase with dye concentration (what is obvious); in Fig 1 the curves are normalized to unity at the highest maximum (702 nm – **1**, 699 – **2**). However, the changes in the band shapes and in the intensity ratios in the spectral region 628–670 nm of the sample **2** indicate the presence of some aggregates. Selected absorption parameters of the samples in chloroform are gathered in Table 1. The first observation is very diverse behavior of **1** and

**Table 1**
The selected absorption parameters of the dyes in chloroform and Langmuir monolayers of **1** and **2**.

| Sample 1 | | | | | | | | Sample 2 | | | | | | | | | | | |
|---|---|---|---|---|---|---|---|---|---|---|---|---|---|---|---|---|---|---|---|
| In chloroform | | | | In Langmuir monolayer | | | | In chloroform | | | | | | | | In Langmuir monolayer | | | |
| $c = 10^{-6}$ M | | | | $\pi = 10$ mN m$^{-1}$ | | | | $c = 10^{-6}$ M | | | | $c = 10^{-4}$ M | | | | $\pi = 10$ mN m$^{-1}$ | | | |
| $\lambda_{max}$ | FWHM | Band | $\chi^2$ | $\lambda_{max}$ | FWHM | Band | $\chi^2$ | $\lambda_{max}$ | FWHM | Band | $\chi^2$ | $\lambda_{max}$ | FWHM | Band | $\chi^2$ | $\lambda_{max}$ | FWHM | Band | $\chi^2$ |
| – | – | – | 0.017 | 740 | 581 | Q–/Q+ | 0.001 | – | – | – | 0.026 | – | – | – | 0.025 | 765 | 529 | – | 0.001 |
| 702 | 251 | Q(00) | | – | – | – | | 699 | 246 | Q(00) | | 699 | 249 | Q(00) | | 699 | 592 | Q(00) | |
| 672 | 440 | – | | 667 | 1297 | Q–/Q+ | | 670 | 590 | Q+ | | 666 | 874 | Q+ | | 658 | 587 | Q+ | |
| 632 | 297 | Q(01) | | 630 | 490 | Q(01) | | 628 | 285 | Q(01) | | 628 | 301 | Q(01) | | 639 | 1282 | Q(01) | |
| 607 | 180 | – | | 578 | 841 | – | | 601 | 230 | – | | 601 | 201 | – | | – | – | – | |

Band intensity ratio

| Sample 1 | | | | Sample 2 | | | | | |
|---|---|---|---|---|---|---|---|---|---|
| In chloroform | | In Langmuir monolayer | | In chloroform | | | | In Langmuir monolayer | |
| $c = 10^{-6}$ M | | $\pi = 10$ mN m$^{-1}$ | | $c = 10^{-6}$ M | | $c = 10^{-4}$M | | $\pi = 10$ mN m$^{-1}$ | |
| 702/632 | 5.14 | – | – | 699/628 | 3.89 | 699/628 | 5.08 | 699/639 | 1.03 |
| 702/672 | 5.76 | – | – | 699/670 | 3.42 | 699/666 | 5.79 | 699/658 | 0.82 |
| 672/632 | 0.93 | 667/630 | 1.22 | 670/628 | 1.14 | 666/628 | 0.88 | 658/639 | 1.26 |

$\lambda_{max}$ – wavelength of band maximum (nm), FWHM – full width at half maximum (cm$^{-1}$), $c$ – concentration,
$\chi^2$ – residual sum of squares, $\pi$ – surface pressure.

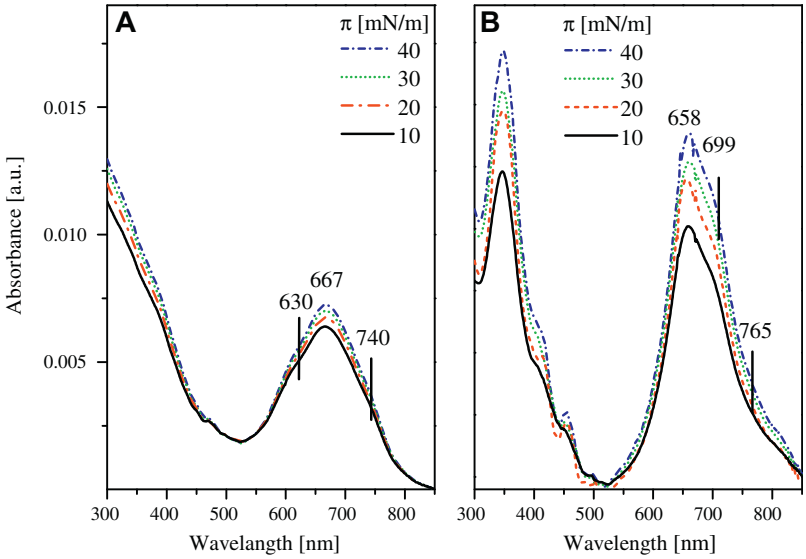


**Fig. 2.** *In situ* light absorption spectra of **1** (A) and **2** (B).

**2** in the concentrated sample ($10^{-4}$ M). When the $10^{-4}$ M dye spectra are compared with those of the monomeric sample in chloroform ($10^{-6}$ M) all differences become apparent.

It is evident that the band's intensities relation *versus* concentration depends on the dye molecular structures of **1** and **2**. The small shoulder at about 670 nm observed in absorption spectra of diluted solutions could be ascribed to very small amount of dimer structures [24,27,28]; whereas the changes in the band shapes and in intensity ratios of **2** evidently confirm the presence of some aggregates (Fig. 1, Table 1). The 550–800 nm absorption spectra in solution are dominated by electronic Q00 and vibronic replicas of this transition Q01. The dissimilarity in the ability to aggregate creation of the dyes could have a source in central ions (In or Ga covalently linked to Cl); the peripheral groups are the same in the two dyes thus their influence can be rather neglected. As the only molecular difference between the samples **1** and **2** is the presence of different ions covalently bond to Cl in the main molecular frame one can say that the results confirm a strong influence of metal on the interaction between the individual molecules **1** and **2**. However, on the basis of the results presented in Fig. 1 we cannot unambiguously declare the type of molecular aggregates because we do not observe the main Q band shifts (and other changes typical for aggregates creation); the changes in the values of the full width at half maximum (*FWHM* at 628–670 nm) are more or less observed. This is seen particularly in the sample **2** (Fig. 1B). The reason of the different ability of the dyes to form aggregates is the different configuration of the dipole transitions in **1** and **2**. The absorption intensity of a shoulder increases in the longwavelength part of the spectra of **2** (in the region from 628 to 680 nm) when the dye concentration increases ($10^{-4}$ M) and it becomes broader due to the presence of aggregates. Thus, the increase of the 628 nm band and of the shoulder at about 666 nm confirm the aggregate formation [28]. Moreover, we cannot exclude admixture of charge-transfer states as observed for GaPc crystal particles in polymer matrix [29]. Creation of aggregates of metallic tetrasubstituted phthalocyanines and related porphyrin compounds and the dimer structure was discussed and confirmed by spectroscopic and atomic force microscopy studies in solutions, polymer matrix and solid thin films [4,9,27–31].

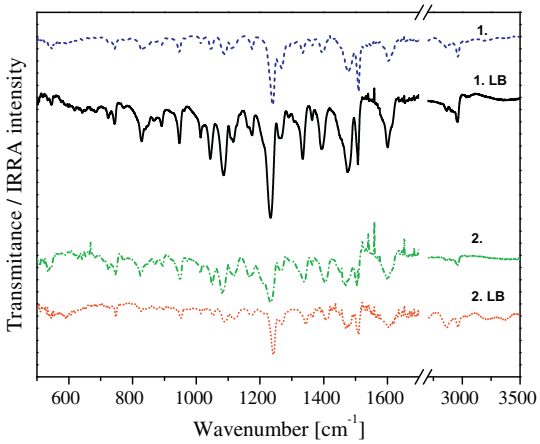


**Fig. 3.** Vibrational spectra of **1** and **2** in KBr and of LB layers deposited on gold substrate recorded with non-polarized light.

*In situ measurements of light absorption of dye Langmuir monolayers*

On the basis of the L layer investigations we have found a confirmation of the dye ability to form aggregated structures. The results of the *in situ* measurements and those in chloroform can help us to discuss the type of aggregates created in the L monolayers. Spectral behavior of the dyes **1** and **2** when compressed in the L layer is shown in Fig. 2A and B. The *in situ* studies are monitored under various surface pressure from 10 to 40 mN/m in a similar way as it was done in our previous papers [8,32–34]. The spectral changes are observed in the dye samples when one compares the *in situ* results with those in chloroform. The dimers are observed

**Table 2**
IR wavenumbers and band assignments of selected bands in KBr pellet and LB layers as well as the tilt angle Ω between selected transition moment $M_i$ and the normal to the sample surface.

| Sample 1 | | | Sample 2 | | | Band assignment |
|---|---|---|---|---|---|---|
| Wavenumber of band ($cm^{-1}$) | | Tilt angle Ω | Wavenumber of band ($cm^{-1}$) | | Tilt angle Ω | |
| in KBr | in LB | | in KBr | in LB | | |
| 547 | 547 | | 533 | – | | C—H b, oop; N—H b, ip; C—N—C b |
| 722 | 724 | | 724 | – | | C—H b, oop; N—H b, oop |
| 742 | 744 | | 745 | 747 | | C—H b, oop; N—H b, ip |
| 828 | 829 | 27 | 825 | 828 | 21 | |
| 892 | 893 | | 870 | 873 | | C—H b, oop |
| 946 | 947 | 32 | 948 | 951 | 22 | C—H b, oop; C—C b, oop |
| 1012 | 1014 | | 1013 | 1013 | | C—H b, ip |
| 1043 | 1045 | | 1051 | 1052 | | C—H b, ip; N—H b, ip |
| 1086 | 1088 | 24 | 1080 | 1088 | 22 | C—H b, ip; N—H b, ip |
| 1117 | 1117 | | 1116 | 1120 | | C—H b, ip; N—H b, ip |
| 1175 | 1175 | | 1169 | 1170 | | C—H b, ip |
| 1233 | 1240 | | 1232 | 1241 | | C—H b, ip; N—H h, oop; N—H b, C—N s |
| 1263 | 1268 | | 1267 | 1267 | | C—H b, ip |
| 1333 | 1333 | 33 | 1338 | 1343 | 34 | C—N s; C—C—S d; N—C—N h; C—H b, oop |
| 1362 | 1364 | | 1363 | 1365 | | C—N s; N—H h; C—C s |
| 1393 | 1394 | 28 | 1403 | 1408 | 28 | C—N s; C—N—C b |
| 1475 | 1475 | 37 | 1468 | 1469 | 37 | C—N s, N—H b, ip; C—H b, ip |
| 1507 | 1508 | | 1503 | 1509 | | C—N s; C—N—C b |
| 1601 | 1603 | 34 | 1599 | 1602 | | C=N s; C=N d |
| 2959 | 2962 | | 2958 | 2964 | | C—H s |

b – bending, s – stretching, d – deformation, h – heaving, oop – out-of-plane, ip – in-plane.

in the L layers (*versus* those in chloroform) because of much stronger interaction between the molecules due to the shorter geometrical distance in the L layer than that in chloroform. The *in situ* results evidently confirm strong interaction between the dye molecules in the layers. In the L absorption spectra two sets of bands are well seen – the intensive bands in the Soret region (300–520 nm) and the broad bands in the Q part (550–800 nm). The spectroscopic behavior of the dyes in the L layers is markedly different. In **1** both structural-less Soret bands with maximum beyond 300 nm and the Q bands (with the main maximum at about 670 nm) are very broad (Fig. 2A) due to the superimposition of several bands localized at about 630, 667 nm and also 740 nm. According to Kasha vector model [35] a blue shift is expected for H aggregates (in the ideal H-dimer the molecular frame is oriented face-to-face), whereas the longwavelength shifts result from J-dimers with in-line transition dipoles oriented face-to-tail. In the oblique configuration a composition of the in-face and out-of-face transition dipole arrangement leads to decreasing and increasing energy of the excited states of double molecules [36–39]. Usually dimerization results in the band shift (longwavelength or shortwavelength), in change of the band intensity ratio and also in the value of the band full width at half maximum. Dimerization also can cause a changes in $\pi$–$\pi^*$ transition dipole moments and give rise to the Q and Soret bands. The shape of the Q broad band of **1** (Fig. 2A) indicates unambiguously the presence of more than one molecular species in the L film. The main band very well seen at 667 and two humps at about 630 and 740 nm can be recognized in the L spectra. On the basis of the obtained results it is rather difficult to finally resolve what kind of dimeric species (oblique or stacked) are present in the samples. It is well known that phthalocyanines (and related porphyrin compounds) have tendency to create stacked dimers in an aqueous surrounding [40]. The presence of such sort of aggregates cannot be neglected in our samples due to interaction of molecules with aqueous surface during Langmuir layer formation. The band at 667 nm appears as a result of domination of the components of oblique aggregates (Q+/Q−). Also the increasing the values of *FWHM* parameters confirm conclusion on the presence of aggregates. The bands at 740 nm in the spectra of **1** in the L layers can originate from oblique coplanar aggregates [36–39]. Thus, the Q band of the sample **1** is found to be composed of two bands 630 (assigned to the monomeric species) and 740 nm around the band with a maximum at 667 indicating the oblique aggregates.

Otherwise, the Langmuir spectra of the sample **2** are more clear. In **2** two sets of the explicitly splitted bands of high intensities are observed: in the Soret part (maximum at 340 nm) and in the Q region. We pay our attention to the Q band results because we are not able to discuss the shapes of the Soret bands of **2** *versus* **1**. A new band at 658 nm and the 699 nm shoulder in the longwavelength part appear after the L layer formation (Fig. 2B). The large "blue" shift of 41 nm (from 699 nm to 658 nm) is observed in **2** and it can result from creation of H aggregates. The shoulder at 699 nm can be assigned to the monomers coexisting with the H aggregates in the monolayers. To our knowledge the origin of the 765 nm hump is unknown (e.g. it could be a kind of aggregate formed in the presence of water [31] in a Langmuir trough). On the basis of the results presented in Fig. 2A and in 2B as well as obtained for the concentrated samples **1** and **2** in chloroform one can draw some conclusions regarding interaction of the dyes in the L monolayers. As seen the *in situ* results depend markedly on the dyes used in the experiments; the central ion (In or Ga) is responsible for the variety of the *in situ* data. Since, the only molecular dissimilarity between the samples **1** and **2** is the presence of different metal ions in the main molecular frame, one can say the results confirm an influence of ion. Thus, the presence of different ions in the macroring affects strongly interaction between the individual dyes in the aggregate and interaction between metallic ion and Cl by the covalent bonding and/or by space in the In-ClTPc and Ga-ClTPc molecules in the L layers. This is clearly confirmed when one compares the *in situ* measurements (Fig. 2) with those in chloroform (Fig. 1). The presence of aggregates in the L layers is obvious and found confirmation in the literature by spectroscopic [36] and atomic force microscopy data [41–43]. In our previous papers regarding creation of zinc and copper phthalocyanines substituted with different peripheral groups and a corrole dye in L layers, it was shown that the type of aggregates (oblique or H) depends strongly on the dye molecular structure. The kind of metal ion in the macroring and substituents attached to the main dye molecule core have a great influence on aggregation creation [8,32–34].

There are several reasons of the dissimilarity between the **1** and **2** structures in the aggregates formation. The aggregates of **1** and **2** display clearly strong influence of ion covalently linked to Cl. The interaction of the electron-rich macroring and metal should also affect the dye ability to form aggregates. The physicochemical properties of indium and gallium complexed with chlorine incorporated in the molecular macroring affect the observed disparity between the aggregates of **1** and **2.** The basic properties of indium and gallium like e.g. electronegativity, ionization energy, electron affinity, Van der Waals radius are similar. However, their electronic configuration, atomic radius, covalent radius, etc. differ one another and it can lead to the marked distinctions between aggregated structures. Because of the different ground state electronic configurations of In ([Kr] $4d^{10}5s^25p^1$) and of Ga ([Ar] $3d^{10}4s^24p^1$) [44–47] the dissimilarity of the covalent bonding between In–Cl and Ga–Cl can lead to the various electron distribution in the $\pi$-electron-reach macrorings and hence to the different aggregate formation. Moreover, the presence of different metal ions (In, Ga) can also affect the dye aggregation ability due to diverse distortion of the $\pi$-electron macrorings. The remarkable distortions of phthalocyanine molecules were also observed in [48], mainly as the central atom trends towards the substrate to minimize the atom-substrate distance.

### *IR investigations in KBr and in Langmuir–Blodgett layers*

#### *In unpolarized light*

The IR transmission spectra of both metallophthalocyanines (Fig. 3A and B) recorded in the KBr pellet (in bulk) are very similar. It seems to be comprehensible because the organic part of the central ring of both molecules is the same. However some of the bands

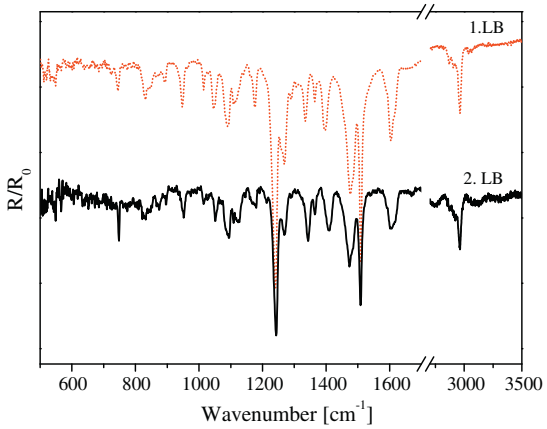


**Fig. 4.** Polarized reflection–absorption spectra of LB layers of **1** and **2** on gold substrate; the angle incidence 80°.

**Table 3**
The wavenumbers and band assignment of selected Raman bands in powder and LB layers of phthalocyanines.

| Sample 1 | | Sample 2 | | Band assignment |
|---|---|---|---|---|
| Wavenumber of band ($cm^{-1}$) | | Wavenumber of band ($cm^{-1}$) | | |
| LB | Powder | LB | Powder | |
| 1615 | 1608 | 1615 | 1610 | C—C s; C—C b, ip |
| 1587 | 1579 | 1592 | 1588 | C—N s; |
| 1508 | 1498 | 1530 | 1527 | C—N s; C—N—C b, ip |
| 1478 | – | 1485 | 1485 | C—H ip; C—C b, oop |
| 1394 | 1389 | 1401 | 1400 | C—C s; C—H b, ip |
| 1344 | 1338 | 1344 | 1339 | C—H b, oop; C—C s |
| 1268 | 1267 | 1268 | 1269 | N—H ip; C—N s |
| 1230 | 1232 | 1230 | 1234 | N—H ip; C—N s |
| 1194 | 1193 | 1194 | 1194 | C—H oop |

b – bending, s – stretching, d – deformation, h – heaving, oop – out-of-plane, ip – in-plane.

are shifted and/or changed in their intensities. The comparison of the strongest and the most characteristic vibrational bands in the "finger" region of the investigated compounds (400–3500 $cm^{-1}$) are gathered in Table 2 and shown in Fig. 3. The shape of some bands of **1** is changed in comparison with those in the adequate region of **2**. For example, we observe strong vibrational bands at 533, 724, 745, 825 and 870 $cm^{-1}$ in the spectrum of **2** whereas for **1** these peaks are slightly shifted to 547, 722, 742, 828 and 892 $cm^{-1}$, respectively. In this region one can find also the C—H out-of-plane bending and deformation of the skeletons of both samples. In the region 1000–1200 $cm^{-1}$ the most intensive bands are connected with the in-plane C—H bending. For stretching vibrations of the C—N groups in phthalocyanines, the small frequency shift of 1338 $cm^{-1}$ (**2**) *versus* 1333 $cm^{-1}$ (**1**) is observed. The C—N stretching and the C—N—C in-plane bending modes are observed above 1500 $cm^{-1}$ but the C=N stretching modes are located at 1599 and 1601 $cm^{-1}$. The modification is an example showing that a relatively small variation in the molecule composition changes distinctly the IR spectrum of the molecule.

IRRA spectra of the thin film, deposited on a solid gold substrate show some differences in comparison with the spectra of an adequate substance in bulk. The comparison of the spectra in KBr and of the LB film shows that the most of vibrational bands are shifted towards the higher frequencies. Their relative intensities are also altered. These band shifts reflect the changes in the charge distribution in the investigated molecules after their deposition on the gold substrate. The modification can be caused by several reasons. Firstly, the molecules in LB films are ordered more or less parallel. Thus, the intermolecular interaction between them can be distinctly changed in comparison with interaction between randomly oriented molecules. Secondly, interaction between the molecular thin layer and metallic substrate can provoke a charge transfer at the layer-gold substrate interface. Thus, some changes can be related to a modification of the electron density on the molecules as a result of interaction with the gold substrate.

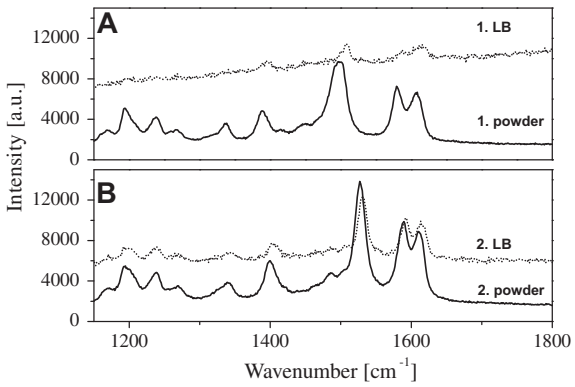


**Fig. 5.** Raman spectra of **1** and **2** in LB layer on gold substrate (A) and in powder (B).

*In polarized light*

As it was mentioned above, an orientation of organic molecules grafted to a metal surface can be determined using IRRA spectroscopy in polarized light. For evaluation of the molecule orientation in the film we have applied the simple method proposed by Debe [21] and described in details by Arnold et al. [20] as well as by us [18]. In our estimations the most intensive band at 1232 $cm^{-1}$ was assumed as a reference band (index j). To determine orientation of the phthalocyanine central ring an analysis of the selected bands of vibrations of the bonds lying in the plane of the central part of a molecule (especially the C—N bending) are performed.

The typical IRRA spectrum of **1** and **2** for the *p*-polarization of light are shown in Fig. 4; the tilt angles are calculated according to Eq. (1). They are collected in Table 2. Analyzing the data one can see that the angles $\Omega$ of the central parts of the investigated metal phthalocyanines are centered between 21° and 37°. It suggests that the phthalocyanine molecules are oriented rather vertically in relation to the gold substrate.

Thus, we can conclude that both phthalocyanines in the LB layers are similarly oriented. We suggest that the type of metal in the central part of the molecules does not affect the organization of molecular layers perceptible. Some differences in the values of the angle $\Omega$ evaluated on the basis of the various vibrational bands may suggest that the central cycle of the investigated phthalocyanines is not exactly flat.

*Raman scattering examinations*

The basic Raman selection rules allow the $A_{1g}$, $B_{1g}$, $B_{2g}$ and $E_g$ modes to be active in the normal Raman scattering [49]. The $A_{2g}$ modes occur in the resonance spectrum as a result of the vibronic coupling between two electronic excited states of metallophthalocyanine.

The position of the bands observed in the spectral region from 1350 to 1550 $cm^{-1}$ is closely linked to metal ion complexed to phthalocyanine macroring. From our experiment point of view we put attention on the mode represented by the maximum at about 1500 $cm^{-1}$ because of at least several reasons: (i) this mode is responsible for interaction of metal with nitrogen in the macroring of phthalocyanine, (ii) the only difference between our samples **1** and **2** is the presence of indium or gallium ions in the central rings, (iii) the major changes in Raman spectra for the two metallophthalocyanine thin layers are observed in this spectral region, (iv) this region corresponds to the nitrogen in-plane stretching and bending vibrations as well as to displacements of the C—N—C bridge bond (see Table 3), and (v) the changes in locations of the 1500 $cm^{-1}$ band in the LB layer Raman spectra *versus* those in powder.

Thus, we can take advantage of the Raman experiment and use this mode as a marker for distinguishing interaction of the metallophthalocyanines in the thin film. In Fig. 5 we present the Raman spectra of **1** and **2** in the LB layer and in powder. As seen, the Raman band at 1500 $cm^{-1}$ in the LB layers (associated with central metal) is shifted with respect to that in powder of about 10 $cm^{-1}$. The band shift is caused by interaction between the dye molecule and the gold substrate and confirms markedly that interaction between the dye molecules and the plate is stronger than molecule–molecule interaction in powder.

One can evidently see the difference in the position of the bands associated with central metal in the molecules. We record this band at 1508 $cm^{-1}$ and 1530 $cm^{-1}$ for the sample **1** and **2**, respectively. The band shift of about 20 $cm^{-1}$ (1508 $cm^{-1}$ *versus* 1530 $cm^{-1}$) is caused by the different metal ion (In or Ga) in the central ring – metal ion sizes, cavity diameters of phthalocyanines, mass of metal ion and electronic structure of the atoms.

Both IR spectra and Raman spectra confirm the results obtained with the use of the *in situ* experiments.

## Conclusions

On the basis of our *in situ* measurements of light absorption of the dyes in the Langmuir monolayers, UV–Vis examinations in chloroform, IR and Raman spectroscopies of the dye Langmuir–Blodgett nanolayers we can draw following conclusions:

1. The dye **1** (In-ClTPc) does not show tendency to aggregate in chloroform even in the highly concentrated samples; otherwise the dye **2** (Ga-ClTPc) shows trend towards aggregate creation.
2. In the L layers the presence of aggregates of both dyes are monitored but their molecular structures depend strongly on the kind of metal in the main dye molecule macrorings – the dye **1** (In-ClTPc) presents a trend to form the oblique aggregates, while the dye **2** (Ga-ClTPc) forms the H-type one.
3. The IR transmission spectra of the investigated metal phthalocyanines in KBr are very similar; central metal (In or Ga) does not distinctly change the spectra of these molecules; however in the LB nanolayers some bands are shifted towards higher energy and indicate stronger interaction between the dye molecules and the gold substrate.
4. The orientation of the central parts of the investigated metal phthalocyanines determined on the basis of IRRA spectroscopy is similar; the molecules are oriented nearly vertically in relation to the gold substrate.
5. The most intense band in the Raman spectrum (at about 1500 $cm^{-1}$) is uniquely sensitive to the metal ion present in the complex. The reason is a large displacement on the C—N—C bridges between the isoindole groups. This leads to a frequency shift that is dependent not only on the strength of the bridge bonds but also on the effect of different metal ion on the ring shape It confirms the essential influence of In and Ga on the strong interaction with the Au substrate.

## Acknowledgements

The paper was supported by Poznan University of Technology (grant 06/62/DSPB/0214; B.B., D.W., A.B., K.K. and 06/64/DSPB/0414; M.S) and by the National Science Center of Poland (Post-doctoral internship No. 2012/04/S/ST5/00071; K.L.).

## Appendix A. Supplementary material

Supplementary data associated with this article can be found, in the online version, at http://dx.doi.org/10.1016/j.saa.2014.02.178.

## References

[1] N.B. McKeown, Phthalocyanine Materials, Synthesis, Structure and Function, Cambridge University Press, Cambridge, 1998.
[2] C.C. Lesnoff, A.B.P. Lever, Phthalocyanines. Properties and Application, VCH, New York, 1996.
[3] I. Rosenthal, Photochem. Photobiol. 53 (1991) 859–870.
[4] Y.L. Lee, Y.C. Chen, C.H. Chang, Y.M. Yang, J.R. Maa, Thin Solid Films 370 (2000) 278–284.
[5] J.-H. Yum, S.-R. Jang, R. Humphry-Baker, M. Grätzel, J.-J. Cid, T. Torres, Md.K. Nazeeruddin, Langmuir 24 (2008) 5636–5640.
[6] R.B. Ostler, A.D. Scully, A.G. Taylor, I.R. Gould, T.A. Smith, A. Waite, D. Phillips, Photochem. Photobiol. 71 (2000) 397–404.
[7] I. Beletskaya, V.S. Tyurin, A.Y. Tsivadze, R. Guilard, C. Stern, Chem. Rev. 109 (2009) 1659–1713.
[8] A. Biadasz, B. Bursa, B. Barszcz, A. Bogucki, B. Laskowska, A. Graja, D. Wróbel, Dyes Pigments 89 (2011) 86–92.
[9] Z. Wang, W. Mao, H. Chen, F. Zhang, X. Fan, G. Qian, Catal. Commun. 7 (2006) 518–552.
[10] H. Yanik, D. Aidyn, M. Durmaş, V. Ahsen, J. Photochem. Photobiol. A: Chem. 206 (2009) 18–26.
[11] W.R. Barger, A.W. Snow, H. Wohltjen, N.L. Jarvis, Thin Solid Films 133 (1985) 197–204.
[12] J. Souto, J.A. De Saja, M.I. Gobernado-Mitre, M.L. Rodriguez, R. Aroka, Opt. Appl. 15–16 (1993) 306–11.
[13] D.P. Dilella, W.R. Barger, A.W. Snow, R.R. Smardzewski, Thin Solid Films 133 (1985) 207–217.
[14] J.P. Borgoin, S. Palacin, Langmuir 14 (1998) 3967–3970.
[15] W.R. Barger, J. Dote, M. Klusty, R. Mowery, R. Price, A.W. Snow, Thin Solid Films 159 (1988) 369–378.
[16] C.G. Cannon, G.B.B.M. Sutherland, Spectrochim. Acta 4 (1951) 373–395.
[17] J.P. Linski, T.R. Paul, R.S. Nohr, M.E. Kenney, Inorg. Chem. 19 (1980) 3131–3135.
[18] A. Graja, K. Lewandowska, B. Laskowska, A. Łapiński, D. Wróbel, Chem. Phys. 352 (2008) 339–344.
[19] K. Lewandowska, A. Graja, B. Barszcz, A. Biadasz, D. Wróbel, New J. Chem. 35 (2011) 1291–1295.
[20] R. Arnold, A. Terfort, Ch. Wöll, Langmuir 17 (2001) 4980–4989.
[21] M.K. Debe, J. Appl. Phys. 55 (1984) 3354–3366.
[22] M. Szybowicz, W. Bała, K. Fabisiak, K. Paprocki, M. Drozdowski, Cryst. Res. Technol. 45 (2010) 1265–1271.
[23] M. Gouterman, G.H. Wagniere, L.C. Snyder, J. Mol. Spectrosc. 11 (1963) 108–127.
[24] J.A. Shelnutt, J. Phys. Chem. 88 (1984) 4988–4992.
[25] J. Mack, M.J. Stillman, J. Am. Chem. Soc. 116 (1994) 1292–1304.
[26] J. Leclaire, R. Dagiral, A. Pla-Quintana, A-M. Caminade, J.-P. Majoral, Eur. J. Inorg. Chem. (2007) 2890–2896.
[27] N. Kabayashi, Coord. Chem. Rev. 227 (2002) 129–152.
[28] B. Brożek-Płuska, I. Szymczyk, H. Abramczyk, J. Mol. Struct. 744–747 (2005) 481–485.
[29] K. Yamasaki, O. Okada, K. Inami, K. Oka, M. Kotani, H. Hamada, J Phys. Chem. B 101 (1997) 13–19.
[30] K. Uehara, M. Mimuro, Y. Fujita, M. Tanaka, Photochem. Photobiol. 48 (1988) 725–732.
[31] H. Imahori, K. Lehara, M. Mituro, M. Tanaka, Photochem. Photobiol. 53 (2008) 371–377.
[32] B. Barszcz, A. Bogucki, A. Biadasz, B. Bursa, D. Wróbel, A. Graja, J. Photochem. Photobiol. A: Chem. 218 (2011) 48–55.
[33] B. Bursa, D. Wrobel, K. Lewandowska, A. Graja, M. Grzybowski, D.T. Gryko, Synth. Met. 176 (2013) 18–25.
[34] B. Bursa, A. Biadasz, K. Kędzierski, D. Wróbel, J. Lumin. 145 (2014) 779–786.
[35] M. Kasha, H.R. Rowls, M.A. El-Bayoumi, Pure Appl. Chem. 11 (1965) 371–392.
[36] E. Orti, J.L. Bredas, C.J. Clarisse, J. Chem. Phys. 92 (1990) 1228–1235.
[37] N.C. Maiti, S. Mazumdar, N. Rediasamy, J. Phys. Chem. 102 (1999) 1528–1538.
[38] E.S. Dodworth, A.B.P. Lever, P. Seymur, C.C. Leznoff, J. Phys. Chem. 98 (1985) 5658–5705.
[39] Z. Gasyna, N. Kibayasi, M.J. Stilmann, J. Chem. Soc. Dalton Trans. 14 (1989) 2397–2405.
[40] H. Abramczyk, I. Szymczyk, J. Mol. Liquids 110 (2004) 51–56.
[41] A. Rebecca, P. Zangmeister, P.E. Smolenyak, A.S. Drager, D.F. O'Brien, N.R. Armstrong, Langmuir 7 (2001) 7071–7078.
[42] K. Mutsumi, W. Kazumi, O. Kazuchika, K. Hanabusa, H. Shirai, N. Kobayashi, Macromolecules 34 (2001) 4706–4711.
[43] C. Ingrosso, M.L. Curri, P. Fini, G. Giancane, A. Agostiano, L. Valli, Langmuir 25 (2009) 10305–10313.
[44] W.C. Martin, W.L. Wiese in: G.W.F. Drake (Ed.), AIP, Woodbury, New York, 1996, pp. 135–153.
[45] L. Pauling, The nature of the chemical bond. IV. The energy of single bonds and the relative electronegativity of atoms, J. Am. Chem. Soc. 54 (1932) 3570–3582.
[46] D.R. Lide (Ed.), Ionization potentials of atoms and atomic ions, Handbook of Chemistry and Physics, CRC Press, Boca Raton, 1992.
[47] W.W. Williams, D.L. Carpenter, A.M. Covington, M.C. Koepnick, D. Calabrese, J.S. Thompson, J Phys. B: Atom Mol. Opt. Phys. 31 (1998) 341–345.
[48] A. Hauschild, K. Karki, B.C. Cowie, M. Rohlfing, F.S. Tautz, M. Sokolowski, Phys. Rev. Lett. 94 (2005) 036106.
[49] M. Szybowicz, W. Bała, K. Fabisiak, K. Paprocki, M. Drozdowski, J. Mater. Sci. 46 (2011) 6589–6595.

**Praca nr 2**

**[Bursa, JL 2014]** B. Bursa, A. Biadasz, K. Kędzierski, D. Wróbel, *Quantum dot with zinc and copper substituted phthalocyanines. 1. Energy transfer in solution and in-situ light absorption in Langmuir monolayers*, Journal of Luminescence, **145** (2014) 779-786

Journal of Luminescence 145 (2014) 779–786

Contents lists available at ScienceDirect

Journal of Luminescence

journal homepage: www.elsevier.com/locate/jlumin

# Quantum dot with zinc and copper substituted phthalocyanines. 1. Energy transfer in solution and *in-situ* light absorption in Langmuir monolayers

B. Bursa, A. Biadasz, K. Kędzierski, D. Wróbel *

*Faculty of Technical Physics, Institute of Physics, Poznan University of Technology, 60-965 Poznań, Poland*

ARTICLE INFO

*Article history:*
Received 11 June 2013
Received in revised form
22 August 2013
Accepted 23 August 2013
Available online 4 September 2013

*Keywords:*
Phthalocyanines
Quantum dot
Langmuir monolayer
*In-situ* absorption
Fluorescence
Energy transfer

ABSTRACT

The paper deals with spectroscopic characterization of a core/shell CdSe/ZnS quantum dot and phthalocyanines substituted with butyl and octakis(octyloxy) peripheral groups: zinc (II) and copper (II) 2,9,16,23-tetra-tert-butyl-29H,31H-phthalocyanine, zinc (II) and copper (II) 2,3,9,10,16,17,23,24-octakis(octyloxy)-29H,31H-phthalocyanine in chloroform as well as in a form of 2D Langmuir monolayers. The isotherms of surface pressure as a function of the mean area per molecule are examined and the *in-situ* absorption study of the Langmuir monolayer is also studied. The influence of the substituents attached to the phthalocyanine macroring and of the presence of the quantum dot on dye spectroscopic properties (absorption and fluorescence) is shown. Molecular arrangement of the molecular skeleton of the phthalocyanines on water substrate is evaluated. A comparison of the *in-situ* absorption of the phthalocyanine monolayers and electronic absorption spectra of the dyes in chloroform supports the existence of dye aggregates in the monolayer. Interaction between the phthalocyanine dyes and CdSe/ZnS quantum dot observed as dot fluorescence quenching is also discussed.



## 1. Introduction

Quantum dot (**QD**) is a very tiny semiconductor crystal (between nanometers to a few microns) of singular properties. It confines electrons, holes or electron-pairs to the zero dimension. Its electronic properties are closely related to the size and shape of the individual crystal which determine the energy gap; thus the color of the light emitted by quantum dots is dictated by their size [1–3]. Quantum dots are extremely promising as new electronic materials in many scientific and life science areas, like *e.g.*: optical and electronic devices, quantum computing, information storage, cascade lasers, IR photodetectors, biology/medicine and many others. Thus, researchers study quantum dots for transistors, solar cells, LEDs, and diode lasers, *etc.* They have also investigated quantum dots as agents for medical imaging and also hope to use them as qubits. Therefore, the study of their spectral, electric and other important properties seems to be essential.

On the other hand, over the past decades phthalocyanines (Pc's) have also been a subject of numerous papers because of their unique spectroscopic, photoelectric and magnetic properties [4]. Pc's are usually characterized by large absorption coefficients and are known as thermally stable molecular materials. They are able to create coordination bonding, aggregates, organic polymers and low-dimensional semiconductors [4,5]. They are still a subject of many studies also because of their very practical applications in many fields, *e.g.* photoconversion of light energy to electric energy, photodynamic therapy, modeling of photosynthesis, photocatalysis and sensors [4–7].

Characterization of nanolayers (mono- and multi-layers) seems to be important since organic materials are usually in close contact with metal or semiconductive electrodes in many molecular electronic and optoelectronic devices. Therefore, it seems to be interesting to follow interfacial phenomena occurring in ultra-thin films with densely packed dye molecules. In thin films their thickness is controllable on the order of nanometers and they can give information on organic material-interface and organic molecule interaction. Moreover, functionality of the films and their molecular arrangement can be also controlled before using them for operation in electronic devices. Since a number of phthalocyanine dyes are rather insoluble in organic solvents, substitution of the dyes with peripheral groups provides enhancing their solubility. Tetra-tert-butyl and octakis(octyloxy) derivatives of zinc and copper phthalocyanines fulfill the solubility requirement and thus their solutions in chloroform are used in our experiments. Moreover, some phthalocyanines have tendency to create aggregated structures when the molecules are densely packed in highly concentrated solutions or thin films [5,8], what we have also taken under consideration in our paper.

Thin films can be characterized by the use of different techniques (UV–vis, FTIR, reflectance–absorption IR, resonance Raman spectroscopies, transmission-electron and atomic force microscopy's [9–14]).

*Abbreviations:* Pc, phthalocyanine; ZnPc, zinc phthalocyanine; CuPc, copper phthalocyanine; QD, quantum dot

* Corresponding author. Tel.: +48 616653179; fax: +48 616653178.
*E-mail address:* danuta.wrobel@put.poznan.pl (D. Wróbel).

0022-2313/$ - see front matter © 2013 Elsevier B.V. All rights reserved.
http://dx.doi.org/10.1016/j.jlumin.2013.08.053

In ultra-thin film a testing depth is often much larger than the thickness of layers. Moreover, charge photogeneration takes place practically only in a thin molecular monolayer nearby heterojunction. Thus, in this paper we have decided to take an advantage from a Langmuir technique supported by an *in-situ* light absorption method. With this experimental approach we can get information on interaction of molecules with their close vicinity (subphase and neighbor molecules) by study of the phthalocyanine monolayers, because many spectroscopic methods are rather unsuitable for characterization of such thin layers. It is worth to mention that investigations of systems composed of organic dyes like phthalocyanines and of non-organic **QD** in a form of thin layers is a great interest for their future applications in new generation of solar energy conversion devices, as perfect photosensitizers in photodynamic cancer therapy, in non-linear optics [5] and others (see for example [5,15–17]).

In our present investigations we have characterized Langmuir monolayers of the dyes in the absence and presence of **QD**. In our previous paper [8] we presented the results of *in-situ* light absorption of Langmuir monolayers of copper Pc's substituted with tetra-tert-butyl and octakis(octyloxy) groups but in the absence of **QD**. In this paper we present the influence of: (i) the peripheral group attached to the main π-electron-system (tetra-tert-butyl or octakis(octyloxy)), and (ii) CdSe/ZnS **QD** on some spectroscopic behavior of the dyes in chloroform and monolayers. Thus, firstly we would like to perform our UV–vis *in-situ* absorption studies of: ZnPc's substituted with butyl or octakis(octyloxy) peripheral groups, and ZnPc-**QD** systems in an organic solvent and in Langmuir monolayers. Secondly, we have extended our investigations with experimental data of copper phthalocyanines described in [8] when they are in the neighborhood and interact with **QD** (CuPc-**QD** systems). As far as we know the *in-situ* light absorption spectroscopy of ZnPc dyes and CdSe/ZnS **QD** have been done for the first time. Also the molecular arrangement of the dyes in the Langmuir monolayers is evaluated. Fluorescence studies of dyes without and with **QD** in solution were also performed. Electronic absorption and fluorescence in the wide range of dye concentrations are presented. As standard samples we have used our components in chloroform (or toluene).

## 2. Materials and methods

The studies have been performed for two symmetric dyes of ZnPc and CuPc (Scheme 1) as well as core/shell CdSe/ZnS **QD**. All the dye samples were obtained from Aldrich Chemical Company and used as received. The CdSe/ZnS **QD** in toluene was purchased from Sigma-Aldrich and used without further purification; its size is 4 nm (Sigma-Aldrich data). We have used following notes for the samples: zinc (II) 2,9,16,23-tetra-tert-butyl-29H,31H-phthalocyanine – **1,** zinc (II) 2,3,9,10,16,17,23,24-octakis(octyloxy)-29H,31H phthalocyanine – **2**, copper (II) 2,9,16,23-tetra-tert-butyl-29H,31H-phthalocyanine – **3,** copper (II) 2,3,9,10,16,17,23,24-octakis(octyloxy)-29H,31H phthalocyanine – **4**, and the core/shell CdSe/ZnS quantum dot – **QD.** The samples after evaporation from toluene are dissolved in chloroform because of their perfect solubility in this solvent (concentrations of the dyes in solution range from $10^{-4}$ to $5\times10^{-7}$ M), which is required for making a good Langmuir layer; thus chloroform solution is used to form Langmuir monolayers.

Langmuir monolayers of the samples are created with a KSV 2000 minitrough (KSV Instruments Ltd.) equipped with a temperature control system. The Langmuir trough area was $364\times75$ mm$^2$. Temperature of subphase is achieved and kept constant (20 °C) with a cooling circulator. Deionized water (electrical resistivity 18.2 MΩ cm) as the subphase was obtained with a Mili-Q water purification system (Millipore Corp.). The sample dissolved in chloroform ($10^{-4}$ M) was spread carefully onto the subphase and

| Molecular structure | Chemical name | Short name |
|---|---|---|
| 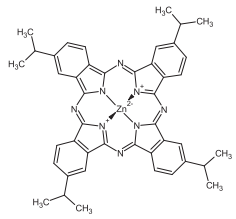 | Zinc (II) 2,9,16,23 – tetra-tert-butyl-29H, 31H – phthalocyanine | **1** |
| 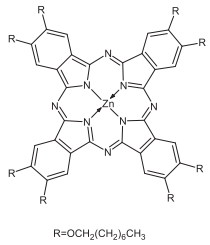 | Zinc 2,3,9,10,16,17,23,24 octakis (octyloxy) – 29H, 31H - phthalocyanine | **2** |
| 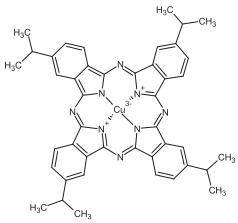 | Copper (II) 2,9,16,23 – tetra-tert-butyl-29H, 31H – phthalocyanine | **3** |
| 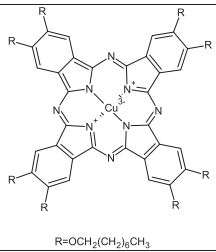 | Copper (II) 2, 3, 9, 10, 17, 23, 24 – octakis (octyloksy) – 29H31H phthalocyanine | **4** |

**Scheme 1.** Molecular structure of the dyes under study.

chloroform evaporation takes 15 min. The floating film of the Langmuir layer was compressed symmetrically from both sides with motion barrier speed of 5 mm/min.

The *in-situ* electronic absorption spectra of the Langmuir layers were recorded in the range 300–800 nm with an Ocean Optics spectrometer QE65000, which was localized in proximity to a quartz window of the KSV instrument. Electronic absorption spectra of the dyes in chloroform were performed with the use of a spectrophotometer Cary 4000 (Varian) in the range 300–800 nm.

Steady-state fluorescence spectra were collected with a fluorescence spectrophotometer Hitachi 4500 (500–800 nm) and the samples were excited at the wide wavelength range (320–650 nm). The relative fluorescence quantum yield ($\Phi_F$) of the samples was evaluated on the basis of the absorption and fluorescence spectra according to the methods described elsewhere [18–20]

$$\Phi_F = \Phi_R \frac{I}{I_R}\frac{A_R}{A}\frac{n^2}{n_R{}^2}, \quad (1)$$

where $\Phi_R$ is the fluorescence quantum yield of a reference sample (chlorophyll *a* in [20]), $I$ and $I_R$ are the integrated fluorescence of the sample and reference, respectively, $A$ and $A_R$ are the absorbance of the sample and reference, respectively and $n$ and $n_R$ are the refractive indices of the sample and reference, respectively. Corrections for re-absorption of fluorescence light and secondary fluorescence effects were taken into account and the maximal error does not exceed 5%. The value of the energy transfer yield was estimated using the values of proper fluorescence of donor without acceptor ($F_D$) and fluorescence of donor with acceptor ($F_{DA}$) [21]

$$\Phi_{ET} = \left(1 - \frac{F_{DA}}{F_D}\right). \quad (2)$$

## 3. Results and discussion

### 3.1. Electronic spectroscopy of samples in solution and in-situ absorption of Langmuir layers

In the first stage of our investigations we have done spectroscopic measurements of absorption and fluorescence spectra of **QD** in chloroform (Fig. 1). The absorption spectrum of **QD** in chloroform shows several exciton transitions, with the lowest energy peak at 575 nm (broad bands in the range between 300 and 615 nm). The differences between maxima location of the **QD** bands depend on solvent used; *e.g.* in toluene the maximum is placed at 550 nm [22]. The shapes of the fluorescence spectra of **QD** when excited with light of the wide wavelength region (from 320 nm to 530 nm) are found to be only slightly dependent on the excitation. Electronic absorption spectra of the dyes **1**–**4** without **QD** and of the dyes with **QD** in chloroform are shown in Fig. 2 A and B, respectively. Selected absorption and fluorescence parameters of the samples in chloroform (and in the Langmuir monolayers) are gathered in Table 1. Some experimental studies of **3** and **4** without **QD** were presented in our previous paper [8]. In Ref. [8] the electronic absorption spectra in chloroform (dye concentrations: $10^{-6}$, $10^{-5}$ and $10^{-4}$ M) and the *in-situ* light absorption of the copper phthalocyanine monolayers (**3** and **4**) show the existence of aggregates in highly concentrated solution as well as in the Langmuir layers; it was shown that aggregation architecture depended on the dye molecular structure of **3** and **4** – the H and oblique dimers, respectively [7,8,23–25]. In the presence of **QD**, one does not observe particular influence of **QD** on the dyes absorption behavior (Fig. 2). It indicates rather weak interaction of **QD** with the dye molecules in their ground state. We have also done absorption experiments for the dyes in chloroform at various concentrations ($c = 10^{-6}$, $10^{-5}$ and $10^{-4}$ M) – the results of these absorption studies of **1** and **2** are shown in Fig. 3 A and B (spectra normalized to unity at 680 nm); (for **3** and **4** this experiment was already done in Ref. [8]). The concentration examinations by the electronic absorption of our samples in solution let us to have a deep insight into ability of the samples to create of the aggregated structures – the $10^{-6}$ M sample is used to minimize the presence of aggregates and serves as a standard sample (the second derivative absorption spectra of the dye samples confirm this supposition – not shown). There is no particular difference in the dye band shapes monitored in the range of 680 nm at various concentrations. The absorption parameters of the concentrated samples are practically not changed with respect to those of monomers and indicate strong domination of the monomeric dyes in the samples in chloroform [5,23,25].

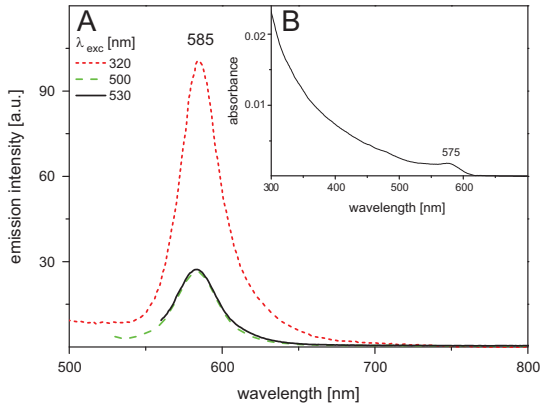


**Fig. 1.** Fluorescence spectra; (A) – exc 320 nm, and absorption (B) of **QD** in chloroform.

The Langmuir layer investigations let as to find confirmation of dye ability to form aggregated structures and the results of the *in-situ* light absorption and those in chloroform can help us to discuss the type of aggregates created in the Langmuir monolayers. Spectral behavior of the dyes **1**–**4** when compressed to a form of Langmuir layers is shown in Fig. 4 A, C, E and G. The *in-situ* absorption spectra of the dyes were monitored under various surface pressures from 10 to 25 mN/m in the same way as it was done before [8]. The spectral changes are observed in all the dye samples when compare the *in-situ* results with those in chloroform. The results evidently confirm strong interaction between the dye molecules in the Langmuir layers. In each *in situ* absorption spectrum one or more bands in the Soret region (300–500 nm) and two clearly seen wide bands (or the band with a hump) between 550 and 800 nm are observed. Nevertheless, the features of the *in-situ* absorption depend markedly on the dyes used in the experiments. In the spectra presented in Fig. 4 A, C, E, and G (dyes without **QD**) it is evidently seen that the long-wavelength Q region bands (600–800 nm) are splitting into separate bands in distinct manner depending on dye. Moreover, a band shift towards the "red" part of the spectra is also observed from 612–680 nm in chloroform to about 615–700 nm in the Langmuir layers. The variety of the *in-situ* absorption spectra of the investigated dyes could lie in the different central ions (Zn and Cu) and the peripheral groups (tetra-tert-butyl and octakis(octyloxy)). Since the only molecular dissimilarity among the samples **1, 3** and **2, 4** is the presence of different ions in the main molecular frame, thus we can say that the results confirm an influence of ion on the interaction between individual ZnPc molecules and CuPc species in the Langmuir layers. The second important observation is that the shapes of the *in-situ* spectra depend substantially on the peripheral groups attached to the main molecular phthalocyanine core – two bands (or one band with a hump) in the "red" part of the spectra and well recognized bands in the Soret region (300–450 nm) are seen. The results of the tetra-tert-butyl samples (**1** and **3**) and octakis(octyloxy) samples (**2** and **4**) are very nice examples; they show the great influence of these groups on the phthalocyanine *in-situ* absorption properties seen as the new bands, splitting bands and/or extending full width at half maximum (FWHM) (Table 1). According to the Kasha vector model [26] the blue shift is expected for H aggregates (in the ideal H-dimer the molecular frame is oriented face-to-face with parallel dipole moments of interacting monomer units), whereas the long-wavelength shifts result from the J-dimer with in-line transition dipoles oriented face-to-tail. In the oblique configuration a composition of the in-face and out-of-face transition dipole arrangement leads to decreasing and increasing energy of the excited states of double molecules [26–30]. The spectacular changes in the *in-situ* results are seen for all the samples; two separate bands (**1** and **4**) or wide bands (**2** and **3**) are very well seen. The bands in the spectra of **1**, **2** (this paper) and of **4** [8] originate from formation of

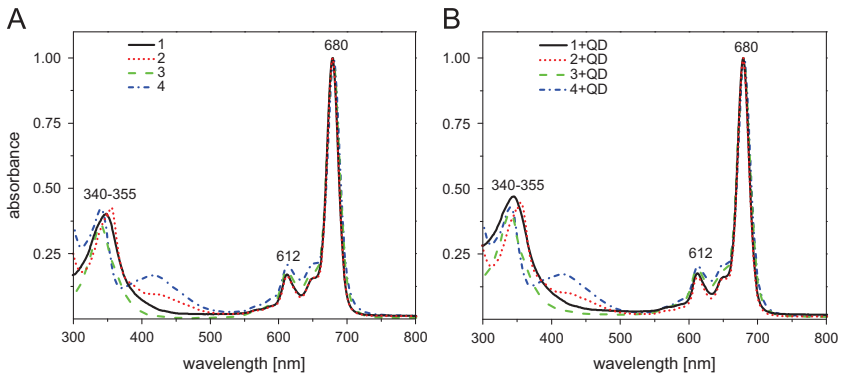


**Fig. 2.** Absorption spectra of dyes **1–4** in chloroform (dye concentration $10^{-6}$ M) in the absence (A) and presence of **QD** (B); normalized to 1 at 680 nm; **3** and **4** without **QD** (A) on the basis of [8].

**Table 1**
Selected absorption and fluorescence parameters of the dyes and dyes with **QD** in chloroform and in Langmuir monolayers.

| Sample | Absorption maxima[a] [nm] | FWHM [a] [$cm^{-1}$] | | | Absorption maxima [b] [nm] | | | FWHM [b][cm] | | | Q band intensity ratio [b] | $\Phi_F$ [a] |
|---|---|---|---|---|---|---|---|---|---|---|---|---|
| **QD** | 575 (585-fluo) | – | | | – | | | – | | | – | – |
| **1** | 612, 648, 680 | 301 | 414 | 227 | – | 633 | 693 | – | 923 | 483 | 1.06; (689/633) | 0.16 |
| **1**+**QD** | 612, 648, 680 | 227 | 385 | 227 | 625 | 656 | 693 | 470 | 236 | 352 | 3.52; (685/627) | 0.18 |
| **2** | 612, 648, 680 | 282 | 409 | 217 | – | 636 | 706 | – | 701 | 629 | 0.42; (693/636) | 0.15 |
| **2**+**QD** | 612, 648, 680 | 290 | 358 | 217 | – | 636 | 706 | – | 971 | 564 | 0.51; (693/635) | 0.16 |
| **3** | 612, 648, 680 | 362 | 373 | 247 | 615 | 674 | – | 843 | 1235 | – | 0.60; (675/623) | – |
| **3**+**QD** | 612, 648, 680 | 324 | 439 | 231 | 615 | 674 | – | 932 | 1259 | – | 0.60; (675/623) | – |
| **4** | 612, 648, 680 | 337 | 529 | 217 | 586 | 635 | 702 | 929 | 769 | 922 | 1.13; (696/654) | – |
| **4**+**QD** | 612, 648, 680 | 395 | 324 | 238 | 586 | 635 | 710 | 667 | 779 | 963 | 0.99; (696/654) | – |

FWHM – full width at half maximum (calculated with the Gaussian component program), $\Phi_F$ – fluorescence quantum yield
The date of the absorption maxima evaluated on the basis of Gaussian decomposition.

[a] in chloroform.
[b] in Langmuir monolayer.

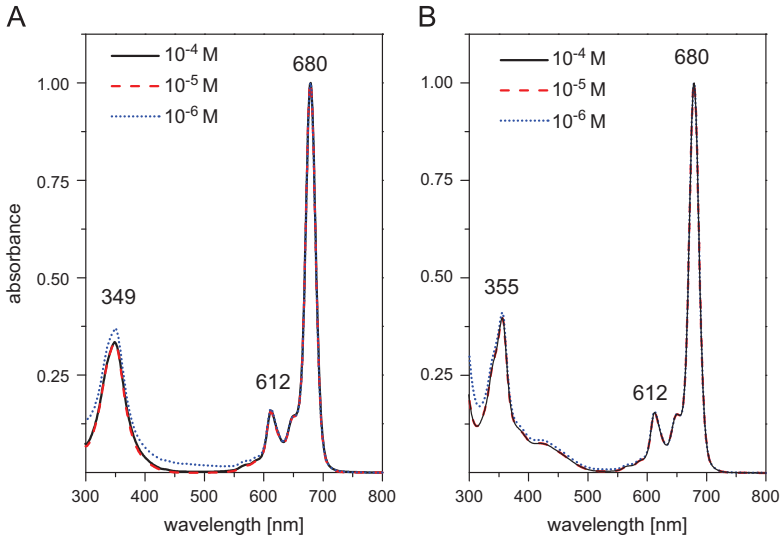


**Fig. 3.** Absorption spectra of **1** (A) and **2** (B) in chloroform in the absence of **QD** at different dye concentration ($10^{-6}$, $10^{-5}$, $10^{-4}$ M); spectra normalized to 1 at 680 nm.

the oblique coplanar aggregates (Fig. 4 A, C and G) while the large "blue" shift observed in **3** (Fig. 4 E) could mostly result from domination of the H aggregates since the new band (the "blue" shift) is observed; a hump in the region 670–690 nm can be assigned to the monomers coexisting with the H aggregates in the monolayers. Of course, we realize that the geometrical distance between the dye molecules in the Langmuir layer is much shorter than that between molecules in $10^{-4}$ M solution. Thus, the package of molecules in the Langmuir layers is denser than that in $10^{-4}$ M solution. Just for this reason, it is obvious that amount of aggregated dyes in layers exceeds quantity of those in chloroform. It is clearly seen when one compares the results of the *in-situ* light absorption with those in chloroform. Nevertheless, our absorption results confirm the presence of aggregates. Of course

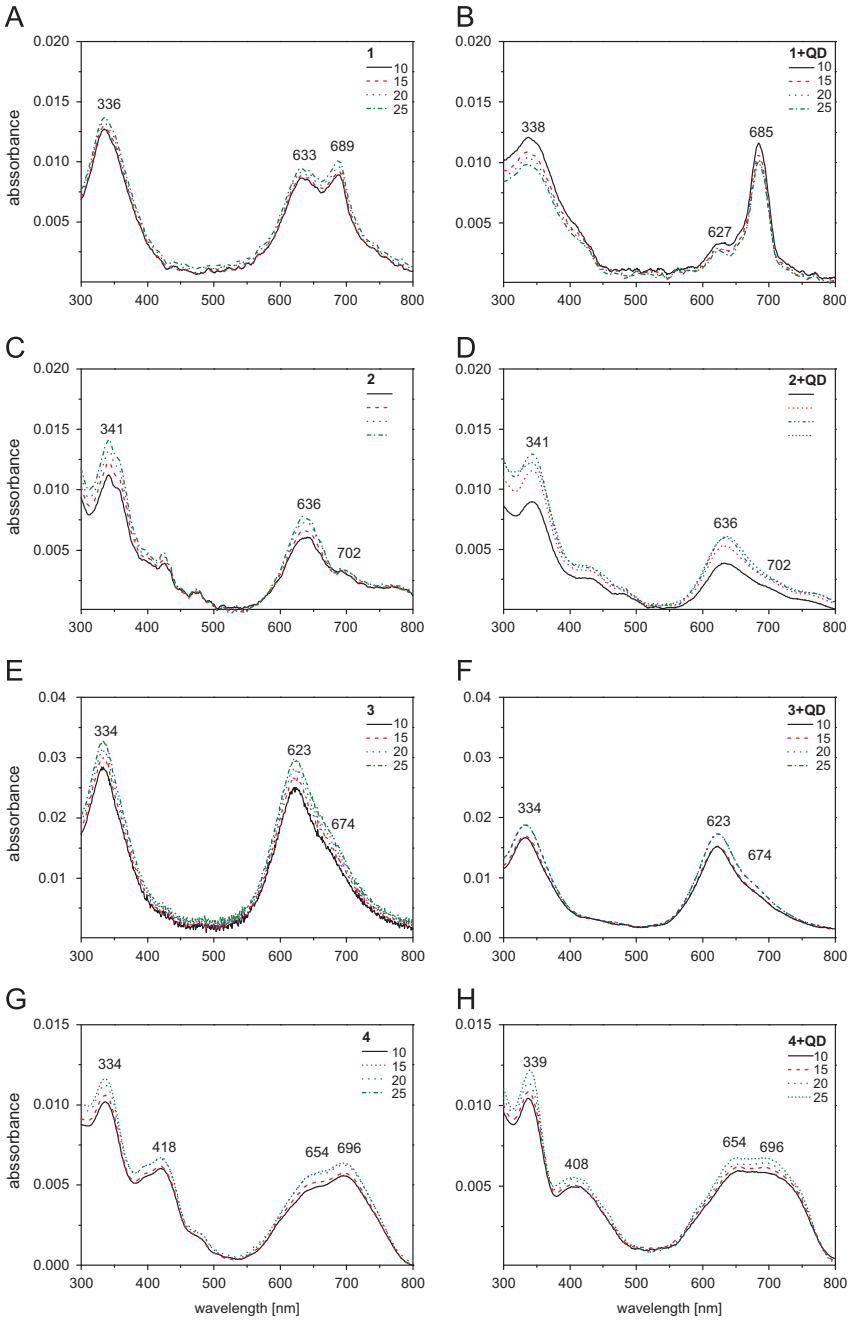


**Fig. 4.** *In-situ* light absorption of Langmuir layers of **1**–**4** without **QD** (A, C, E, and G) and with **QD** (B, D, F, and H); 10, 15, 20 and 25 mN/m – surface pressures.

we realize the coexistence of aggregates and monomers in all our dye samples.

The presence of aggregates in the Langmuir layer is obvious and found confirmation in the literature by spectroscopic [27] and atomic force microscopy data [31–33]. Nevertheless, in this paper we wish to indicate the influence of different peripheral groups in **1**–**4** on the aggregates architecture in the Langmuir monolayers.

Very interesting conclusions we can draw from the *in-situ* absorption results of the dyes without **QD** *versus* those in chloroform (Fig. 4 A, C, E, and G *versus* Figs. 2 and 3) and of the dyes in the vicinity of **QD** (Fig. 4 A, C, E, and G *versus* Fig. 4B, D, F, and H). First of all, new locations of the Q dye bands in the monolayer with respect to those in chloroform are observed (see Table 1) and can be explained by creation of aggregates and changing electronic energy of the dye molecules. Secondly, from comparison of the *in-situ* spectra of the dyes with **QD** and the *in-situ* absorption spectra of their counterpart (*in-situ* of the individual dyes) one can evidently see their disparity. All figures presenting the results of the samples **1**–**4** with **QD** differ more or less from those of the *in-situ* absorption of the individual dyes, both in the Soret region and in the Q part of the spectra. The first observation is the appearance of bands with different maximum locations. The intensive double

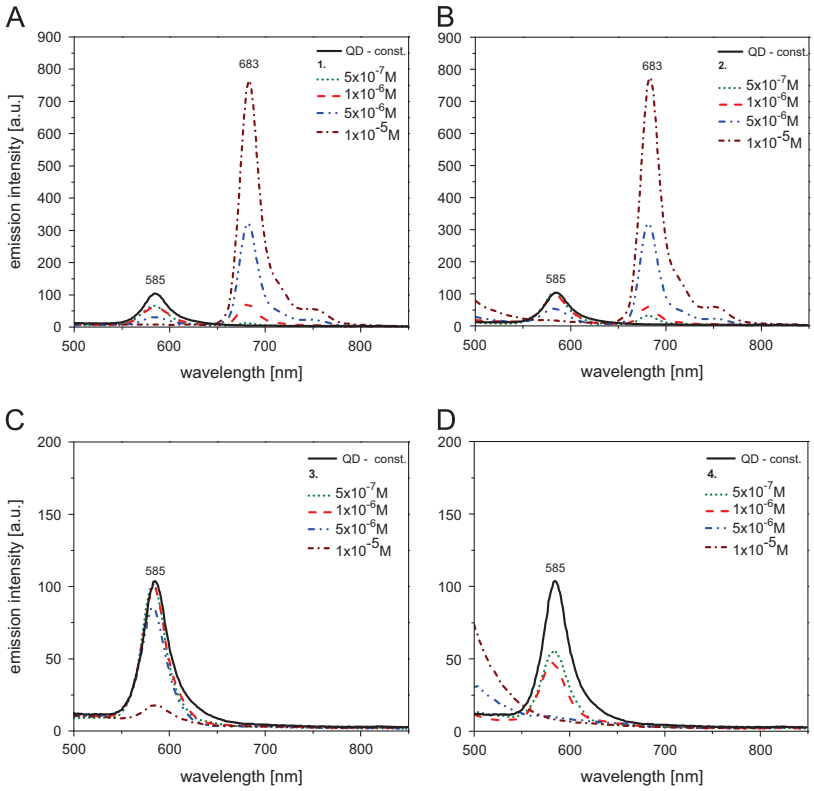


**Fig. 5.** Fluorescence spectra of dyes **1**–**4** with **QD** in chloroform at different **QD**:dye ratios; $\lambda_{exc}$=320 nm.

bands in the "red" region in the spectra of the dye samples without **QD** support domination of dimers over monomers [26,30]. The second evidence is a change in the Soret to Q band intensity ratios; the intensity ratio changes in the dyes samples without **QD** *versus* those with **QD**. On the basis of Fig. 4 and Table 1 it is obvious that the most spectacular changes in the *in-situ* absorption are seen for the sample **1** and inconsiderable changes are observed in **3**. Then, let us discuss first the samples **1** and **3**. The shapes of the Q part of spectra of **1** are drastically changed upon the presence of **QD** – the double splitting vanishes and the bands with the maximum at 685 and at 627 nm are observed instead of two bands with maxima at 689 nm and 633 nm (Fig. 4). The new location of the bands 685 and 627 nm in the monolayer of **1** with **QD** spectra can be explained by increasing energy states of the dye due to the presence of **QD** in its vicinity. The dissimilarity clearly displays strong influence of **QD** on the dye **1** when it is in the Langmuir monolayer. Moreover, the shapes of the *in-situ* absorption of **1** in the vicinity of **QD** indicate destruction of the oblique dimer. In **3** no changes are observed. In the samples **2** and **4** in the vicinity of **QD** the locations of the bands are not significantly changed as it is observed in **1** indicating rather weak influence of **QD** on aggregation of these dyes in the Langmuir layers. Nevertheless, these results still settle the presence of the oblique dimer in **2** and **4** and also domination of the H-dimer in **3**. The observed differences in aggregation properties of the sample **1**, **2** and **4** *versus* **3** could lie in the physic-chemical properties of zinc and copper ions incorporated in the molecular macroring and the presence of various peripheral groups. As mention above the only dissimilarity between the dyes **1** and **3** is the presence of different ions in the molecular core which could cause so marked disparity in aggregates formation in the Langmuir layers. Even that basic properties of zinc and copper ions (electronic configurations, electronegativities, ionization energies, atomic radius, Pauling's ionic radius, covalent radius, metallic radius, Van der Waals radius *etc.*) are very similar, the different ability to form aggregation structures could rather be their marked distinctions in electron affinity (Zn – 0 kJ/mol *versus* Cu – 1185 kJ/mol). Moreover, the presence of different metal ions (Zn, Cu) also can affect dye aggregation ability due to distortion of the π-electron microrings. On the other hand, the peripheral tetra-tert butyl groups and octakis(octyloxy) chains can also strongly affect dye behavior in the studied layers. This supposition is supported when compared the results of the pairs of the samples: **1**–**2** and **3**–**4**. The presence of **QD** modifies the aggregation behavior of the dye layers. It is very well seen in Fig. 4. The marked changes in the *in-situ* light absorption spectra are particularly observed in the Langmuir layers of the sample **1**, and also not so markedly in **2** and **4**; it means in the samples with the oblique coplanar aggregates. Otherwise, in the sample with the H-aggregates (**3**) the alternation of the *in-situ* spectra upon **QD** is rather not so spectacular. These results evidently indicate very weak impact of **QD** on the closely packed copper dye H-aggregates (CuPc substituted with octakis (octyloxy) chains) and harmful influence of **QD** when the dyes create the oblique aggregates due to strong interaction of **QD** with the π-electron dye systems – the best example is the sample **1**.

### 3.2. *Fluorescence of samples in solution*

Fluorescence behavior of the dyes samples depends very strongly on metal ion incorporated into the main molecular π-electron core – fluorescence of ZnPc's is very strong whereas CuPc's show only vestige emission independently of the excitation wavelength (although a fluorescent dimer of copper tetrasulfonated phthalocyanine in ethanol was observed [34]). As seen,

distortion of the nominally planar phthalocyanines (zinc *versus* copper in the macrorings) results in excited state energy [35]. On the other hand, in comparison to many organic chromophores quantum dots possess superior fluorescence properties – strong fluorescence emission, relatively long fluorescence life-time and relatively low photobleaching. For fluorescence study the investigated samples are prepared without and with **QD** at different ratios of **QD** to dyes; the **QD** amount is constant in all investigated **QD**-dye samples and the dye concentration range from $5\times10^{-7}$ to $10^{-5}$ M. The results of our fluorescence examinations done at 320 nm excitation for the samples **1**–**4** in the presence of **QD** at different **QD**:dye ratios are shown in Fig. 5. The zinc sample (**1** and **2**) fluorescence spectra (not shown) are in accordance with the literature data [5,36] – their shapes and locations of fluorescence maxima are independent of excitations what confirms the presence of emitting species. We are not able to follow fluorescence of **3** because of its extremely weak emission; fluorescence of **4** is also weak but detectable. When the samples are excited in the region of the dye absorption (612, 650 nm) only their fluorescence is seen as expected (not shown). The most spectacular evidences of the presence of the emitting **QD** are observed when the samples are excited in the absorption of **QD**. When excitation 320 nm is used the maxima characteristic for **QD** fluorescence (585 nm) and the dye emission (650–780 nm) are observed. On the other hand, **QD** emission in the presence of the dyes is not as intensive as seen for **QD** in the absence of the dyes. The **QD** fluorescence intensity decreases with increasing amount of the dyes. However, the **QD** fluorescence intensities do not decrease proportionally with increasing dye concentration, what can be well seen in Fig. 5A and B. It can be explained as follows: when the samples are excited at 612 and 650 nm the fluorescence comes directly from the excited dyes only. Otherwise, when the samples are excited at 320 nm one can observe emission at 585 nm originating from **QD** and from the dyes **1** and **2** (600–800 nm); the latest one due to the direct excitation of the dyes and also because of energy transfer from **QD**. Thus, it is evident that in the samples with the low **QD:** dye ratios almost all energy absorbed by **QD** is transferred to the dye thanks to the Förster resonant mechanism occurring between donor and acceptor (spectral requirement of **QD** fluorescence and dye absorption overlapping is fulfilled) (Figs. 1 and 2). The overlapped of emission spectra of **QD** and absorption of the dyes strongly confirm that energy transfer process from **QD** to the dyes can occur with the dye as an acceptor and **QD** as a donor. Two effects can occur in the samples: energy transfer and fluorescence of the dyes. On the other hand, when **QD** prevails over the dye concentration the **QD** fluorescence is quenched and fluorescence originating from the dye is weakly observed. Our fluorescence data (Fig. 5) strongly confirm the resonance energy transfer in the sample of **QD** in the presence of the dye. On the basis of Eq. (2) we have estimated the yield of energy transfer between **QD** and **1, QD** and **2**. The value of $\Phi_{ET}$ can reach up of about 90%. According to [22,37–39] **QD** transfers energy to phthalocyanine with efficiency of 0.12–0.25 (estimated on the basis of fluorescence quenching and/or life-times). The difference between our results and those presented in [22,37–39] can lie in different solvent (chloroform *versus* toluene, dimethylsulfoxide and others), type of quantum dot, different molecular structures of chromophores and the different ratio of **QD** to a dye. As mentioned above the dyes **3** and **4** do not emit fluorescence (or very slightly). Thus, the character of the fluorescence spectra shown in Fig. 5C and D is different from those of **1** and **2**. As seen only the **QD** fluorescence in the region 550–650 nm and the diminishing **QD** emission by fluorescence quenching (also of about 80–90%) through interaction with the dyes **3** or **4** are observed. These results also confirm the Förster resonant energy transfer from **QD** (donor) to CuPc dye (acceptor). It is also worth to mention that we have also done EPR examinations of our samples (data not published) and we found that fluorescence quenching by electron transfer between two moieties **QD** and a dye cannot be excluded (this is a topic of our forthcoming paper).

## 4. Conclusions

On the basis of our absorption and fluorescence examinations of the dyes in the Langmuir monolayers and in chloroform we can draw following conclusions:

1. We have shown the interaction between non-organic **QD** (core/shell CdSe/ZnS) and organic chromophores (ZnPc and CuPc). It was stated that the influence of **QD** on the investigated dyes are rather weak when the dyes are in the electronic ground state in solution; particular no changes are monitored in the absorption spectra of the dyes when compared with those of the same dyes in the presence of **QD**.
2. Aggregated ZnPc and CuPc forms are detected in the Langmuir monolayers. The sort of the aggregates depends strongly on the kind of ion in the molecular macroring and on substituents attached to the main dye molecule core. The marked changes of the *in-situ* absorption spectra upon **QD** are observed when the oblique coplanar aggregates in **1, 2** and **4** in the Langmuir layers are found. In the sample **3** with domination of the H-aggregates the alternation of the *in-situ* spectra upon **QD** is not so spectacular. These results evidently indicate weak impact of **QD** on the closely packed dye H-aggregates (**3**), and harmful influence of **QD** when the dyes create the oblique aggregates (**1**, **2**, **4**) due to strong interaction of **QD** with the π-electron dye systems (the strongest **QD** affection is found for the sample **1**).
3. The much stronger influence of the presence of **QD** on the dye behavior is found if the dyes are excided. It is caused by the stronger interaction between **QD** and the dyes.
4. The fluorescence quenching of **QD** is observed when it is in vicinity of the dyes. The energy absorbed by **QD** is transferred to chromophores with very high efficiency (up to 90%).

## References


[1] A.I. Ekimov, A.A. Onushchenko, JETP Lett. 34 (1981) 345.
[2] S. Li, M.L. Steigerwald, L.E. Brus, ASC Nano 3 (2009) 1267.
[3] M.A. Reed, J.N. Randall, R.J. Aggarwal, R.J. Matyi, T.M. Moore, A.E. Wetsel, Phys. Rev. Lett. 60 (1988) 535.
[4] N.B. McKeown, Phthalocyanine Materials, Synthesis, Structure and Function, Cambridge University Press, Cambridge, 1998.
[5] C.C. Lesnoff, A.B.P. Lever, Phthalocyanines. Properties and Application, VCH, New York, 1996.
[6] I. Rosenthal, Photochem. Photobiol. 53 (1991) 859.
[7] Y.L. Lee, Y.C. Chen, C.H. Chang, Y.M. Yang, J.R. Maa, Thin Solid Films 370 (2000) 278.
[8] A. Biadasz, B. Bursa, B. Barszcz, A. Bogucki, B. Laskowska, A. Graja, D. Wróbel, Dyes Pigm. 89 (2011) 86.
[9] W.R. Barger, A.W. Snow, H. Wohltjen, N.L. Jarvis, Thin Solid Films 133 (1985) 197.
[10] J. Souto, J.A. De Saja, M.I. Gobernado-Mitre, M.L. Rodriguez, R. Aroka, Sens. Actuators B 15–16 (1993) 306.
[11] D.P. Dilella, W.R. Barger, A.W. Snow, R.R. Smardzewski, Thin Solid Films 133 (1985) 207.
[12] J.P. Borgoin, S. Palacin, Langmuir 14 (1998) 3967.
[13] W.R. Barger, J. Dote, M. Klusty, R. Mowery, R. Price, A.W. Snow, Thin Solid Films 159 (1988) 369.
[14] C.G. Cannon, G.B.B.M. Sutherland, Spectrochim. Acta 4 (1951) 373.
[15] J.-H. Yum, S. Jang, R. Humphry-Baker, M. Grätzel, J.-J. Cid, T. Torres, M.d. K. Nazeeruddin, Langmuir 24 (2008) 5636.
[16] R.B. Ostler, A.D. Scully, A.G. Taylor, I.R. Gould, T.A. Smith, A. Waite, D. Phillips, Photochem. Photobiol. 71 (2000) 397.
[17] I. Beletskaya, V.S. Tyurin, A.Y. Tsivadze, R. Guilard, C. Stern, Chem. Rev. 109 (2009) 1659.
[18] M.A.M.J. Van Zandvoort, D. Wróbel, P. Lettinga, G. Van Ginkel, Y.K. Levine, Photochem. Photobiol. A: Chem. 62 (1995) 279.

[19] J. Lakowicz, Principles of Fluorescence Spectroscopy, Plenum Press, New York, 1999.
[20] H. Scheer, Chlorophylls, CRC-Press, Boca Raton, 1991.
[21] T. Förster, T. Naturwissenschaften 33 (1946) 166.
[22] M. Nyk, K. Palewska, L. Kępinski, K.A. Wilk, W. Stręk, M. Samoć, J. Lumin. 130 (2010) 2487.
[23] B. Brożek-Płuska, I. Szymczyk, H. Abramczyk, J. Mol. Struct. 744-747 (2005) 481.
[24] G.L. Gaines Jr., Insoluble Monolayers at the Liquid-Gas Interfaces, Wiley, New York, 1966.
[25] Y.C. Yang, J.R. Ward, R.P. Seiders, Inorg. Chem. 24 (1985) 1765.
[26] M. Kasha, H.R. Rowls, M.A. Bayoumi, Pure Appl. Chem. 11 (1965) 371.
[27] E. Orti, J.L. Bredas, C.J. Clarisse, J. Chem. Phys. 92 (1990) 1228.
[28] N.C. Maiti, S. Mazumdar, N. Rediasamy, J. Phys. Chem. 102 (1999) 1528.
[29] E.S. Dodworth, A.B.P. Lever, P. Seymur, C.C. Lesnoff, J. Phys. Chem. 98 (1985) 5658.
[30] Z. Kasyna, N. Kibayasi, M.J. Stilmann, J. Chem. Soc. Dalton Trans. 14 (1989) 2397.
[31] A. Rebecca, P. Zangmeister, P.E. Smolenyak, A.S. Drager, D.F. O'Brien, N. R. Armstrong, Langmuir 7 (2001) 7071.
[32] K. Mutsumi, W. Kazumi, O. Kazuchika, K. Hanabusa, H. Shirai, N. Kobayashi, Macromolecules 34 (2001) 4706.
[33] C. Ingrosso, M.L. Curri, P. Fini, G. Giancane, A. Agostiano, L. Valli, Langmuir 25 (2009) 10305.
[34] N.M. Speirs, W.J. Ebenezer, A.C. Jones, J. Photochem. Photobiol. 75 (2002) 247.
[35] J.M. Retsek, C.J. Medforth, D.J. Nurko, S. Gentenman, V.S. Chirvony, K.M. Smith, D.J. Holten, J. Phys. Chem. B 105 (2001) 6396.
[36] M. Durmuş, T. Nyokong, Spectrochim. Acta Part A 69 (2008) 1170.
[37] K.E. Sekhosana, E. Antunes, S. Khene, S. D'Souza, T. Nyokong, J. Lumin. 136 (2013) 255.
[38] O. Adegoke, E. Antunes, T. Nyokong, J. Photochem. Photobiol. A: Chem. 257 (2013) 11.
[39] K.E. Sekhosana, E. Antunes, T. Nyokong, Polyhedron 54 (2013) 294.

**Praca nr 3**

**[Bursa, PCCP 2015]** B. Bursa, B. Barszcz, W. Bednarski, J.P. Lewtak D. Koszelewski, O. Valulyuk, D.T. Gryko, D. Wróbel, *New meso-substituted corroles possessing pentafluorophenyl groups - Synthesis and spectroscopic characterization*, Phys. Chem. Chem. Phys. **17** (2015) 7411 – 7423

PCCP

PAPER

View Article Online
View Journal | View Issue



Cite this: *Phys. Chem. Chem. Phys.*, 2015, **17**, 7411

# New *meso*-substituted corroles possessing pentafluorophenyl groups – synthesis and spectroscopic characterization†

Bartosz Bursa,[a] Bolesław Barszcz,[b] Waldemar Bednarski,[b] Jan Paweł Lewtak,[c] Dominik Koszelewski,[c] Olena Vakuliuk,[c] Daniel T. Gryko*[c] and Danuta Wróbel*[a]

Received 4th December 2014,
Accepted 30th January 2015

DOI: 10.1039/c4cp05648e

www.rsc.org/pccp

The investigation presented in this paper deals with new free-base corroles substituted with different peripheral groups. These aromatic macrocycles were efficiently synthesized by a [2+1] approach from dipyrromethanes. Moreover, the basic spectroscopic studies of the dyes in chloroform were conducted, and the UV-Vis absorption, fluorescence and ESR parameters were estimated. The experimental data were supported by quantum chemical calculations. The presence of monomeric dye structures is concentration independent ($10^{-6}$–$10^{-4}$ M), as expected for dyes in a solvent of low polarity, and rules out aggregate formation of corroles dissolved in chloroform. The excitation emission and fluorescence life-time values confirm the monomeric structure of the corroles. The spectra were compared with the time-dependent density functional theory (TD-DFT) results for the HOMO–LUMO states. The ESR examinations strongly show that for any type of studied fluorine corrole an unpaired electron is localized on the corrole macroring but not on the substituents both before and after light illumination. Laser illumination creates additional radicals, however with different effectiveness depending on the sample.

## 1. Introduction

Corroles are synthetic aromatic porphyrin-analogue dyes, in which one *meso* carbon bridge is absent[1–8] which leads to the redistribution of electron density when one compares them to porphyrins[9] and in consequence this can result in changes of spectroscopic properties and make them promising candidates as photoactive agents. The similar but not the same molecular structure of corroles with respect to porphyrins, large delocalized π-electron conjugation, reasonable stability and very good matching of their absorption spectrum range to sunlight make them new excellent organic materials for light energy collection and conversion. Thus, in some laboratories corroles have attracted considerable interest because of their potential applications as photoconductors, in electronic devices, as gas sensors, solar cells and in other photo-electroactive items.[10–18]

Selected photophysical properties of some corroles have been previously studied by us with the use of various spectroscopic methods: UV-Vis spectroscopy, infrared absorption, Raman scattering and electron paramagnetic resonance.[19–21] Our experimental methods were supported by quantum chemical calculations. In this paper we wish to describe the synthesis and to present the spectroscopic characterization of six new *meso*-substituted corroles possessing various groups of different electronic and steric character. In particular corroles bearing naphthalene-1-yl substituents (and analogous ones) at position 10 were studied. Thus, the general purpose of the presented paper is to investigate the fundamental electronic properties by UV-vis spectroscopy (absorption, fluorescence, and electron spin resonance (ESR)) supported by quantum-chemical calculations. Gaining in-depth knowledge of the relationship between structure and optical properties is essential for potential applications of corroles in optoelectronics and related fields.

## 2. Materials and methods

### 2.1. Synthesis

2,7-Dimethoxynaphthalene, 4,7-dimethoxy-1-naphthaldehyde, 2,3-dichloro-5,6-dicyano-*p*-benzoquinone (DDQ), indium(III) chloride and pyrrole were purchased from Sigma-Aldrich. All chemicals were used as received unless otherwise noted. Reagent grade solvents (DCM, hexanes) were distilled prior to use. All reported $^1$H NMR spectra were collected using a 400 or

[a] *Faculty of Technical Physics, Institute of Physics, Poznan University of Technology, 60-965 Poznań, Poland. E-mail: danuta.wrobel@put.poznan.pl*
[b] *Institute of Molecular Physics, Polish Academy of Sciences, 60-179 Poznań, Poland*
[c] *Institute of Organic Chemistry, Polish Academy of Sciences, 01-224 Warsaw, Poland. E-mail: daniel@icho.edu.pl*

† Electronic supplementary information (ESI) available. See DOI: 10.1039/c4cp05648e

500 MHz spectrometer. Chemical shifts ($\delta$ ppm) were determined with TMS as the internal reference; $J$ values are given in Hz. The UV-Vis absorption spectra were recorded in THF. The absorption wavelengths are reported in nm. Flash column chromatography was performed on silica (200–400 mesh). The mass spectra were obtained by field desorption MS (FD-MS) and electrospray ionisation (ESI-MS). The following compounds have been prepared according to literature procedures: 2,7-dimethoxy-1-naphthalenecarbaldehyde,[22] 5-pentafluorophenyldipyrromethane,[23] 8-methoxy-4-quinolinecarboxaldehyde[24], 4-formyl-7,8-dimethoxycoumarin,[25] corrole **5**[26] and corrole **6**.[27]

**10-(4,7-Dimethoxynaphthalen-1-yl)-5,15-bis(pentafluorophenyl)-corrole (1).** 4,7-Dimethoxy-1-naphthaldehyde (108 mg, 0.5 mmol) and 5-pentafluorophenyldipyrromethane (312 mg, 1 mmol) were dissolved in MeOH (50 mL). Subsequently, a solution of $HCl_{aq}$ (36%, 2.5 mL) in $H_2O$ (50 mL) was added, and the reaction was stirred at room temperature for 1 h. The mixture was extracted with $CHCl_3$ (2 × 50 mL), and the organic layer was washed twice with $H_2O$, dried ($Na_2SO_4$), filtered, and diluted to 250 mL with $CHCl_3$. DDQ (300 mg, 1.3 mmol) was added, and the mixture was stirred for 0.5 h at room temperature. The reaction mixture was concentrated to half the volume and was passed through a silica column (silica, DCM/hexanes, 1 : 1). All fractions containing corrole were combined and evaporated to dryness. Flash column chromatography (silica, DCM/hexanes, 1 : 4) afforded the title compound as a dark solid. The resulting solid was precipitated from hot DCM by adding cyclohexane. The crystals were filtered off and dried under vacuum to give 115 mg of pure corrole **1** (28%). $R_f$ (DCM/hexanes, 1 : 1) = 0.57; $^1$H NMR (400 MHz, $CDCl_3$, $Me_4Si$, ppm) $\delta$ (−2.5)–(−1) (br s, 3H, NH), 2.94 (s, 3H, $OCH_3$), 4.24 (s, 3H, $OCH_3$), 6.47 (d, 1H, $J$ = 2.3 Hz, naphtha.), 7.08 (d, 1H, $J$ = 7.9 Hz, naphtha.), 7.15 (dd, 1H, $J_1$ = 2.5, $J_2$ = 9.3 Hz, naphtha.), 8.02 (d, 1H, $J$ = 7.9 Hz, naphtha.), 8.46 (d, 1H, $J$ = 9.3 Hz, naphtha.), 8.50 (d, 2H, $J$ = 4.6 Hz, β-H), 8.56 (br s, 2H, β-H), 8.60 (d, 2H, $J$ = 4.4 Hz, β-H), 9.10 (d, 2H, $J$ = 4.0 Hz, β-H); HRMS (ESI): [$MH^+$] 817.1678 $C_{43}H_{23}F_{10}N_4O_2$ requires: 817.1655. Anal. calcd for $C_{43}H_{22}F_{10}N_4O_2$: C, 63.24; H, 2.72; N, 6.86. Found: 63.33; H, 2.70; N, 6.71.

**10-(2,7-Dimethoxynaphthalen-1-yl)-5,15-bis(pentafluorophenyl)-corrole (2)**

*Method A.* 2,7-Dimethoxy-1-naphthalenecarbaldehyde (108 mg, 0.5 mmol) and 5-pentafluorophenyldipyrromethane (312 mg, 1 mmol) were dissolved in MeOH (50 mL). Subsequently, a solution of $HCl_{aq}$ (36%, 2.5 mL) in $H_2O$ (50 mL) was added, and the reaction was stirred at room temperature for 1 h. The mixture was extracted with $CHCl_3$ (2 × 50 mL), and the organic layer was washed twice with $H_2O$, dried ($Na_2SO_4$), filtered, and diluted to 250 mL with $CHCl_3$. DDQ (300 mg, 1.3 mmol) was added, and the mixture was stirred overnight at room temperature. The reaction mixture was concentrated to half the volume and was passed through a column (silica, DCM/hexanes, 1 : 3). All fractions containing corrole were combined and evaporated to dryness. Flash column chromatography (silica, DCM/hexanes, 1 : 9 → 1 : 4) afforded the title compound as a dark solid. The resulting solid was suspended in hot MeOH, cooled, and filtered to give pure corrole **2** (19 mg, 4.7%).

*Method B.* 2,7-Dimethoxy-1-naphthalenecarbaldehyde (108 mg, 0.5 mmol) and 5-pentafluorophenyldipyrromethane (312 mg, 1 mmol) were dissolved in a pre-prepared solution of TFA (10 μL) in DCM (10 mL). After 1 h at room temperature the reaction mixture was dissolved in DCM (800 mL), a solution of DDQ (300 mg, 1.3 mmol) in toluene (3 mL) was added, and the reaction was stirred at room temperature for an additional 0.5 h. The reaction mixture was passed through a silica column (silica, DCM/hexanes, 1 : 3). All fractions containing corrole were combined and evaporated to dryness. Flash column chromatography (silica, DCM/hexanes, 1 : 9 → 1 : 4) afforded the title compound as a dark solid. The resulting solid was suspended in hot MeOH, cooled, and filtered to give pure corrole **2** (73 mg, 18%). $R_f$ (DCM/hexanes, 1 : 1) = 0.60; $^1$H NMR (400 MHz, $CDCl_3$, $Me_4Si$, ppm) $\delta$ (−3)–(−1) (br s, 3H, NH), 2.87 (s, 3H, $OCH_3$), 3.61 (s, 3H, $OCH_3$), 6.20 (d, 1H, $J$ = 2.5 Hz, naphtha.), 7.03 (dd, 1H, $J_1$ = 2.5, $J_2$ = 9 Hz, naphtha.), 7.54 (d, 1H, $J$ = 9.1 Hz, naphtha.), 7.94 (d, 1H, $J$ = 9.1 Hz, naphtha.), 8.20 (d, 1H, $J$ = 9.0 Hz, naphtha.), 8.41 (d, 2H, $J$ = 4.6 Hz, β-H), 8.53 (d, 2H, $J$ = 3.2 Hz, β-H), 8.58 (d, 2H, $J$ = 4.8 Hz, β-H), 9.07 (d, 2H, $J$ = 4.3 Hz, β-H); HRMS (FD): [$M^+$] 816.1606 $C_{43}H_{22}F_{10}N_4O_2$ requires: 816.1583. Anal. calcd for $C_{43}H_{22}F_{10}N_4O_2$: C, 63.24; H, 2.72; F, 23.26, N, 6.86. Found: 63.01; H, 2.78; F, 23.18, N, 6.97.

**10-(8-Methoxyquinolin-4-yl)-5,15-bis(pentafluorophenyl)-corrole (3).** 8-Methoxy-4-quinolinecarboxaldehyde (160 mg, 0.85 mmol) and 5-pentafluorophenyldipyrromethane (530 mg, 1.7 mmol) were dissolved in DCM (55 mL). To the resulting mixture TFA (200 μL) was added and the reaction mixture was stirred for 30 min. Subsequently $Et_3N$ (400 μL) was added and, after diluting with DCM to 300 mL, a solution of DDQ (550 mg, 2.38 mmol) in toluene (10 mL) was added, and the reaction was stirred at room temperature for a further 0.5 h. The reaction mixture was passed through a silica pad (silica, DCM/acetone, 95 : 5). All fractions containing corrole were combined and evaporated to dryness. Flash column chromatography (silica, DCM/acetone, 95 : 5) afforded the title compound as a dark solid. The resulting solid was precipitated from hot DCM by adding hexanes. The crystals were filtered off and dried under vacuum to give 121 mg of corrole **3** (18%). $R_f$ (DCM/MeOH 99 : 1) = 0.50; $^1$H NMR (500 MHz, $CDCl_3$, $Me_4Si$, ppm) $\delta$ (−3)–(−1) (br s, 3H, NH), 3.00 (s, 3H, $OCH_3$), 6.52 (d, 1H, $J$ = 2.8 Hz, quin.), 7.42 (dd, 1H, $J_1$ = 2.8, $J_2$ = 9.4 Hz, quin.), 8.04 (d, 1H, $J$ = 4.2 Hz, quin.), 8.24 (d, 1H, $J$ = 9.4Hz, quin.), 8.41 (d, 2H, $J$ = 4.8 Hz, β-H), 8.59 (d, 2H, $J$ = 4.1 Hz, β-H), 8.65 (d, 2H, $J$ = 4.6 Hz, β-H), 9.07 (d, 1H, $J$ = 4.2 Hz, quin.), 9.14 (d, 2H, $J$ = 4.3 Hz, β-H); HRMS (TOF MS FD): [$M^+$]: 787.1457 $C_{41}H_{19}N_5OF_{10}$ requires: 787.1430. UV-vis (THF) $\lambda$ 328, 412, 566, 609 nm.

**10-(7,8-Dimethoxycoumarin-4-yl)-5,15-bis(pentafluorophenyl)-corrole (4).** 4-Formyl-7,8-dimethoxycoumarin (47 mg, 0.20 mmol) and 5-pentafluorophenyldipyrromethane (125 mg, 0.4 mmol) were dissolved in a pre-prepared solution of TFA (20 μL) in DCM (10 mL). After 20 min at room temperature the reaction mixture was diluted with DCM (50 mL) and a solution of DDQ (118 mg, 0.52 mmol) in toluene (2 mL) was added, and the reaction was stirred at room temperature for an additional 0.5 h. The reaction mixture was passed through a silica pad (silica, DCM/acetone, 95 : 5). All fractions containing corrole

 

were combined and evaporated to dryness. Flash column chromatography (silica, DCM/acetone, 95 : 5) afforded the title compound as a dark solid. The resulting solid was precipitated from hot DCM by adding hexanes. The crystals were filtered off and dried under vacuum to give 121 mg of corrole **4** (16%). $R_f$ (DCM/acetone 98 : 2) = 0.58; $^1$H NMR (400 MHz, $CDCl_3$, $Me_4Si$, ppm) $\delta$ (−3)–(−2) (br s, 3H, NH), 3.83 (s, 3H, $OCH_3$), 4.20 (s, 3H, $OCH_3$), 6.49 (s, 2H, coumar.), 6.99 (s, 1H, coumar.), 8.57 (br s, 2H, β-H), 8.72–8.75 (m, 4H, β-H), 9.13 (br s, 2H, β-H); HRMS (TOF MS ESI): [$MH^+$]: 835.1397 $C_{42}H_{21}F_{10}N_4O_4$ requires: 835.1364; UV-vis (THF) $\lambda$ 413, 422, 566, 607 nm.

### 2.2. Spectroscopic investigations

UV-Vis spectra of the samples **1–6** in chloroform ($\varepsilon$ = 4.80) were recorded with the use of a Cary 4000 UV-Vis spectrometer in the range 300–800 nm, and fluorescence emission ($\lambda_{exc}$ = 405 nm) and excitation spectra ($\lambda_{em}$ = 700 nm) were recorded with the use of a Hitachi 4500 Fluorometer. Absorption and fluorescence spectra in solution were recorded for $10^{-4}$, $10^{-5}$ and $10^{-6}$ M concentrations. Fluorescence kinetics were determined with the use of a PTI instrument. The values of the life-time were evaluated with the use of the Launch EasyLife V program.

Continuous wave X-band ESR experiments were carried out using a Bruker ELEXSYS 500 EPR spectrometer equipped with a Super High Sensitivity Probehead resonator and a helium gas-flow cryostat (ESR900, Oxford Instruments). Dark and light spectra were recorded at 250 K for a chloroform solution with a $10^{-5}$ M fluorine corrole concentration. Light spectra were recorded immediately after solution illumination (30 mW $cm^{-2}$, 1 min) which was performed directly in the resonator with 405 nm semiconductor laser light. The number of radicals was obtained after double integration of the EPR spectra and comparison with a DPPH standard. The concentration of free radicals was calculated in relation to the number of corrole molecules.

### 2.3. Computational details

In order to interpret the experimental UV-Vis spectra we performed calculations of the transition energies by means of time-dependent density functional theory (TD-DFT). The calculations were performed using the B3LYP hybrid functional (Becke 3-parameter exchange functional combined with Lee–Yang–Parr correlational functional) and the standard 6-31G basis set. The choice of the functional was made taking into account the results published in ref. 28, in which a few functionals were applied to the TD-DFT calculations of corroles. It was concluded that to reproduce the energetic relations between the electronic transitions, the use of hybrid functionals like B3LYP is most reasonable. The calculations were run on the equilibrium geometries of isolated molecules obtained from the optimization procedure performed earlier for all the investigated corroles (DFT, B3LYP/6-31G).[45] The Gaussian 03 program package was used for that purpose.[29] The first 200 transitions have been calculated. To convolute the resulting transition energies and oscillator strengths into the absorption spectra the GaussSum program was used.[30] The spectra were generated assuming a FWHM (full width at half maximum) parameter equal to 3000 $cm^{-1}$ for all transitions.

### 2.4. Photophysical parameters

Fluorescence quantum yield ($\Phi_F$) is determined by the comparative method according to eqn (1)[31,32]

$$\Phi_F = \Phi_{Ref}\frac{F \cdot A_{Ref} \cdot n^2}{F_{Ref} \cdot A \cdot n_{Ref}^2} \quad (1)$$

where $F$ and $F_{Ref}$ are the areas under the fluorescence emission curves of samples **1–6** and the references, respectively; $A$ and $A_{Ref}$ are the relative absorbance of the sample and the references at the excitation wavelength; $n$ and $n_{Ref}$ are the refractive indices of the solvents and the references. As a reference chlorophyll *a* in methanol was used ($\Phi_{Ref}$ = 0.32[33]). The samples and the reference were excited at the same wavelength (405 nm).

## 3. Results and discussion

### 3.1. Design and synthesis

Six carefully designed corroles were synthesized for this study. *meso*-substituted *trans*-$A_2B$-corroles possessing two pentafluorophenyl substituents at positions 5 and 15 were chosen as a key motif due to their stability[12,27] which is crucial in advanced photophysical studies. Structural diversity has been achieved by attaching substituents differing in steric and electronic effects at position 10. We selected the following substituents: 4-nitrophenyl (strongly electron-withdrawing, lack of steric hindrance), 2,7-dimethoxynaphthalen-1-yl and 4,7-dimethoxynaphthalen-1-yl (electron-donating, steric hindrance), 4-methoxyquinoliny-1-yl (basic nitrogen atom, steric hindrance) and 5,6-dimethoxycoumarin-1-yl (strongly polarized, steric hindrance). 5,10,15-Tris(pentafluorophenyl)corrole (**5**) has also been studied as a reference point. The synthesis of all the *trans*-$A_2B$-corroles was performed according to the well-known [2+1] condensation of dipyrromethanes[34] with aldehydes under either classical TFA–DCM[27] or in the $H_2O$–MeOH–HCl system[35] (Scheme 1). The corresponding aldehydes were prepared following literature procedures.[22,24,25] Interestingly the yield of corroles **1–4** depends both on the conditions and on the electronic character of the aldehyde. In the case of 4,7-dimethoxynaphthaldehyde, the condensation in polar solvents afforded corrole **1** in high yield (Scheme 1). On the other hand, the analogous reaction involving 2,7-dimethoxynaphthaldehyde led to the corresponding corrole **2** in 5% yield only. This can be partly rationalized based on the lipophilic character of that aldehyde, which is not compatible with the $H_2O$–MeOH–HCl system. The same reaction performed in $CH_2Cl_2$ afforded corrole **2** in 18% yield. The same conditions were also used for formyl-coumarin to give corrole **4** in 16% yield. *meso*-substituted corroles, bearing a coumarin moiety attached to a corrole core by various linkers have been prepared before.[37,38] It is worth noting that the yield of corrole **4** was significantly higher than the efficiency of the condensation of 5-pentafluorophenyldipyrromenthane with other formyl-coumarins leading to previously described coumarin-corroles (~5–8%).[37,38] This can be rationalized by the much weaker polarization of 4-formyl-7,8-dimethoxycoumarin compared

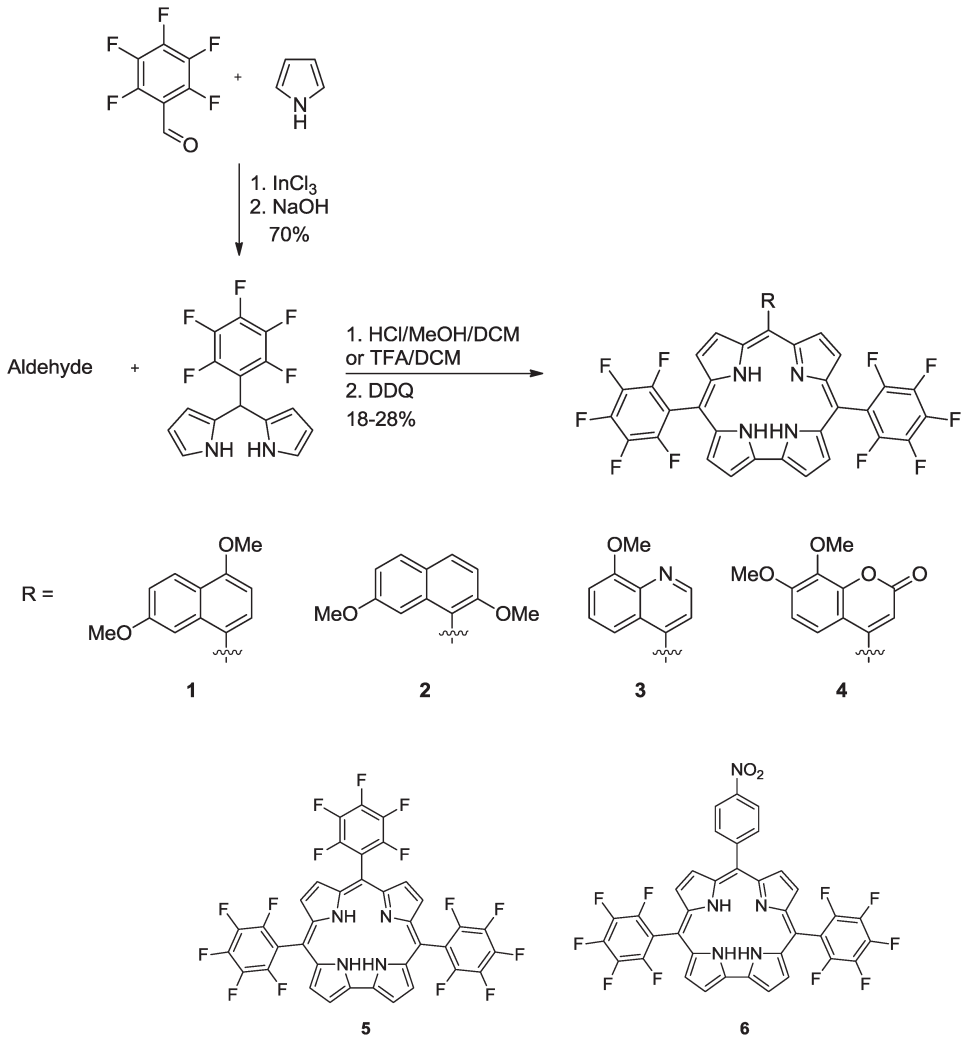


Scheme 1 Synthesis and molecular structures of the investigated corroles.

to previously employed formyl-coumarins, which leads to a lower number of side-reactions. For the condensation of 4-formyl-8-methoxyquinoline, the conditions previously optimized for aldehydes bearing basic nitrogen atoms were utilized,[36] giving corrole **3** in 18% yield (Scheme 1). Corroles **5** and **6** were prepared following known procedures.[26,27]

### 3.2. Electronic absorption spectra

**Experimental.** The electronic absorption spectra of corroles **1–6** in chloroform at three concentrations ($10^{-6}$, $10^{-5}$ and $10^{-4}$ M) have been measured. In Fig. 1 we present representative spectra of the corroles **1** and **5**. The spectra are normalized to unity at the highest Soret band. The second derivative spectra of **1** and **5** are also shown as an example. For the remaining dyes one does not observe any influence of concentration on the spectra shape, as expected for dyes in solvent of low polarity. The spectra of the dyes are slightly different in their shapes. Similarities of the shapes of samples **2** and **6** to that of sample **1**, and the shapes of samples **3** and **4** to that of sample **5**, are shown. The location of the bands and the full widths at half maximum (FWHM) are almost independent of the dye concentration; this indicates the presence (or high predominance) of monomeric dye structures in the whole range of dye concentrations. This conclusion is in agreement with Ziegler *et al.*;[39] they ruled out the presence of aggregates in corroles dissolved in non-polar chloroform.

The two-structural band in the Soret region with maxima at 410 and 427 nm indicates the presence of at least two electronic transitions. Also the band in Fig. 1 observed at 562 nm is broad and split into two bands at 556 and 573 nm. Additionally, the long wavelength band (638 nm) is also present. Table 1A gathers the band intensity ratios as well as the values of the FWHM (of the dyes at a concentration of $10^{-6}$ M).

The previously described coumarin-corroles[37,38] usually contained either π-expanded coumarins or strongly polarized

 

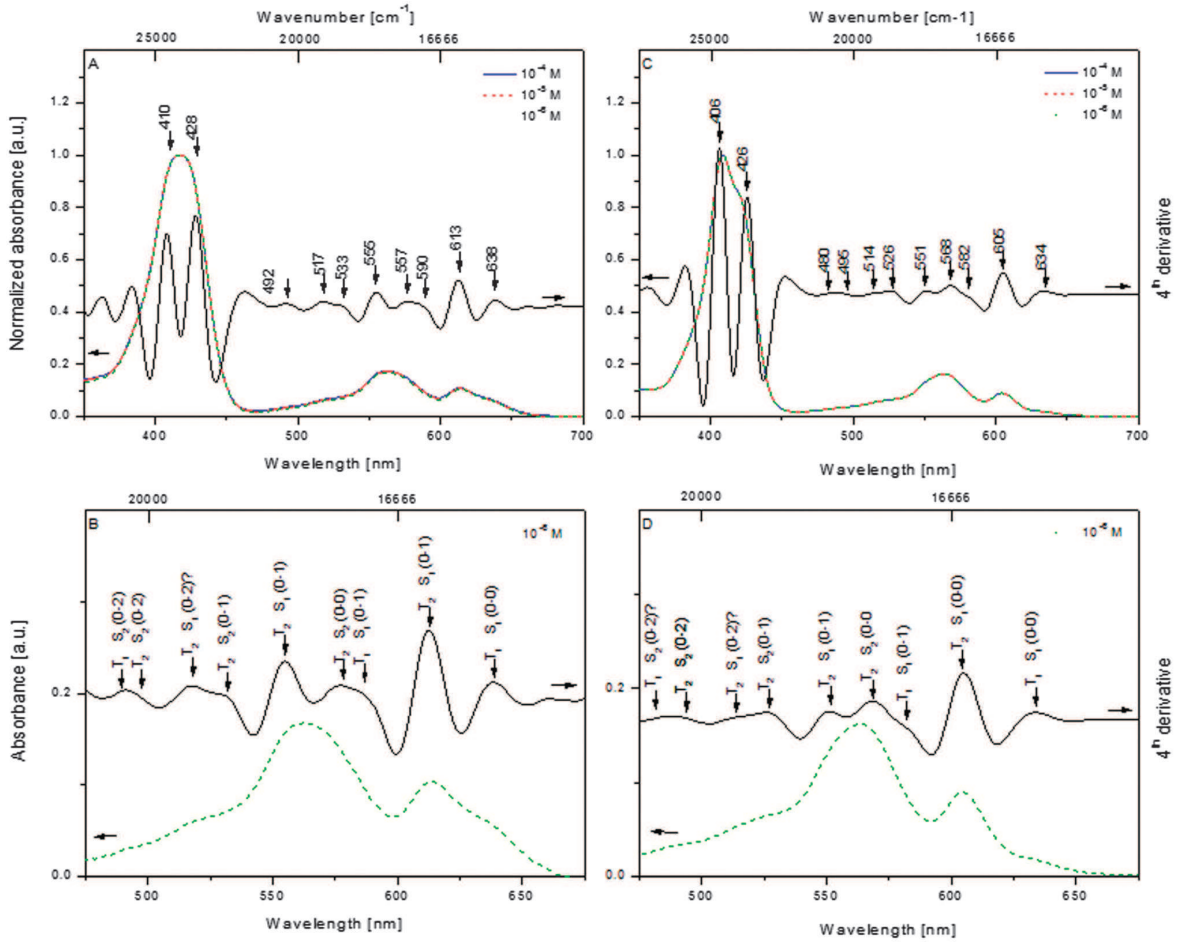


Fig. 1 Representative absorption spectra and derivative spectra of corroles **1** (A, B) and **5** (C, D) in chloroform; concentration $10^{-4}$–$10^{-6}$ M; normalized to unity at the highest Soret band. The remaining dyes show concentration independence. B and D show the range 450–700 nm with notation of the transition assignments.

coumarins bearing an electron-donating group at position 7. In spite of these differences both the absorption and emission spectra of corrole **4** (Fig. 5–7) bear a strong resemblance to previous dyads with a very visible shoulder on the Soret band and two distinct Q-bands (560–570 nm and 610–620 nm).

The origin of the absorption bands is discussed on the basis of Gouterman's four orbital model[40] and our TD-DFT calculations presented in this paper. The corroles are much less symmetric (their symmetry is $C_{2v}$) whereas porphyrins are characterized by $D_{2h}$ or $D_{4h}$ symmetry.[41,42] Nevertheless, the four-orbital model refers also to corrole systems.[43,44] The reduced symmetry strongly affects the absorption properties.[43,44] The absorption bands of corroles contain intense Soret bands and weaker Q bands. In our absorption experiments two sets of bands are well recognized, in the region of 400–450 nm and of 500–700 nm. In the decomposition of the Soret and Q bands it is useful to analyze the spectra and assign the bands of the tautomer electronic transitions as proposed by Beenken *et al.*[28] Two different types of tautomers of the studied corroles are expected and can be identified – they are denoted as T1 and T2 (Table 1B). Five of them belong to the $A_2B$-type corroles (two *meso*-positions are occupied with different groups – samples **1–4** and **6**) and one corrole is the $A_3$-type (*meso*-positions are substituted with the same groups – sample **5**). We conducted our absorption experiments at room temperature, thus it should be expected that a thermodynamic equilibrium with a balance of the two tautomers T1 and T2 in coexistence would be obtained. The results of the experimental data, supported by means of the derivative absorption Gaussian analysis and by the Gouterman model of the electronic transitions of the two tautomers T1 and T2, are gathered in Table 1B. The four-orbital model predicts the presence of four electronic transitions. On the basis of Table 1B the following electronic transitions can be identified as belonging to the tautomers T1 and T2. The $S_1(0–0)$ transitions can be assigned to T1 and T2 in the ranges of 635–638 nm and 605–613 nm, respectively. The $S_2(0–0)$ transitions are observed in the range of 568–577 nm. Some overtones $S_1(0–1)$, $S_2(0–1)$ and $S_2(0–2)$ are also identified. At this point of our discussion it is worth noting that in one of our papers[45] we have also presented

Table 1 (A) Selected absorption and fluorescence parameters; the data of the absorption maxima were evaluated on the basis of the Gaussian decomposition.[a] (B) Band analysis of the absorption spectra of the studied corroles at room temperature by means of fourth derivative minima, and the band assignment to the transitions of the tautomers T1 and T2 in the Q-band range by means of the Gouterman model[b 40]

(A)

| Dye | $\Phi_F$ | Band intensity ratio | | Absorption maximum [nm] | | | | FHWM [$cm^{-1}$] | | | | $R^2$ | $\tau$ [ns] | $\chi^2$ |
|---|---|---|---|---|---|---|---|---|---|---|---|---|---|---|
| 1 | 0.31 | 410/427 | 1.05 | 374 | 394 | 410 | 427 | 722 | 750 | 580 | 636 | 0.9990 | 3.96 ± 0.09 | 1.51 |
| 2 | 0.30 | 407/423 | 0.98 | 371 | 391 | 407 | 423 | 626 | 766 | 522 | 700 | 0.9977 | 4.27 ± 0.11 | 0.95 |
| 3 | 0.27 | 408/425 | 1.12 | 380 | 392 | 408 | 425 | 477 | 477 | 580 | 617 | 0.9894 | 4.30 ± 0.14 | 1.45 |
| 4 | 0.25 | 410/425 | 1.15 | 380 | 390 | 410 | 425 | 667 | 534 | 486 | 644 | 0.9955 | 4.37 ± 0.15 | 1.27 |
| 5 | 0.21 | 407/424 | 1.22 | 379 | 392 | 407 | 424 | 637 | 475 | 545 | 568 | 0.9925 | 4.95 ± 0.41 | 1.38 |
| 6 | 0.07 | 407/427 | 1.06 | 374 | 390 | 407 | 427 | 755 | 562 | 723 | 1045 | 0.9932 | 1.26 ± 0.09 | 0.86 |

(B)

| | | Experimental maximum position | | | Assignment | |
|---|---|---|---|---|---|---|
| Dye | Corrole type | nm | $cm^{-1}$ | Gouterman model | T1 | T2 |
| 1 | $A_2B$ | 638 | 15 674 | 15 740 | $S_1(0–0)$ | |
| | | 613 | 16 313 | 16 695 | | $S_1(0–0)$ |
| | | 590 | 16 949 | 17 040 | $S_1(0–1)$ | |
| | | 577 | 17 331 | 17 570 | | $S_2(0–0)$ |
| | | 555 | 18 018 | 17 995 | | $S_1(0–1)$ |
| | | **548** | | **18 250** | **$S_2(0–0)$** | |
| | | **545** | | **18 340** | **$S_1(0–2)$?** | |
| | | 533 | 18 762 | 18 870 | | $S_2(0–1)$ |
| | | 517 | 19 342 | 19 295 | | $S_1(0–2)$? |
| | | 510 | 19 608 | 19 550 | $S_2(0–1)$ | |
| | | 492 | 20 325 | 20 170 | | $S_2(0–2)$ |
| | | 480 | 20 833 | 20 850 | $S_2(0–2)$? | |
| 2 | $A_2B$ | 638 | 15 674 | 15 740 | $S_1(0–0)$ | |
| | | 612 | 16 340 | 16 695 | | $S_1(0–0)$ |
| | | 588 | 17 007 | 17 040 | $S_1(0–1)$ | |
| | | 575 | 17 391 | 17 570 | | $S_2(0–0)$ |
| | | 554 | 18 051 | 17 995 | | $S_1(0–1)$ |
| | | **548** | | **18 250** | **$S_2(0–0)$** | |
| | | **545** | | **18 340** | **$S_1(0–2)$?** | |
| | | 530 | 18 868 | 18 870 | | $S_2(0–1)$ |
| | | 518 | 19 305 | 19 295 | | $S_1(0–2)$? |
| | | 512 | 19 531 | 19 550 | $S_2(0–1)$ | |
| | | 495 | 20 202 | 20 170 | | $S_2(0–2)$ |
| | | 483 | 20 704 | 20 850 | $S_2(0–2)$? | |
| 3 | $A_2B$ | 638 | 15 674 | 15 740 | $S_1(0–0)$ | |
| | | 609 | 16 420 | 16 695 | | $S_1(0–0)$ |
| | | 583 | 17 153 | 17 040 | $S_1(0–1)$ | |
| | | 573 | 17 545 | 17 570 | | $S_2(0–0)$ |
| | | 553 | 18 083 | 17 995 | | $S_1(0–1)$ |
| | | **548** | | **18 250** | **$S_2(0–0)$** | |
| | | **545** | | **18 340** | **$S_1(0–2)$?** | |
| | | 529 | 18 904 | 18 870 | | $S_2(0–1)$ |
| | | 514 | 19 455 | 19 295 | | $S_1(0–2)$? |
| | | 507 | 19 724 | 19 550 | $S_2(0–1)$ | |
| | | 491 | 20 367 | 20 170 | | $S_2(0–2)$ |
| | | 478 | 20 921 | 20 850 | $S_2(0–2)$? | |
| 4 | $A_2B$ | 636 | 15 724 | 15 740 | $S_1(0–0)$ | |
| | | 608 | 16 447 | 16 695 | | $S_1(0–0)$ |
| | | 583 | 17 153 | 17 040 | **$S_1(0–1)$** | |
| | | 571 | 17 513 | 17 570 | | $S_2(0–0)$ |
| | | 553 | 18 083 | 17 995 | | $S_1(0–1)$ |
| | | **548** | | **18 250** | **$S_2(0–0)$** | |
| | | **545** | | **18 340** | **$S_1(0–2)$?** | |
| | | 528 | 18 939 | 18 870 | | $S_2(0–1)$ |
| | | 515 | 19 417 | 19 295 | | $S_1(0–2)$? |
| | | 509 | 19 646 | 19 550 | $S_2(0–1)$ | |
| | | 492 | 20 325 | 20 170 | | $S_2(0–2)$ |
| | | 483 | 20 704 | 20 850 | $S_2(0–2)$? | |
| 5 | $A_3$ | 634 | 15 773 | 15 740 | $S_1(0–0)$ | |
| | | 605 | 16 529 | 16 695 | | $S_1(0–0)$ |

 

Table 1 (*continued*)

(B)

| Dye | Corrole type | Experimental maximum position | | Gouterman model | Assignment | |
|---|---|---|---|---|---|---|
| | | nm | $cm^{-1}$ | | T1 | T2 |
| | | 582 | 17 182 | 17 040 | $S_1$(0–1) | |
| | | 568 | 17 606 | 17 570 | | $S_2$(0–0) |
| | | 551 | 18 149 | 17 995 | | $S_1$(0–1) |
| | | **548** | | **18 250** | **$S_2$(0–0)** | |
| | | **545** | | **18 340** | **$S_1$(0–2)?** | |
| | | 526 | 19 011 | 18 870 | | $S_2$(0–1) |
| | | 514 | 19 455 | 19 295 | | $S_1$(0–2)? |
| | | 508 | 19 685 | 19 550 | $S_2$(0–1) | |
| | | 495 | 20 202 | 20 170 | | $S_2$(0–2) |
| | | 480 | 20 833 | 20 850 | $S_2$(0–2)? | |
| 6 | $A_2B$ | 640 | 15 625 | 15 740 | $S_1$(0–0) | |
| | | 610 | 16 393 | 16 695 | | $S_1$(0–0) |
| | | 587 | 17 036 | 17 040 | $S_1$(0–1) | |
| | | 573 | 17 452 | 17 570 | | $S_2$(0–0) |
| | | 555 | 18 018 | 17 995 | | $S_1$(0–1) |
| | | **548** | | **18 250** | **$S_2$(0–0)** | |
| | | **545** | | **18 340** | **$S_1$(0–2)?** | |
| | | 531 | 18 832 | 18 870 | | $S_2$(0–1) |
| | | 517 | 19 342 | 19 295 | | $S_1$(0–2)? |
| | | 510 | 19 608 | 19 550 | **$S_2$(0–1)** | |
| | | 496 | 20 161 | 20 170 | | $S_2$(0–2) |
| | | 480 | 20 833 | 20 850 | **$S_2$(0–2)?** | |

[a] FWHM – full width at half maximum (calculated with the Gaussian component program), $R^2$ – coefficient of determination, $\Phi_F$ – fluorescence quantum yield, $\tau$ – fluorescence life-time, $\chi^2$ – chi square. [b] Bands expected by the model but not found in the analysis of the experimental spectrum are given in bold. Questionable assignments are marked by "?", precision ± 0.5 nm.

the results of some vibrational bands and also the combination bands with the use of very sensitive infrared photoacoustic examinations. However, a few bands predicted in the Gouterman model are not seen (*e.g.* $S_1$(0–2) and $S_2$(0–0)).

**Quantum chemical calculations.** Our supposition as to the spectral behavior of the corrole dyes was confirmed by quantum-chemical calculations. The electronic transitions (oscillator strengths *versus* wavelength) calculated by the TD-DFT method for all investigated corroles are presented in Fig. 2. In all cases the Soret band (about 400 nm) consists of 3–4 intense transitions. However, the spectral distance between the transitions is quite small and they appear in the resulting spectra as single bands. In the experimental spectra the Soret band is observed also as a single band (with some components visible), so there is an

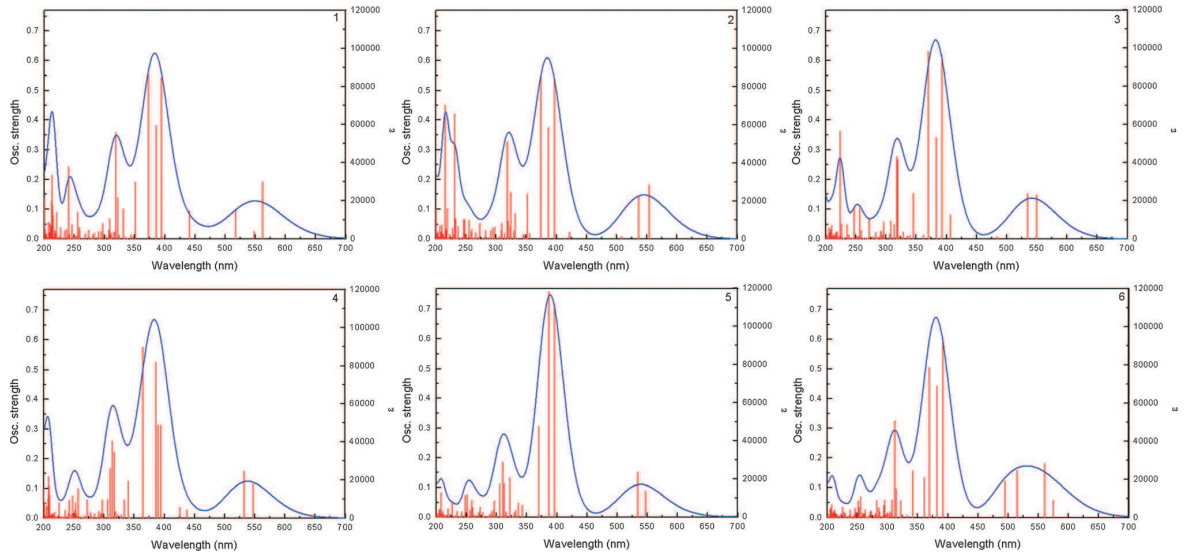


Fig. 2 Electronic transitions (oscillator strengths *versus* wavelength) calculated by the TD-DFT method for all the investigated corroles.

agreement between the calculated and experimental spectra. In the Q band spectral region, two bands are observed in all the experimental spectra (614 and 638 nm). In the calculated spectra, the band is not separated but can be seen in Fig. 2; there are two (or more) intense transitions in this region. A similar result has been obtained in calculations done by Salvatori *et al.*[46] for a set of free-base and copper corroles. The electronic transition related to the appearance of the Q band involves mainly the HOMO (highest occupied molecular orbital) and LUMO (lowest unoccupied molecular orbital). Of course other orbitals also take part but the dominant contribution arises from the HOMO → LUMO transition. The main transitions with appropriate descriptions are collected in Table 3. The HOMO and LUMO energies and the HOMO–LUMO energy gap values calculated for the investigated corroles are collected in Table 2 and Fig. 3 while the contour plots of the mentioned orbitals are gathered in Fig. 4.

Table 2 HOMO and LUMO energies and the HOMO–LUMO energy gap values calculated for the investigated corroles (eV). The values calculated for similar free base corroles by Salvatori and Beenken are provided for comparison

| | 1 | 2 | 3 | 4 | 5 | 6 | Ref. 46 | Ref. 28 |
|---|---|---|---|---|---|---|---|---|
| $E_{total}$ (hartree) | −3018.805 | −3018.802 | −2920.335 | −3129.867 | −3132.251 | −2840.650 | | |
| HOMO | −5.20 | −5.14 | −5.39 | −5.58 | −5.63 | −5.58 | −4.76 | −5.244 |
| LUMO | −2.75 | −2.69 | −2.91 | −3.05 | −3.10 | −3.16 | −2.30 | −2.595 |
| $\Delta_{H-L}$ | 2.45 | 2.45 | 2.48 | 2.53 | 2.53 | 2.42 | 2.46 | 2.649 |

Table 3 Selected electronic transitions calculated for the investigated corroles using the TD-DFT (B3LYP/6-31G) method. The major contributions of the involved orbitals are also given. The table is limited to the transitions with wavelength > 350 nm and oscillator strengths > 0.1

| Wavelength (nm) | Oscillator strength | Major contribution |
|---|---|---|
| **1** | | |
| 562.1 | 0.1918 | H − 2 → LUMO (15%), HOMO → LUMO (63%) |
| 394.3 | 0.5418 | H − 1 → L + 1 (13%), HOMO → L + 1 (26%) |
| 385.5 | 0.3818 | H − 4 → LUMO (40%), H − 2 → L + 1 (16%), H − 1 → L + 1 (12%) |
| 372.4 | 0.554 | H − 4 → LUMO (45%), H − 1 → L + 1 (17%) |
| 351.1 | 0.1907 | HOMO → L + 2 (68%) |
| **2** | | |
| 553.5 | 0.1816 | H − 1 → LUMO (22%), H − 1 → L + 1 (14%), HOMO → LUMO (43%), HOMO → L + 1 (15%) |
| 536.4 | 0.1418 | H − 1 → LUMO (40%), HOMO → LUMO (24%), HOMO → L + 1 (21%) |
| 396.8 | 0.5368 | H − 1 → LUMO (14%), HOMO → L + 1 (38%) |
| 387.0 | 0.3744 | H − 4 → LUMO (42%), H − 1 → L + 1 (23%) |
| 374.1 | 0.5476 | H − 4 → LUMO (45%), H − 1 → L + 1 (23%) |
| 351.6 | 0.1501 | HOMO → L + 2 (56%), HOMO → L + 3 (14%) |
| **3** | | |
| 549.3 | 0.1476 | H − 1 → LUMO (28%), H − 1 → L + 1 (12%), HOMO → LUMO (36%), HOMO → L + 1 (19%) |
| 534.6 | 0.1521 | H − 1 → LUMO (34%), H − 1 → L + 1 (10%), HOMO → LUMO (30%), HOMO → L + 1 (19%) |
| 392.3 | 0.6197 | H − 1 → LUMO (14%), HOMO → L + 1 (35%) |
| 383.1 | 0.3415 | H − 4 → LUMO (42%), H − 2 → L + 1 (13%), H − 1 → L + 1 (14%) |
| 370.0 | 0.6289 | H − 4 → LUMO (39%), H − 1 → L + 1 (21%) |
| **4** | | |
| 547.2 | 0.1142 | H − 1 → LUMO (32%), H − 1 → L + 1 (11%), HOMO → LUMO (31%), HOMO → L + 1 (22%) |
| 531.9 | 0.1582 | H − 1 → LUMO (28%), H − 1 → L + 1 (13%), HOMO → LUMO (35%), HOMO → L + 1 (17%) |
| 394.1 | 0.3133 | H − 1 → L + 1 (26%), H − 1 → L + 2 (30%) |
| 389.2 | 0.3133 | H − 1 → L + 2 (47%), HOMO → L + 1 (15%) |
| 385.9 | 0.5257 | H − 2 → L + 1 (15%), H − 1 → L + 1 (14%), H − 1 → L + 2 (14%), HOMO → L + 1 (16%) |
| 364.3 | 0.5745 | H − 4 → LUMO (18%), H − 2 → L + 1 (41%), H − 1 → L + 1 (13%) |
| **5** | | |
| 534.2 | 0.1511 | H − 1 → LUMO (21%), H − 1 → L + 1 (16%), HOMO → LUMO (40%), HOMO → L + 1 (15%) |
| 395.7 | 0.7181 | H − 1 → LUMO (18%), HOMO → L + 1 (33%) |
| 386.8 | 0.7593 | H − 2 → LUMO (16%), H − 1 → L + 1 (37%) |
| 369.7 | 0.3045 | H − 2 → LUMO (74%), H − 1 → L + 1 (10%) |
| **6** | | |
| 560.3 | 0.1808 | H − 1 → LUMO (19%), H − 1 → L + 2 (10%), HOMO → LUMO (46%) |
| 514.6 | 0.1576 | H − 1 → LUMO (22%), H − 1 → L + 1 (14%), HOMO → L + 1 (24%), HOMO → L + 2 (33%) |
| 494.7 | 0.1214 | H − 1 → LUMO (13%), H − 1 → L + 1 (60%), H − 1 → L + 2 (11%) |
| 391.3 | 0.6029 | H − 1 → LUMO (12%), HOMO → L + 2 (38%) |
| 381.8 | 0.4419 | H − 2 → LUMO (32%), H − 2 → L + 1 (11%), H − 1 → L + 2 (29%) |
| 368.9 | 0.505 | H − 2 → LUMO (55%), H − 1 → L + 2 (22%) |
| 360.8 | 0.1345 | H − 2 → L + 1 (76%) |

 

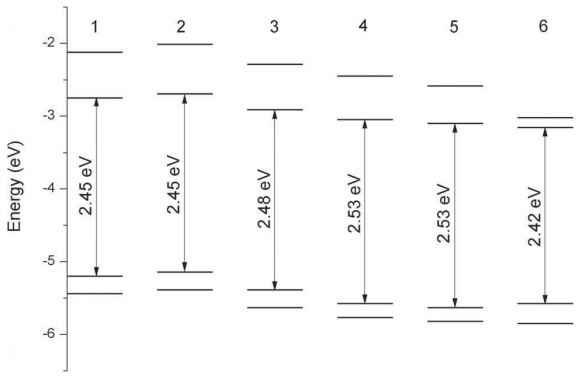


Fig. 3 HOMO–LUMO energy gap values calculated for the investigated corroles.

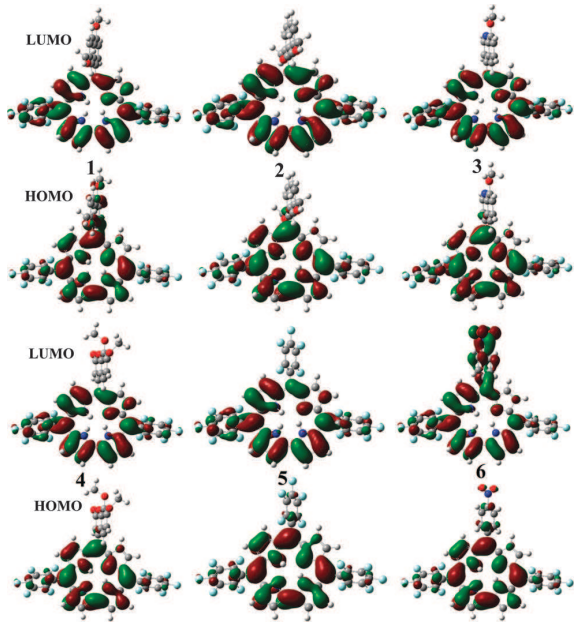


Fig. 4 Contour plots of the corrole molecular orbitals.

It is easy to notice some differences in the HOMO and LUMO energy values. The greatest differences are between the HOMO levels of **5** and **2** (0.49 eV) and the LUMO levels of **6** and **2** (0.47 eV). Despite that, the energy gap between the HOMO and LUMO is very similar for all the investigated corroles – the greatest difference is between that of **6** and those of **4**/**5** (0.11 eV). The energy gap and the HOMO–LUMO energy values are also similar to the ones calculated by Salvatori[46] and Beenken[28] for similar free-base corroles (see Table 2 for comparison).

In the investigated molecules both the HOMO and the LUMO are localized on the corrole ring and not on the substituents. The only exception is the LUMO of **6** which is localized on the corrole macroring and on one of the substituents. The reason for this is the presence of the electron-withdrawing nitro group in the substituent. Selected electronic transitions calculated for the investigated corroles using the TD-DFT (B3LYP/6-31G) method are shown in Table 3. The major contributions of the involved orbitals are also given. The table is limited to the transitions with wavelengths > 350 nm and oscillator strengths > 0.1.

### 3.3. Fluorescence studies

The studied corroles exhibit strong fluorescence; Fig. 5 shows the results for all the dyes in chloroform when excited at 405 nm. The character of the fluorescence spectra is typical for the porphyrin-like corroles. As seen, the spectra are dependent on the samples and differ from each other in shapes and location of the maxima. The bands of samples **1** and **6** are located at about 651 nm and the bands of **2–5** at about 642 nm; weak bands in the range 700–750 nm are also seen. Moreover, the fluorescence of the samples is characterized by small humps observed in the shorter wavelength range (600–625 nm), which are very well seen in the spectra of samples **2–6** and much less in that of sample **1**. The differences in the shapes of the fluorescence spectra can be compared with our TD-DFT results and the tautomer T1 and T2 absorption band analysis by means of the Gouterman model. Thus, the predominant fluorescence is seen in the long wavelength region and can be assigned to the emission of the tautomer T1; the less intense shorter wavelength humps can have their origin in the fluorescence of T2.[28,47] The differences in the sample fluorescence behavior come from the presence of the various substituents attached to the main corrole core. Similar fluorescence behavior was shown by Kruk *et al.*[13] for other NH *meso*-(dichloropyrimidinyl)corrole tautomers, although the T2 tautomer emission in their work was much more intense than that of our samples.

The higher intensity of T2 seems to be influenced strongly by the electron-withdrawing character of the substituents at position 10. Both $C_6F_5$ (corrole **5**) and pyranone (corrole **4**) are electron-deficient. The same holds true for the nitro group (corrole **6**), but the nitro group quenches emission so its effect on the T1/T2 ratio is more complex.

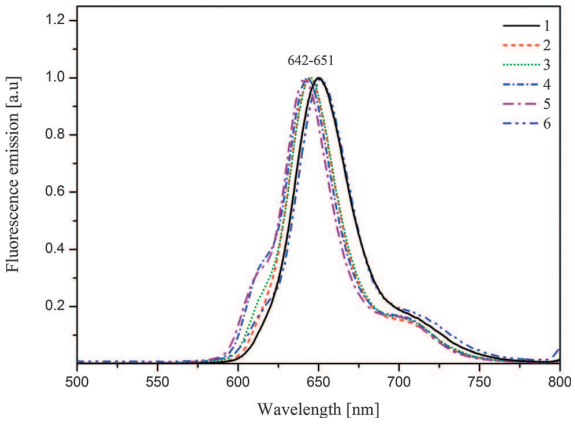


Fig. 5 Fluorescence spectra of the dyes in chloroform; excitation at 405 nm.

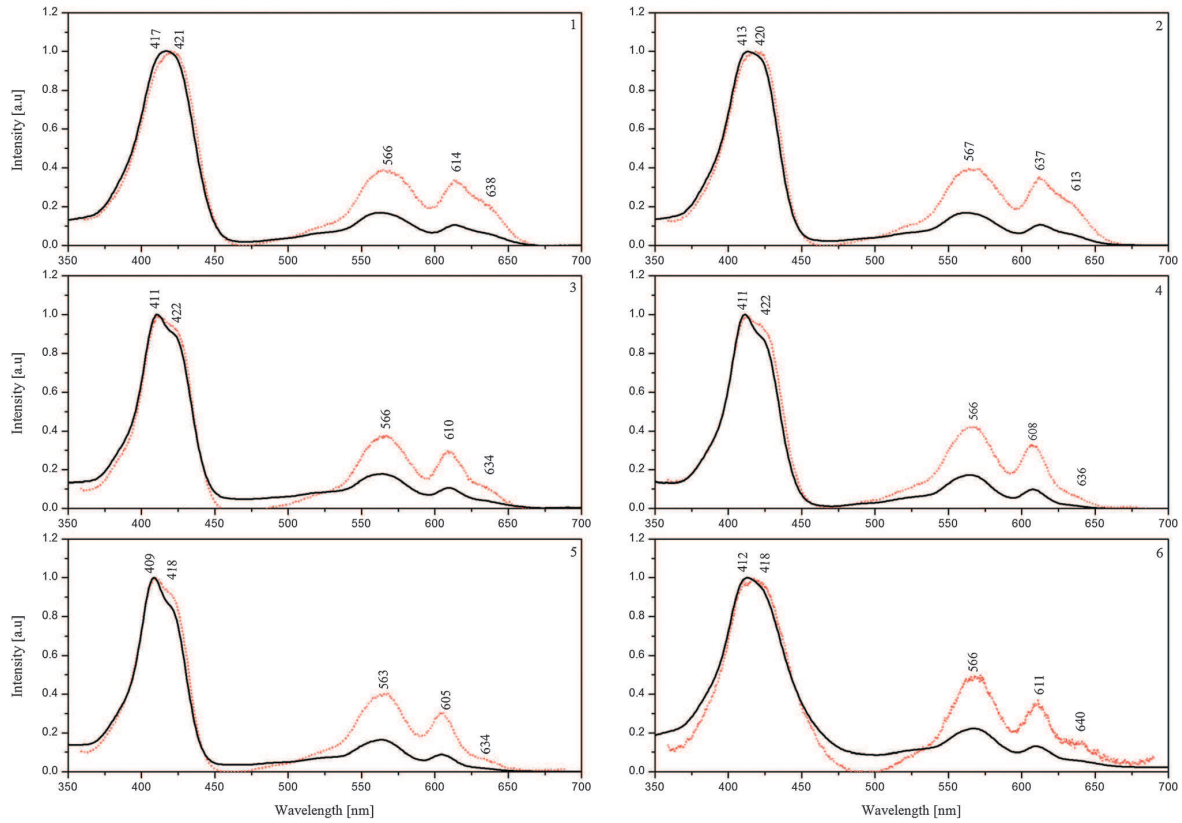


Fig. 6 Excitation emission spectra of the corroles observed at 700 nm.

The shapes of the excitation emission spectra observed at 700 nm correspond to those of the absorption spectra in the range 350–680 nm (Fig. 6). However, the exception is the slightly split band in the Soret region, which confirms the presence of the T1 and T2 tautomers.

The fluorescence decays of two selected dyes (1 and 6) in chloroform are shown in Fig. 7. On the basis of the fluorescence kinetics the life-time values are evaluated and the results are shown in Table 1A. The life-time values of 1.26–4.95 ns (depending on the dye) are characteristic of porphyrin-like dyes and confirm monomeric corrole emission. The results of the deconvolution procedure give the typical monoexponential decay; however we are not able to recognize the life-times of tautomers T1 and T2 in our experiment. In Table 1A the values of the fluorescence quantum yields are also collected.

### 3.4. ESR spectroscopy

Fig. 8 presents the qualitative changes in the ESR spectra recorded for samples **1–6** before and after illumination. Each fluorine corrole solution shows an almost symmetrical ESR line characterized by the parameters: line width $\Delta B_{pp}$ = 6.5 (± 0.1) Gs, *g*-factor *g* = 2.0030 (± 0.0002). The lack of differences in the ESR parameter values strongly suggests that for any of the studied fluorine corroles, an unpaired electron is localized on the corrole macroring but not on the substituents. The only noticeable difference among the samples is the ESR line amplitude, which is proportional to the number of radicals created. Because after illumination the shape of the ESR spectrum does not change and one can observe only increased line amplitude in comparison to the dark samples, we conclude that light creates some additional radicals of the same type as those of the samples before illumination.

Fig. 9 presents an example of ESR signal deconvolution for the light-induced sample **2**. Approximations indicate that any spectrum consists of two Gaussian lines. These two lines are characterized by different line widths, $\Delta B_{pp}^{1st}$ = 6 Gs and $\Delta B_{pp}^{2nd}$ = 8 Gs, and *g*-factors, $g^{1st}$ = 2.0030 and $g^{2nd}$ = 2.0032. The two components of the ESR spectrum result from the partial charge separation in the fluorine corrole molecules and the creation of cationic and anionic radicals.

The increase in the number of radicals (proportional to the ESR signal amplitude) under laser illumination and the decrease after the discontinuation of illumination due to partial ionic radical recombination can be described by the exponential function, with characteristic times of growth and decay of the order of a few minutes and a few hours, respectively. The concentrations of radicals in the solutions of the different fluorine corroles before and after 1 minute of illumination are presented in Fig. 10. It is worth mentioning that the ESR results also show radicals in the powdered samples, but their

 

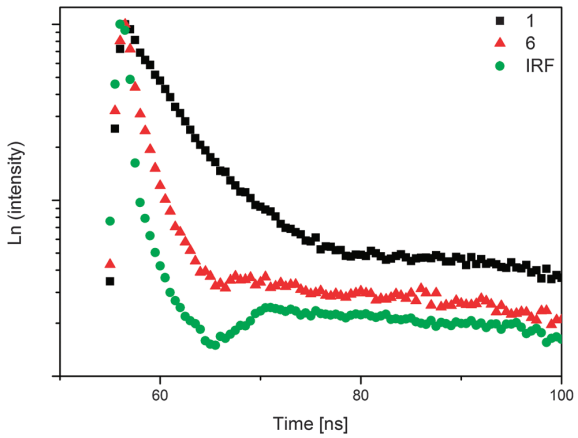


Fig. 7 Fluorescence kinetics of corroles **1** and **6** in chloroform.

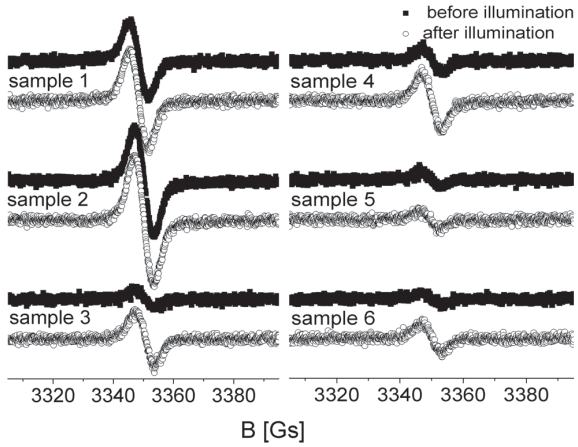


Fig. 8 ESR spectra of corroles **1–6** in chloroform ($10^{-5}$ M), recorded at 250 K before and after laser illumination.

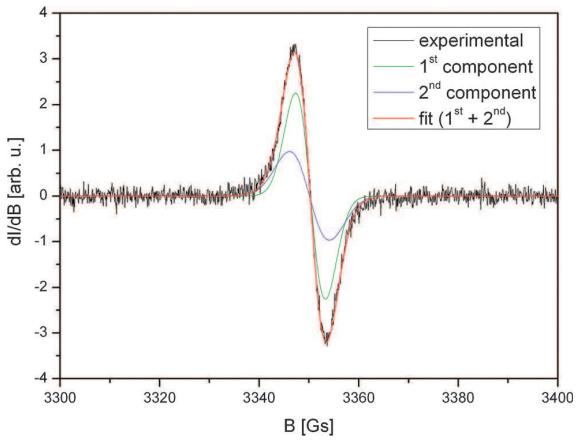


Fig. 9 Experimental and approximated ESR spectra of the light-induced sample **2**.

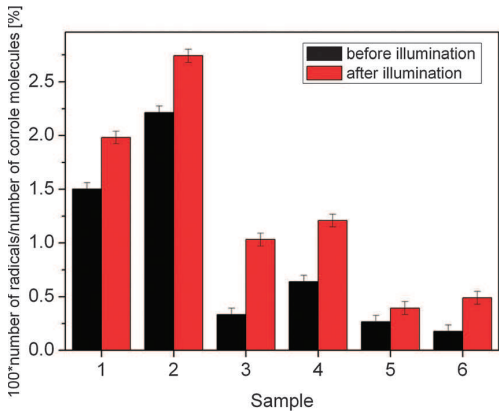


Fig. 10 Concentrations of radicals in corrole solutions before and after laser illumination: 30 mW $cm^{-2}$, 1 min, 405 nm.

concentration is much smaller and does not exceed 0.02% (at least about one order of magnitude less in comparison to those in solution). The creation of radicals most probably results from an activation process. In the case of solution samples the activation energy of radical creation is lowered and leads to an increase of radical concentration. As presented in Fig. 10, samples **1** and **2** show the highest concentrations of radicals (above 1.50%) before laser illumination. Samples **5** and **6** have the lowest concentrations under the same conditions, *i.e.* 0.27% and 0.18%, respectively. One minute of laser illumination creates additional radicals in all of the samples. This process is most effective in sample **3** (0.70% additional radicals) and the least efficient in sample **5** (0.13%).

## 4. Conclusions

In summary we can conclude the following:

(1) The free-base corroles possessing partly polarized structures due to the presence of two strongly electron-withdrawing $C_6F_5$ groups, in chloroform show a monomeric structure even in solutions of high concentrations. This is confirmed by the absorption and excitation emission as well as the fluorescence experiments (intensity ratio, FWHM parameters and fluorescence life-time). The multi-structural character of the bands in the Soret and in the Q-band regions (410–427 nm, 500–650 nm) indicate the presence of more than one electronic transition assigned to the tautomers T1 and T2. The emission spectra evidently show the predominance of the T1 tautomer fluorescence in the room temperature spectra.

(2) The experimental data are supported by quantum chemical calculations (TD-DFT) of the HOMO and LUMO, and the agreement between the experimental and simulated results is evident. In the investigated molecules (samples **1–5**) both the HOMO and the LUMO are localized on the corrole ring and not on the substituents. The only exception is the LUMO of **6**which is localized on the corrole macroring and on the nitro substituent.

(3) The ESR experiments strongly show that an unpaired electron is localized on the corrole macroring but not on the substituents both before and after light illumination – laser illumination creates additional radicals, however with different effectiveness depending on the sample.

## Abbreviations

| | |
|---|---|
| UV-vis | Ultraviolet–visible |
| ESR | Electron spin resonance |
| FWHM | Full width at half maximum |
| TD-DFT | Time-dependent density functional theory |

## Acknowledgements

The paper was supported by the Poznan University of Technology (grant 06/62/DSPB/0215; B.B1, B.B2, D.W.) and by EuroSolarFuels grant.

## References

1 D. T. Gryko, J. P. Fox and D. P. Goldberg, *J. Porphyrins Phthalocyanines*, 2004, **8**, 1091.
2 C. J. Lemon and P. J. Brothers, *J. Porphyrins Phthalocyanines*, 2011, **15**, 809.
3 R. Paolesse, in *The Porphyrin Handbook*, ed. K. M. Kadish, K. M. Smith and R. Guilard, Academic Press, New-York, 2000, vol. 2, p. 201.
4 F.-P. Montforts, M. Glasenapp-Breiling and D. Kusch, in *Houben-Weyl Methods of Organic Chemistry*, ed. E. Schaumann, Thieme, Stuttgart-New York, 1998, vol. E9d, p. 665.
5 D. T. Gryko, *Eur. J. Org. Chem.*, 2002, 1735.
6 R. Guilard, J.-M. Barbe, C. Stern and K. M. Kadish, in *The Porphyrin Handbook*, ed. K. M. Kadish, K. M. Smith and R. Guilard, Elsevier, 2003, vol. 18, p. 303.
7 D. T. Gryko, J. P. Fox and D. P. Goldberg, *J. Porphyrins Phthalocyanines*, 2004, **8**, 1091.
8 S. Nardis, D. Monti and R. Paolesse, *Mini-Rev. Org. Chem.*, 2005, **2**, 355.
9 D. Wróbel and A. Graja, *Coord. Chem. Rev.*, 2011, **255**, 2555.
10 I. Aviv and Z. Gross, *Chem. Commun.*, 2007, 1987 and references therein.
11 L. You, H. Shen, L. Shi, G. Zhang, H. Li, H. Wang and L. Ji, *Sci. China: Phys., Mech. Astron.*, 2010, **53**, 1491.
12 L. Flamigni and D. T. Gryko, *Chem. Soc. Rev.*, 2009, **38**, 1635.
13 M. Kruk, T. H. Ngo, P. Verstappen, A. Starukhin, J. Hofkens, W. Dehaen and W. Maes, *J. Phys. Chem. A*, 2012, **116**, 10695.
14 M. Kruk, T. H. Ngo, V. Savva, A. Starukhin, W. Dehaen and W. Maes, *J. Phys. Chem. A*, 2012, **116**, 10704.
15 Y. B. Ivanova, V. Savva, N. Z. Marmardashvili, A. Starukhin, T. H. Ngo, W. Dehaen, W. Maes and M. Kruk, *J. Phys. Chem. A*, 2012, **116**, 10683.
16 J. M. Barbe, G. Canard, S. Brandés and R. Guilard, *Eur. J. Org. Chem.*, 2005, 4601.
17 J. M. Barbe, G. Canard, S. Brandés and R. Guilard, *Angew. Chem., Int. Ed.*, 2005, **117**, 3163.
18 S.-L. Lai, L. Wang, C. Yang, M.-Y. Chan, X. Guan, C.-C. Kwok and C.-M. Che, *Adv. Funct. Mater.*, 2014, **24**, 4655.
19 K. Lewandowska, B. Barszcz, J. Wolak, A. Graja, M. Grzybowski and D. T. Gryko, *Dyes Pigm.*, 2013, **96**, 249.
20 K. Lewandowska, B. Barszcz, A. Graja, B. Bursa, A. Biadasz, D. Wróbel, W. Bednarski, S. Waplak, M. Grzybowski and D. T. Gryko, *Synth. Met.*, 2013, **166**, 70.
21 B. Bursa, D. Wróbel, K. Lewandowska, A. Graja, M. Grzybowski and D. T. Gryko, *Synth. Met.*, 2013, **176**, 18–25.
22 T. Mizutani, T. Murakami, T. Kurahashi and H. Ogoshi, *J. Org. Chem.*, 1996, **61**, 539.
23 A. Osuka, G. Noya, S. Taniguchi, T. Okada, Y. Nishimura, I. Yamazaki and N. Mataga, *Chem. – Eur. J.*, 2000, **6**, 33.
24 J.-P. Liou, C.-Y. Nien, C.-Y. Chang, J.-Y. Chang, Y.-C. Chen, C.-C. Kuo, H.-P. Hsieh, J.-S. Wu, S.-Y. Wu and J.-Y. Chang, *J. Med. Chem.*, 2010, **53**, 2309.
25 K. Bohra, B. Kumar, V. S. Parmar, A. K. Prasad, D. Sharma and C. E. Olsen, *J. Indian Chem. Soc.*, 2013, **90**, 1885.
26 D. T. Gryko and B. Koszarna, *Org. Biomol. Chem.*, 2003, **1**, 350.
27 D. T. Gryko and B. Koszarna, *Synthesis*, 2004, 2205.
28 W. Beenken, M. Presselt, T. H. Ngo, W. Dehaen, W. Maes and M. Kruk, *J. Phys. Chem. A*, 2014, **118**, 862.
29 M. J. Frisch, G. W. Trucks, H. B. Schlegel, G. E. Scuseria, M. A. Robb, J. R. Cheeseman, J. A. Montgomery, Jr., T. Vreven, K. N. Kudin, J. C. Burant, J. M. Millam, S. S. Iyengar, J. Tomasi, V. Barone, B. Mennucci, M. Cossi, G. Scalmani, N. Rega, G. A. Petersson, H. Nakatsuji, M. Hada, M. Ehara, K. Toyota, R. Fukuda, J. Hasegawa, M. Ishida, T. Nakajima, Y. Honda, O. Kitao, H. Nakai, M. Klene, X. Li, J. E. Knox, H. P. Hratchian, J. B. Cross, C. Adamo, J. Jaramillo, R. Gomperts, R. E. Stratmann, O. Yazyev, A. J. Austin, R. Cammi, C. Pomelli, J. W. Ochterski, P. Y. Ayala, K. Morokuma, G. A. Voth, P. Salvador, J. J. Dannenberg, V. G. Zakrzewski, S. Dapprich, A. D. Daniels, M. C. Strain, O. Farkas, D. K. Malick, A. D. Rabuck, K. Raghavachari, J. B. Foresman, J. V. Ortiz, Q. Cui, A. G. Baboul, S. Clifford, J. Cioslowski, B. B. Stefanov, G. Liu, A. Liashenko, P. Piskorz, I. Komaromi, R. L. Martin, D. J. Fox, T. Keith, M. A. Al-Laham, C. Y. Peng, A. Nanayakkara, M. Challacombe, P. M. W. Gill, B. Johnson, W. Chen, M. W. Wong, C. Gonzalez and J. A. Pople, *Gaussian 03, Revision D.01*, Gaussian, Inc., Pittsburgh, PA, 2003.
30 N. M. O'Boyle, A. L. Tenderholt and K. M. Langner, *J. Comput. Chem.*, 2008, **29**, 839.
31 J. Lakowicz, *Principles of Fluorescence Spectroscopy*, Springer, New York, 3rd edn, 2006.
32 M. A. M. J. Van Zandvoort, D. Wróbel, A. J. Scholten, D. De Jager, G. Ginkel and Y. K. Levine, *Photochem. Photobiol.*, 1993, **58**, 600.
33 H. Scheer, *Chlorophylls*, CRC-Press, Boca Raton, 1991.
34 D. T. Gryko, D. Gryko and C.-H. Lee, *Chem. Soc. Rev.*, 2012, **41**, 3780.

 

35 B. Koszarna and D. T. Gryko, *J. Org. Chem.*, 2006, **71**, 3707.
36 D. T. Gryko and K. E. Piechota, *J. Porphyrins Phthalocyanines*, 2002, **6**, 81.
37 M. Tasior, D. T. Gryko, D. J. Pielacińska, A. Zanelli and L. Flamigni, *Chem. – Asian J.*, 2010, **5**, 130–140.
38 M. Tasior, R. Voloshchuk, Y. M. Poronik, T. Rowicki and D. T. Gryko, *J. Porphyrins Phthalocyanines*, 2011, **15**, 1011–1023.
39 C. J. Ziegler, J. R. Sabin, G. R. Geiger III and V. N. Nemykin, *Chem. Commun.*, 2012, **48**, 4743.
40 M. Gouterman, G. H. Wagnière and L. C. Snyder, *J. Mol. Spectrosc.*, 1963, **11**, 108.
41 A. Biadasz, B. Bursa, B. Barszcz, A. Bogucki, B. Laskowska, A. Graja and D. Wróbel, *Dyes Pigm.*, 2011, **89**, 86.
42 D. Wróbel, A. Siejak and P. Siejak, *Sol. Energy Mater. Sol. Cells*, 2010, **94**, 492.
43 N. S. Hush, J. M. Dyke, M. L. Williams and I. S. Woolsey, *J. Chem. Soc., Dalton Trans.*, 1974, 395.
44 A. Ghosh, T. Wondimagegn and A. B. J. Parusel, *J. Am. Chem. Soc.*, 2000, **122**, 5100.
45 B. Barszcz, D. Wróbel, A. M. Urbańska, J. P. Lewtak, D. Koszelewski, O. Vakuliuk and D. T. Gryko, *Dyes Pigm.*, under review.
46 P. Salvatori, A. Amat, M. Pastore, G. Vitillaro, K. Sudhakar, L. Giribabu, Y. Soujanya and F. De Angelis, *Comput. Theor. Chem.*, 2014, **1030**, 59.
47 R. S. Becker, *Theory and Interpretation of Fluorescence and Phosphorescence*, Wiley Interscience, New York, 1969.

**Praca nr 4**

**[Bursa, PCCP 2016]** B. Bursa, D. Wróbel, B. Barszcz, M. Kotkowiak, O. Valulyuk, D. Gryko, Ł. Kolanowski, M. Baraniak, G. Lota, *Solvent impact on the singlet and triplet states of selected fluorine corroles – absorption, fluorescence and aptoacustic studies,* Phys. Chem. Chem. Phys. **18** (2016) 7216-7228

PCCP

PAPER

View Article Online
View Journal | View Issue

Cite this: *Phys. Chem. Chem. Phys.*, 2016, **18**, 7216

# The impact of solvents on the singlet and triplet states of selected fluorine corroles – absorption, fluorescence, and optoacoustic studies†

Bartosz Bursa,[a] Danuta Wróbel,*[a] Bolesław Barszcz,[ab] Michał Kotkowiak,[a] Olena Vakuliuk,[c] Daniel T. Gryko,*[c] Łukasz Kolanowski,[d] Marek Baraniak[d] and Grzegorz Lota[d]

Received 19th October 2015,
Accepted 3rd February 2016

DOI: 10.1039/c5cp06335c

www.rsc.org/pccp

This paper examines the influence of aprotic solvents on the spectroscopic properties as well as the energy deactivation of two free-base corrole dyes substituted with $C_6F_5$ and/or 4-$NO_2C_6H_4$ groups. Absorption, fluorescence and laser-induced optoacoustic spectroscopy have been used to follow the singlet and triplet states of fluorine corroles belonging to the $A_2B$ and $A_3$ type in toluene (TL), chloroform (CL), dimethylformamide (DMF), dimethyl sulfoxide (DMSO) and also in solvent mixtures. Changes in the absorption and fluorescence spectra are influenced by the type of solvent mixture. The fluorescence behaviors of the two investigated corroles were extremely different – fluorescence of the nitro-corrole in TL is dramatically quenched in the presence of DMF. In contrast, fluorescence quenching of fluorine corroles in DMF–TL mixtures is substantially weakened. Absorption, fluorescence, triplet population as well as singlet oxygen generation parameters are evaluated. The spectral experimental data are supported by quantum chemical calculations – time-dependent density functional theory (TD-DFT) and cyclic voltammetry experiments. The presented results are discussed from a viewpoint of aggregation, tautomerization, and deprotonation effects occurring in the corroles.

## 1. Introduction

Because of their unique properties and abundance, porphyrins have been the most commonly used systems for modeling light-energy harvesting and conversion over the past few decades.[1] Efforts to improve the photophysical properties of porphyrins have encouraged the use of other porphyrinoids such as corroles, a unique family of dyes. Although corroles were first reported several decades ago by Johnson and Kay,[2] they have not been thoroughly investigated due to synthetic challenges. Recent advances in synthetic procedures have improved and advanced corrole chemistry,[3,4] and thus provide a venue for new possible applications.

Corroles are aromatic macrocycles that are analogues to porphyrin dyes, but with one less carbon.[2] They are characterized by the reduced $C_{2v}$ symmetry with regard to the $D_{2h}$ and $D_{4h}$ symmetry of porphyrins due to the absence of one *meso* carbon bridge (direct pyrrole–pyrrole linkage). Consequently, the photophysical characteristics of corroles are different from that of porphyrins including stronger absorption in the red region of the spectrum, greater fluorescence quantum yield, larger Stokes shift, different reactivity and profound differences in coordination chemistry.[2,5–7]

A variety of corroles consisting of different molecular structures and in different solvents[8–14] and in solid matrices[15–18] have been investigated through physical/photophysical and chemical/photochemical experiments to examine their singlet/triplet behavior,[8,19] tautomerization, protonation[11,13,20,21] and interactions with fullerene as an electron acceptor.[18,22–24]

Although the photophysical properties of corroles have been investigated, further studies are needed to make these compounds applicable. In earlier work, our laboratory conducted basic spectral investigations of selected substituted *meso*-corroles and their dyads with fullerene.[21,23,25] In these studies, we discovered that corroles are very good electron donating species when covalently linked to fullerene and provided evidence for their molecular orientation when arranged in solid substrates.[23,25] The influence of solvent polarity on the spectral properties of corroles and the locations of exchangeable

[a] *Faculty of Technical Physics, Institute of Physics, Poznan University of Technology, Piotrowo 3, 60-965 Poznan, Poland. E-mail: danuta.wrobel@put.poznan.pl*
[b] *Institute of Molecular Physics, Polish Academy of Sciences, Smoluchowskiego 17, 60-179 Poznan, Poland*
[c] *Institute of Organic Chemistry, Polish Academy of Sciences, Kasprzaka 44/52, 01-224 Warsaw, Poland. E-mail: dtgryko@icho.edu.pl*
[d] *Institute of Chemistry and Technical Electrochemistry, Poznan University of Technology, Berdychowo 4, 60-965 Poznan, Poland*

† Electronic supplementary information (ESI) available. See DOI: 10.1039/c5cp06335c

protons have been the subjects of a few studies.[5,21,26] However, the question of the protonation and deprotonation effects has not yet been fully resolved although some studies on tautomers of *meso*-pentafluorophenyl-substituted corroles in chloroform have been carried out previously.[21]

In the present study, we focused our attention on the properties of $A_3$-corrole possessing three $C_6F_5$ substituents at *meso*-positions and *trans*-$A_2B$-corrole bearing one 4-$NO_2C_6H_4$ group at position 10. These studies include an investigation of protonation/deprotonation with the use of polar and non-polar solvents and their mixtures. We also provide UV-vis spectra. Moreover, laser-induced optoacoustic spectroscopy (LIOAS) was used for the first time to determine the population of the triplet states, singlet oxygen generation and triplet thermal deactivation. The experimental data are supported by computational calculations *via* time-dependent density functional theory (TD-DFT) to obtain information on the distribution of electron density in the systems.

Computational calculations as well as electrochemical measurements are very important for determining the molecular energy levels of dyes, when embedded in an organic solar cell. The highest occupied molecular orbital (HOMO) and the lowest unoccupied molecular orbital (LUMO) can be determined by means of cyclic voltammetry.[27]

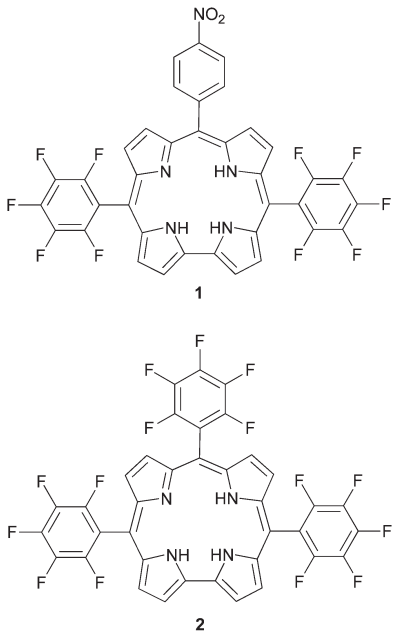


Fig. 1 Molecular structures of investigated corroles.

## 2. Materials and methods

### 2.1. UV-vis absorption and fluorescence

In these studies we present investigations of two free-based corrole dyes 10-(4-nitrophenyl)-5,15-bis(pentafluorophenyl)corrole (**1**) and 5,10,15-tris(pentafluorophenyl)corrole (**2**). The detailed description of the chemical synthesis of dyes was described previously.[28,29] The molecular structures of the dyes under investigations are shown in Fig. 1.

Spectroscopic grade toluene (TL), chloroform (CL), dimethylformamide (DMF) and dimethyl sulfoxide (DMSO) were purchased from POCH Poland S.A. Ground state absorption spectra were monitored using a UV-vis Varian Cary 4000 spectrophotometer in an ES quartz cuvette over the range of 350–700 nm; all measurements were done at room temperature. Fluorescence was measured using a Hitachi F-4500 fluorimeter ($\lambda_{exc}$ = 405 nm). Fluorescence lifetime was obtained using a 1.5 ns pulse, 405 nm LED excitation source. Fluorescence responses were collected over the range of 430–900 nm (excitation and emission spectra).

The fluorescence quantum yields ($\Phi_F$) were determined using the classical formula:

$$\Phi_F = \Phi_{Ref}\frac{F_s(1-10^{-A_r})n_s^2}{F_r(1-10^{-A_s})n_r^2}, \quad (1)$$

where $A$ is the absorbance at the excitation wavelength, $F$ is the area under fluorescence and $n$ is the refraction index. Subscripts r and s refer to the reference and to the sample of unknown quantum yield, respectively. For reference, chlorophyll *a* in methanol was used ($\Phi_{Ref}$ = 0.32).[30] The samples and the reference were excited at the same wavelengths, 405 and 614 nm. Fluorescence lifetimes were estimated by fitting the decay data using a deconvolution procedure based on the EasyLife V software.

### 2.2. Quantum chemical calculations

To improve the interpretation of the experimental UV-vis spectra we performed calculations of the transition energies *via* time-dependent density functional theory (TD-DFT). The chemical calculations were performed using the B3LYP hybrid functional (Becke 3-parameter exchange functional combined with Lee–Yang–Parr correlation functional) and the standard 6-31G basis set. Time dependent DFT calculations were performed using the equilibrium geometries of the molecules obtained from the optimization of the investigated corroles (DFT, B3LYP/6-31G). The influence of solvents (CL, TL and DMSO) was taken into account using the Polarized Continuum Model (PCM) as implemented in the Gaussian 03 program package.[31] The first 200 optical transitions were calculated. To convolute the resulting transition energies and oscillator strengths into the absorption spectra, the GaussSum program was used.[32] The spectra were generated assuming FWHM (Full Width at Half Maximum) parameters at 3000 $cm^{-1}$ for all transitions.

### 2.3. Electrochemical measurements

Cyclic voltammetry experiments were performed using a three-electrode cell: glassy carbon as a working electrode, platinum wire as a counter electrode, and Ag/AgCl as a reference electrode. The working electrode was polished with a suspension of $Al_2O_3$ in water and rinsed in water and acetone under ultrasounds before experiments. Electrochemical measurements were carried out in a solution containing $10^{-5}$ M of examined corroles in methyl alcohol and TL (ratio 1 : 1) as supporting electrolytes.

The electrolyte was purged by nitrogen over 30 min before the test. The potential varied between −3 and 3 V *vs.* Ag/AgCl with a scan rate of 20 mV $s^{-1}$. All electrochemical measurements were performed using the potentiostat/galvanostat VSP (BioLogic, France) equipped with a low current module.

The experiments were performed without and with illumination using a xenon 150 W lamp.

### 2.4. LIOAS studies

To obtain additional information on the influence of the photophysical properties of corroles and the nature of the solvent on photothermal parameters, time-resolved photothermal signals were recorded using the LIOAS method. Specific details of LIOAS apparatus have been described by other groups.[26,33,34] For LIOAS experiments, corrole dyes are dissolved in CL, TL, DMF, and DMSO respectively. Ferrocene (FC), purchased from Sigma-Aldrich, and Ni-substituted pheophytin *a*[35] were chosen as calorimetric references due to their suitable spectral properties for LIOAS experiments. All measurements were carried out at ambient temperature, in air and in an argon atmosphere. The excitation wavelengths were 405 nm or 614 nm; the absorbance of the corrole was equal to 0.1 at the excitation wavelength.

The analysis of the LIOAS waveform was carried out according to the methods of Marti *et al.*[36] In this approach, the first maximum ($H_{max}$) of the LIOAS signal is expressed as

$$H_{max} = k\alpha^{air}E_{h\nu}(1 - 10^{-A}), \quad (2)$$

where $k$ is a proportionality factor that regards geometry and electric impedance of a device, $\alpha^{air}$ is a part of the energy changed into heat in an air atmosphere (in time shorter than a time resolution of the apparatus), $A$ is the absorbance of a sample and $E_{h\nu}$ is the molar energy of incident photons (295.3 kJ $mol^{-1}$ at 405 nm and 194.8 kJ $mol^{-1}$ at 614 nm).

Part of the excitation energy exchanged into heat promptly ($\alpha$ parameter) and was calculated by a direct comparison of the slopes in the linear region of the plots obtained for the corrole and for the reference dye in argon and air.[37]

The quantum efficiency of the triplet state population ($\Phi_T$) could be evaluated using the following equation:

$$E_T\Phi_T = E_{h\nu}(1 - \alpha^{Ar}) - E_S\Phi_F, \quad (3)$$

where $\alpha^{Ar}$ is the fraction of excitation energy exchanged into heat promptly in an argon atmosphere (in time shorter than a time resolution of the apparatus), $E_S$ is the energy of the singlet state in [kJ $mol^{-1}$], $E_T$ is the energy of the triplet state and $\Phi_F$ is the quantum yield of fluorescence (Table 1). However, we do not know the exact value of $E_T$ for the examined samples, therefore the $\Phi_T$ parameter can only be estimated based on $E_T\Phi_T$.

The efficiency of singlet oxygen generation ($\Phi_\Delta$) can be evaluated from the following equation:

$$\Phi_\Delta = \frac{E_{h\nu}}{E_\Delta}(1 - \alpha^{air}) - \frac{E_S}{E_\Delta}\Phi_F, \quad (4)$$

where $E_\Delta$ is the energy of the oxygen singlet state ($E_\Delta$ = 94 kJ $mol^{-1}$).

## 3. Results and discussion

### 3.1. Electronic absorption experiments in solvents and their mixtures

Both studied corroles showed good solubility in many organic solvents, particularly in TL, CL, DMF, and DMSO. The molecular structures and ground state electronic absorption spectra of 10-(4-nitrophenyl)-5,15-bis(pentafluorophenyl)corrole (**1**) and 5,10,15-tris(pentafluorophenyl)corrole (**2**) in TL, DMF and DMSO (concentration $10^{-4}$–$10^{-6}$ M) are shown in Fig. 1 and 2, respectively.

The concentration of the sample had a marked effect on the absorption spectra of corrole **2** in DMSO as indicated by a blue shift in the wavelength maximum and the appearance of a shoulder peak at higher concentrations of **2** (Fig. 2, panel F); no such remarkable effects were observed in the spectra of **2** in TL and DMF (Fig. 2, panels B and D). Even though corroles are closely related to porphyrins, their absorption spectra have distinct differences: their absorption spectra are dominated by π–π* transitions with an intense and broad Soret band and a much lower intensity Q band.

We previously reported the assignment of the π–π* electron transition in the Soret and Q bands of these corroles dissolved in CL.[21] The presence of the tautomeric T1 and T2 forms of the investigated corroles was clearly evident in the Soret regions as a broad band (sample **1**; Fig. 2A) at 424 nm and more or less split bands (samples **1** and **2**; Fig. 2B–F) with the maxima at 412–434 nm, depending on the dye. Some changes were also observed in the Q region of the spectra. No particular changes in

Table 1 The optical parameters, absorption and fluorescence parameters of corroles **1** and **2** in selected solvents; FWHM – full width at half maximum (calculated with the Gaussian component program) $\Phi_F$ – fluorescence quantum yield, $\tau$ – fluorescence life time

| Solvent | $\varepsilon$ | $D$ | Dye | Soret FWHM [$cm^{-1}$] | Major contribution | $\Phi_{F(405)}$ | $\Phi_{F(614)}$ | $\tau$ [ns] |
|---|---|---|---|---|---|---|---|---|
| TL | 2.38 | 0.36 | **1** | 2903 (conc. $10^{-4}$–$10^{-6}$ M) | Fb/mesomeric effect | 0.10 | 0.08 | 6.15 ± 0.04 |
| | | | **2** | 2126 (conc. $10^{-4}$–$10^{-6}$ M) | Fb | 0.10 | 0.08 | 6.21 ± 0.02 |
| DMF | 37 | 3.8 | **1** | 2230 (conc. $10^{-4}$–$10^{-6}$ M) | Mesomeric effect/deprotonated | <0.01 | <0.01 | — |
| | | | **2** | 1523 (conc. $10^{-4}$–$10^{-6}$ M) | Deprotonated | 0.36 | 0.36 | 5.12 ± 0.06 |
| DMSO | 46.7 | 3.9 | **1** | 2465 (conc. $10^{-4}$ M)<br>2219 (conc. $10^{-5}$–$10^{-6}$ M) | Mesomeric effect/deprotonated | <0.01 | — | — |
| | | | **2** | 2323 (conc. $10^{-4}$ M)<br>1363 (conc. $10^{-5}$–$10^{-6}$ M) | Deprotonated | 0.48 | — | 5.33 ± 0.28 (4.45%)<br>0.37 ± 0.07 (95.55%) |

$\varepsilon$ – dielectric constant, $D$ – dipole moment [Debye], Fb – free base corrole.

 

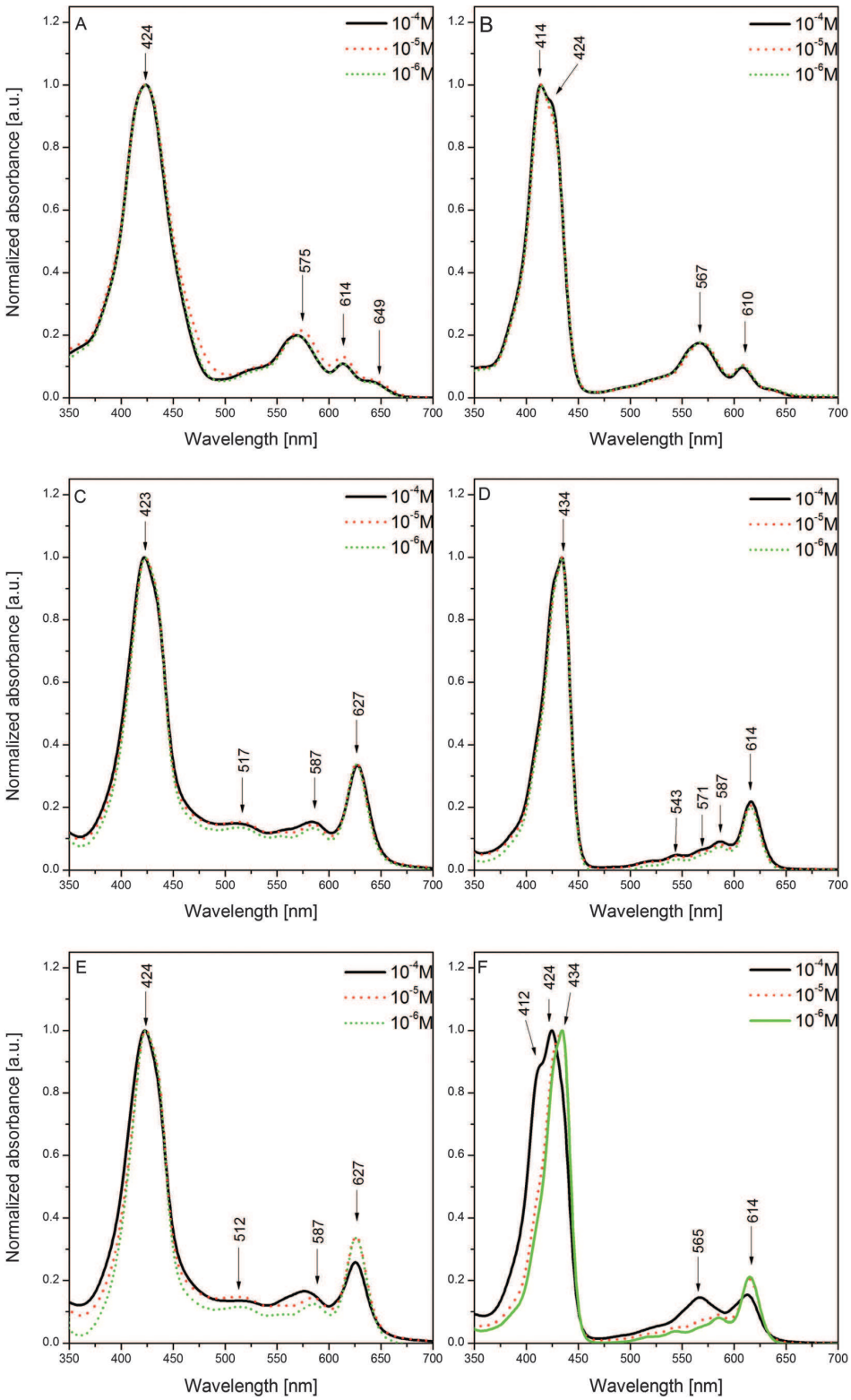


Fig. 2 Absorption spectra of corroles **1** (panels at left) and **2** (panels at right) in TL (A and B), DMF (C and D) and DMSO (E and F); concentration range $10^{-4}$–$10^{-6}$ M. The absorption spectra were normalized to unity at the highest Soret band (424 nm).

the absorption spectra were observed for the samples at different concentrations thus showing the dominance of the tautomers' monomeric forms up to $10^{-4}$ M (except for **2** – Fig. 2F). Solvent properties often cause π–π* dyes to associate into dimers (J and H dimers)[38] or higher aggregated forms which show smaller or larger wavelength shifts. The best example of dimer formation is chlorophyll (Chl)[30] which is a metallic coordinated porphyrin-like pigment. Chlorophyll dimers can be formed *via* direct or indirect interaction between the magnesium of one Chl and an electron donating group of another molecule. However, in our studies, we used non-metallic free-based corroles without metal ions in the main molecular core, pheophytin (Pheo). Pheo is also able to make dimers and its dimerization can occur *via* π–π* interaction at adequately high concentration. Thus, on the basis of behavior of the natural pigments and of other synthetic porphyrin-like molecules,[39–41] one can suppose the presence of poorly defined molecular aggregates; furthermore, this phenomenon cannot be excluded in highly concentrated samples.

DMSO had a great influence on absorption with sample **2**. DMSO was the most polar solvent ($\varepsilon$ = 46.70) that was tested (DMF ($\varepsilon$ = 37), CL ($\varepsilon$ = 4.80) and TL ($\varepsilon$ = 2.38)). A highly concentrated solution of corrole **2** in polar DMF did not show notable changes when compared to the same corrole dissolved in DMSO. However, it is worth noting that most molecular aggregates are not created in polar solvents since polar solvents protect molecules against aggregate formation due to solvation.

The formation of aggregated forms of corroles addresses the phenomena of tautomerization, protonation/deprotonation, and distortion of the pyrrole ring. Solvent effects are evident in our absorption studies (Fig. 2A–E as compared to Fig. 2F). The shape of absorption bands differs mainly in the Soret region of **1** and **2** and the Q region of **2**. This observation can be attributed to differences in the molecular structure of **1** *versus* **2**, for example, the presence of a nitro substituent group (in **1** – $A_2B$ type tautomer) and a pentafluorophenyl substituent (in **2** – $A_3$ type tautomer).

Tautomers T1 and T2 are difficult to distinguish in **1** (in TL – in Fig. 2A) because of their very similar energies. Otherwise, the bands in the Soret peak are clearly visible in the highly concentrated sample **2** in DMSO (Fig. 2F) – the bands with the maxima at 412 and 424 nm ($10^{-4}$ M) are well separated (*versus* the Soret bands in the remaining spectra). This observation could originate from two sources: (i) a change in the relative amounts of T2 and T1, giving rise to varied band intensities at 412, 424, 434 nm, and (ii) the process of deprotonation, resulting in the short wavelength shift of the Soret band of different energies.[9,13,21] In an earlier report,[20] a deprotonation effect was observed in polar DMSO.

We also recorded the absorption spectra of the corroles in mixtures of polar (DMF) and non-polar (TL) solvents (Fig. 3). These studies further confirmed a strong effect of solvents on dye behavior. Differences in the shapes and intensities were obvious in the Soret regions and in the Q bands of **1** and **2**. The most dramatic changes were observed in the Q region of **1** and **2** and also of **2** in the Soret region. The differences in the

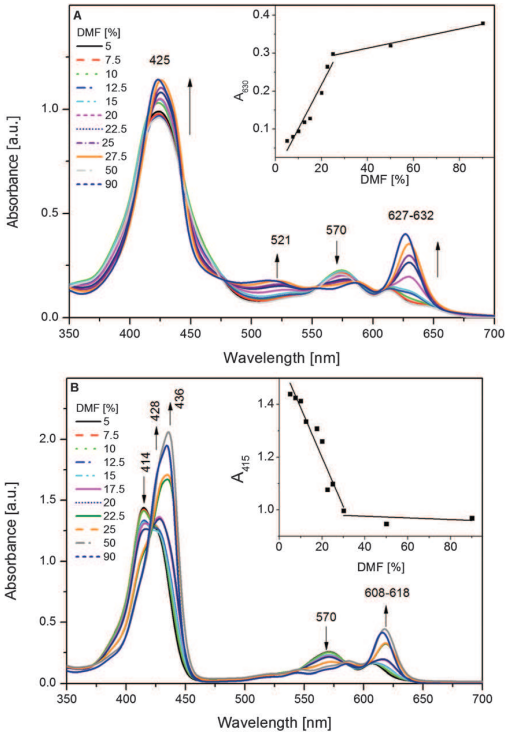


Fig. 3 Absorption spectra of corroles **1** (A) and **2** (B) in DMF and TL mixtures; concentration $10^{-5}$ M. Titration curve for corrole **1** (insert) and corrole **2** (insert).

absorption spectra in the presence of different solvent ratios could be related to the dyes' molecular structures since the substituents in **1** and **2** are structurally different (nitrophenyl and pentafluorophenyl groups). Moreover, the asymmetry in the pyrrole-rings could result in replacing the –NH groups around the main π-core ring, leading to changes in the equilibrium of tautomers T1 and T2;[9] in 100% TL *versus* 100% DMF, the changes in T1 and T2 were evident from the shift of the Soret band towards the longer wavelength, from 414 to 436 nm for **2**. Such an observation is characteristic of a deprotonated corrole.[14] The existence of the deprotonated form of corrole **2** is further confirmed by the appearance of a species with a higher intensity at a longer wavelength, the 0–0 transition with the maximum at 620 nm. In the case of **1**, a bathochromic shift was not observed in the Soret region.

Titration curves (inserts in Fig. 3) showed two stages in the reactive kinetics. The changes in the absorbance value are about 85% in sample **1** (Q band region) and about 93% in sample **2** (Soret region). The distinct changes in band shapes that occurred after the addition of DMF to TL indicated a very strong polar influence of DMF on processes occurring in the dyes. TL is a non-polar solvent, while DMF is a polar-aprotic solvent and their dipole moments are quite different (0.36 D of TL *versus* 3.82 D of DMF). Consequently, the interaction between the corrole and the TL is different compared to the dye and the DMF. The changes in the spectra of the corroles could

 

indicate the formation of aggregates however our previous absorption results and literature data[21] exclude this possibility. Although tautomerization could contribute to alternation of the spectra, our earlier papers[9,10] indicated that tautomerism is a rather weak phenomenon. One of the arguments supporting the slight influence of tautomerization[9,10,21] is the similar energy of both tautomers. A third possibility, from Ding *et al.*,[9] suggested that hydrogen bonding with the –NH group could cause changes in the structure of the molecules that are solvent-dependent. Similar effects were observed in porphyrins in apolar solvents.[42,43] The hydrogen linkage between NH and a solvent molecule was also observed in corroles[44] producing changes in the photophysical properties. Resonance effects related to the electron-withdrawing or electron-donating properties of substituents should also be considered. The changes in the absorption spectra of polar solvents (DMF and DMSO) can also be discussed in terms of a mesomeric effect as shown for a phthalocyanine substituted with fluorine groups.[45]

Based on our experiments on the TL–DMF mixtures and the results presented in other papers,[9,10] we believe that deprotonation is the key influence on the absorption behavior of samples **1** and **2** in the presence of the aprotic solvent DMF.

### 3.2. Fluorescence studies

We acquired the excitation and emission spectra of corrole **2** ($10^{-5}$ and $10^{-6}$ M) in DMSO (Fig. 4A and B). Using DMSO as a reference solvent allowed us to measure the effect of solvents with high polarity and to avoid (or to minimize) molecular aggregate formation. Only corrole **2** in DMSO showed strong fluorescence with maxima at 621–625 and 674 nm (Fig. 4). A similar behavior had also been observed for other corroles.[8,20,46,47] The dominant fluorescence peak was assigned to emission of tautomer T1; the much less intense shorter wavelength humps can have their origin in the fluorescence of T2.[48,49] The fluorescence excitation spectra, when observed at 700 nm, were consistent with the UV-vis absorption spectra. The details of the fluorescence character of the corroles in non-polar CL have been discussed in our previous paper[21] thus we will present the fluorescence spectra of the TL–DMF mixtures of different DMF contribution (%) as shown in (Fig. 5 and 6).

The fluorescence spectra of **1** and **2** (shown in Fig. 4 and 5) differed markedly in their intensity, peak shapes, and location of the maxima. It is well known that the presence of nitro groups typically quenches the fluorescence of organic compounds to the level below the detection limit.[50] Accordingly we observed that the fluorescence quantum yield of corrole **1** is much weaker than that of corrole **2** in TL (Table 1). The $\Phi_F$ value is larger (0.1) compared to the vast majority of known organic dyes of the same family. Furthermore, significant quenching of the fluorescence signal ($\sim$750-fold) was observed for corrole **1** after the addition of DMF to TL. As the more DMF was added, the stronger quenching was observed, the rate of fluorescence quenching at 658 nm is presented in Fig. 5B. Furthermore, the fluorescence bands shifted to shorter wavelengths (from 658 to 624 nm). In corroles and other porphyrin-like dyes, the macrocyclic π-electrons are involved in the fluorescence process. The lack of

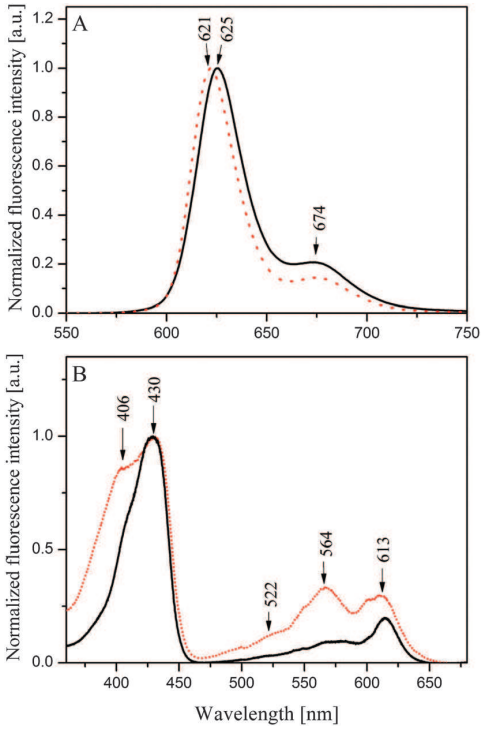


Fig. 4 Fluorescence spectra of corroles **2** and their excitation emission spectra in DMSO normalized at the maximal bands; (A) $\lambda_{exc}$ = 405 nm, (B) $-\lambda_{obs}$ = 700 nm. Concentrations $10^{-5}$ M (dotted red) and $10^{-6}$ M (straight black) were used. The spectra are normalized with respect to the most intense peak.

(or minimal) fluorescence of sample **1** in the presence of DMF can be attributed to the relocation of the majority of the electron density cloud from the macroring and from the nitro group – nitro substituents have a strong electron withdrawing character as shown in Fig. 8. This behavior can only be explained by considering molecule **1** as a conjugated donor–acceptor (D–A) system with the 4-$NO_2C_6H_4$ group acting as an electron acceptor and the corrole core acting as an electron donor. Although the dihedral angle between the corrole core and the benzene ring at position 10 is large (possibly $\sim 68^\circ$)[44] it can still provide means for strong interaction of both moieties. The decrease of fluorescence quantum yield while moving towards polar solvents is a well-known phenomenon for polarized D–A compounds.[50]

Corrole **2** is substituted with $C_6F_5$ groups exclusively and behaves differently. Moreover, the Stokes shifts of the bands with respect to transitions at 658 nm (sample **1**) and at 628–645 nm (sample **2**) were about 20–30 nm, indicating strong deprotonation, mostly observed for the T2 tautomer. The changes in the fluorescence band locations in the TL–DMF mixture can be clearly seen in the inset of Fig. 5, an enlargement of the fluorescence spectra. The band maxima of fluorescence in TL–DMF for dye **1** occur at 658 and 624 nm for a low concentration of DMF (to 30%); the emission maxima or a hump appear in the

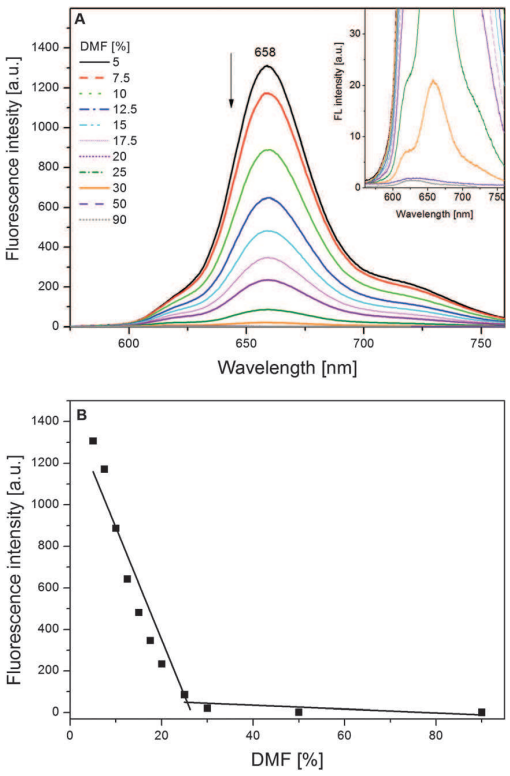


Fig. 5 Fluorescence (A – $\lambda_{exc}$ = 405 nm) in DMF–TL mixture, the same spectra in the enlarged scale (insert); and titration curve (B).

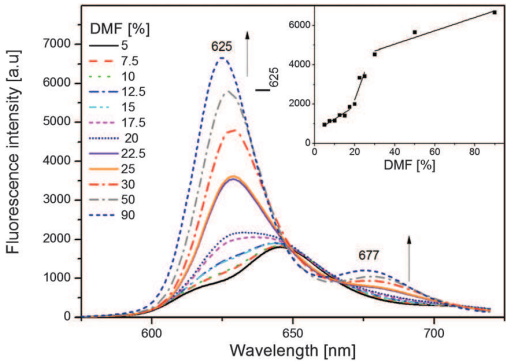


Fig. 6 Fluorescence ($\lambda_{exc}$ = 405 nm) spectra of corrole **2** in the DMF–TL mixture. The titration curve for corrole **2** (insert).

spectra of **1** and are assigned to T1 and T2 emission, respectively. In solvent ratios of 50/50, 90/10 and 100/0, an emission peak at 639 nm originated from the T2 tautomer (the band at 658 nm is actually not seen).[11,21]

In contrast, the influence of the TL–DMF solvent on sample **2** fluorescence was opposite, and quenching by DMF was not observed. The band shapes and main band shifting (from 645 to 624 nm – (0/100)) were nearly unchanged upon the addition of more DMF to the solvent mixture. However, the band shifts

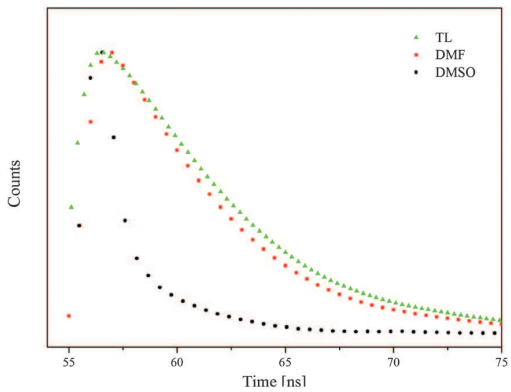


Fig. 7 Fluorescence kinetics of **2** in TL, DMF and DMSO (concentration $10^{-5}$ M); $\lambda_{exc}$ = 405 nm.

towards the higher energy part of the spectrum indicating deprotonation of the corroles. Nevertheless, upon the addition of DMF, a large increase in fluorescence was observed (Fig. 6), supporting a very strong effect of DMF on tautomer T2 fluorescence.

The lack of notable changes in the band shapes upon the addition of DMF to TL was a strong indicator of the negligible influence of DMF on the processes occurring in the corrole dyes. Similar fluorescence behavior has been observed by Kruk *et al.*[20,46] for other NH *meso*-dichloropyrimidinyl corrole tautomers. In their work, the T2 tautomer emission was also intense. Fluorescence studies also confirmed the deprotonation process, as exhibited in sample **2** (the fluorine corrole) in DMSO.

The fluorescence kinetics curves for **2** in different solvents are shown in Fig. 7. The evaluated lifetime values (Table 1) ranged from 5.12 to 6.21 ns (depending on the dye) and are characteristic of porphyrin-like dyes. They confirm the monomeric corrole emission in corroles **1** and **2** in TL and DMF. The deconvolution procedure used in our evaluation gave the typical mono-exponential fluorescence decay curves in TL and DMF in the range of $10^{-4}$–$10^{-6}$ M. However, we were not able to recognize the life times of tautomers T1 and T2. The values of fluorescence quantum yields (Table 1) were markedly different when one compares the results of samples **1** and **2** in TL (0.07–0.10) *versus* those in polar DMF (0.32–0.34) and in DMSO (0.47). In **1**, strong fluorescence quenching was evident (in both DMF and DMSO) – the $\Phi_F$ and $\tau$ values dropped dramatically, almost to zero (see Table 1). The bi-exponential decay observed for sample **2** in DMSO may indicate the presence of emission of two tautomers with different lifetimes.

### 3.3. Quantum chemical calculations

To improve the interpretation of the experimental UV-vis spectra, we calculated the transition energies *via* TD-DFT. We then compared the absorption and fluorescence spectra with the TD-DFT results and the HOMO/LUMO states. In our previous paper[21] we presented the TD-DFT results of the isolated corroles **1** and **2**. Here, we have extended TD-DFT calculations for these corroles in TL, CL and DMSO.

 

Table 2 The TD-DFT calculated values of the molecule dipole moment (in Debye units) and the HOMO and LUMO energies (in eV) of investigated corroles

| | Corrole **1** | | | | Corrole **2** | | | |
|---|---|---|---|---|---|---|---|---|
| Solvent | Dipole moment | HOMO | LUMO | $\Delta_{H-L}$ | Dipole moment | HOMO | LUMO | $\Delta_{H-L}$ |
| None | 6.3172 | −5.58 | −3.13 | 2.45 | 3.7685 | −5.63 | −3.10 | 2.53 |
| TL | 7.4079 | −5.39 | −3.07 | 2.31 | 4.5052 | −5.47 | −2.94 | 2.53 |
| CL | 8.0358 | −5.31 | −3.07 | 2.23 | 4.9068 | −5.39 | −2.83 | 2.56 |
| DMSO | 8.7525 | −5.22 | −3.10 | 2.12 | 5.3455 | −5.31 | −2.78 | 2.53 |

Table 2 illustrates the solvent influence on the calculated energy levels of the frontier molecular orbitals of corroles **1** and **2**. Increasing the relative permittivity of the solvent increased the energy levels. In **2**, both HOMO and LUMO energy increased with the increase in solvent permittivity. Consequently, the energy gap between the HOMO and the LUMO remained constant (2.53 eV). Corrole **1** showed a slightly different behavior. The HOMO level increased, the LUMO level did not change much thus decreasing the HOMO–LUMO energy gap in **1** from 2.45 eV (for isolated corrole) to 2.12 eV (for solution in DMSO). This outcome suggested that corrole **1** is susceptible to solvent effects. The reduction of the energy gap caused by the solvent was also observed by Panda *et al.*[51] for the $A_2B_2$ type porphyrin derivatives. However, these investigators reported that the direction of the changes in the HOMO and LUMO energy levels were opposite (decrease of the orbital energy in solvent). The influence of the solvent on the energy levels of **1** appeared not only in energy values but also in the localization of the molecular orbital. For isolated **1**, the HOMO was localized on the corrole ring while the LUMO was on the corrole ring and partially on the nitro substituent.[21] For **1** in solution (in all the considered solvents), the localization of the HOMO was similar and the LUMO was localized on the nitrophenyl (in DMSO – Fig. 8A) and on both the nitrophenyl substituent and partially on the corrole ring in TL (Fig. 8C). Compound **2** did not exhibit such behavior, indicating that the position of the orbital is solvent-independent (Fig. 8B and D).

The π-electrons in the corrole macrorings are responsible for fluorescence. Taking into account the HOMO–LUMO results presented in Fig. 8, it is evident that a high density of electrons is localized on the 4-$NO_2C_6H_4$ substituent and very slightly on the core ring in corrole **1**. The weak fluorescence of sample **1** may be caused by relocation of the majority of the electron density cloud from the macroring to the nitrophenyl group upon excitation at the LUMO level. This is not the case for **2**, which is substituted with the fluorine groups.

The question now arrives as to the fluorescence of **1** in TL. There were a few examples presented in papers[52,53] showing fluorescence quenching of dyes due to the electron withdrawing character of the nitro group introduced to the maternal dye. On the other hand, it was evidently shown how much the fluorescence of dyes with the nitro group is affected by the molecular dye structure, solvent, the type of substituent linked to dye molecules and the location of a substituent. Many authors have shown quenched fluorescence in dyes containing nitro-groups.[50] There are some evidences presenting how the location of the nitro-substituent can influence dye emission behavior.[52–55] The nitro group is one of the most electrophilic moieties and shows electron deficiency. This group is known as a substituent with the negative mesomeric effect, relatively to the $sp^3$ carbon. However, one also has to take into account the asymmetry in the location of the NH group in the macrocycle. The presence of the three NH groups leads to the asymmetry of the electron density distribution on the pyrrole rings which is evidenced by our TD-DFT results of **1** in TL and shown in Fig. 8C – a high density of electrons is predominantly localized in the nitro group and also partially in the core ring in sample **1** in the LUMO state. Moreover, one cannot exclude the influence of the two

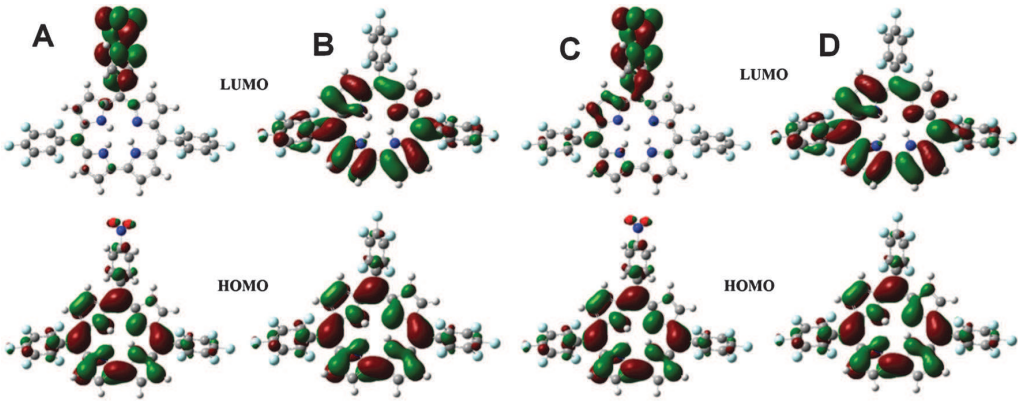


Fig. 8 The contour plots of the TD-DFT calculated frontier molecular orbitals of corrole **1** (A and C) and **2** (B and D); A, B in DMSO; C, D in TL (T2 tautomer).

$C_6F_5$ being near the core π-electrons thus changing the electron density in corrole **1**. Therefore, we have come to the conclusion that the weak fluorescence of sample **1** originates from the π-electron redistribution in the corrole macroring resulting from the NH asymmetry in the presence of fluorine-groups.

The TD-DFT calculated spectra (Fig. 9) of the investigated corroles showed that in the presence of solvents, theoretical calculations showed increased intensity and a red shift in the absorption bands. This result is quite similar to those obtained by Panda *et al.*[51] for porphyrins, where the bands in the calculated solution spectra were also increased and red-shifted in comparison to the gas phase result. A closer look at the transitions involved in the computation of absorption bands revealed that the Soret band in the isolated **2** consisted of three main transitions below 400 nm. The solution spectra show that two bands increased significantly and moved above 400 nm (Fig. 9, right). A similar behavior was observed for the Q band region and the differences between the corrole-solution spectra in TL, CL and DMSO were relatively small. Corrole **1** showed stronger effects – the Soret band behavior was similar to that of **2** (increasing, red-shifted transitions), but the Q band region was different. For the isolated **1** the Q band consisted of four transitions. These transitions not only increased and red-shifted in the corrole-solution spectra, but their shifts and intensities were solvent-dependent. The energetically lowest transitions in the corrole-solvent spectra were observed at 626, 657, and 691 nm for the corroles in TL, CL, and DMSO respectively. Appropriate transitions in the corrole-solution spectra of **2** showed a very small blue shift with increased solvent permittivity (553, 552, 551 nm for TL, CL and DMSO respectively). Major contributions of the calculated transitions are collected in Tables S1 (for **1**) and S2 (for **2**) (ESI†). We observed a completely different behavior for corroles **1** *versus* **2**. For corrole **2**, the dominant contribution (36%) in the mentioned first transition was H−1 → LUMO while the rest of the transition involves other orbitals including the HOMO → LUMO transition (25%). This situation changes when we consider the presence of solvent – the contribution of the HOMO → LUMO transition became dominant and increased up to 50% for **2** in DMSO. Corrole **1** also showed a complex composition of the first transition for the isolated molecule – the dominant contribution was HOMO → L+1 (53%) while the contribution of HOMO → LUMO was similar to that for **2** (22%). However, the influence of the solvent caused the first transition in **1** in the presence of solvents to be almost the pure HOMO → LUMO (89–94%) and the remaining contributions were much less significant. As a consequence, the calculated solution spectra of **1** showed more differences in comparison to the spectra of the isolated species, as compared to corrole **2**. The detailed data of the theoretical calculations are gathered in Tables S1 and S2 (ESI†).

### 3.4. Electrochemical experiments

Cyclic voltammetry is an electrochemical method that provides information on the oxidation and reduction processes of the compounds. It can also be used for the estimation of the HOMO and the LUMO. The oxidation process is associated with the removal of an electron from the HOMO level; on the other hand,

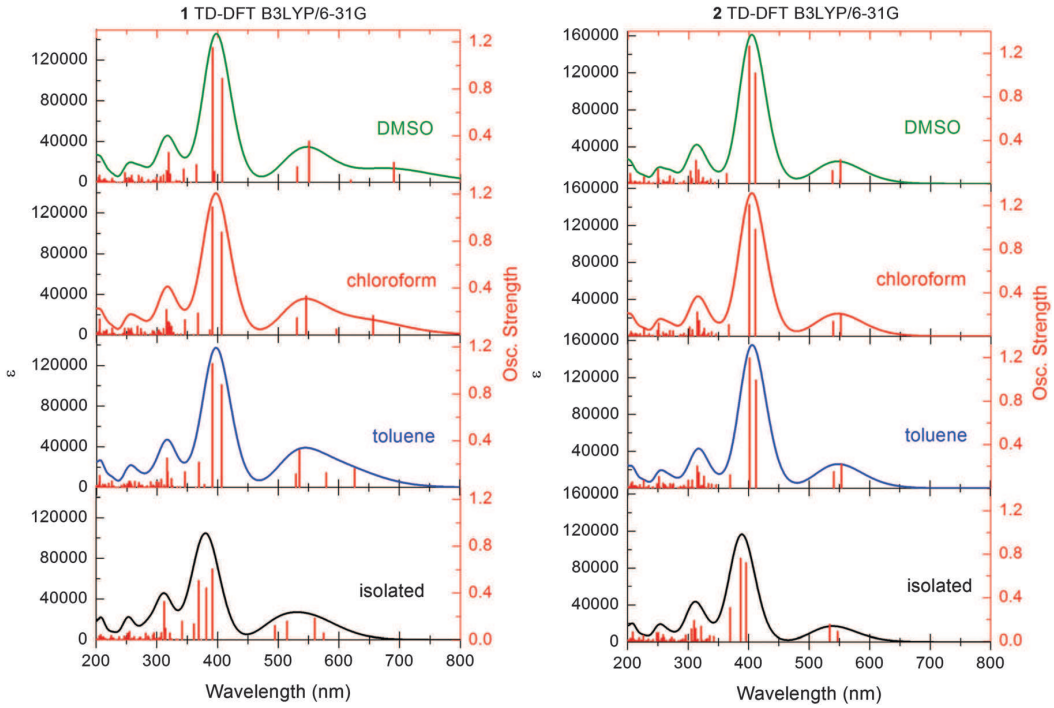


Fig. 9 The TD-DFT calculated electronic transitions (oscillator strengths *versus* wavelength) of corroles **1** (left side) and **2** (right side) together with the convoluted UV-vis spectra.

 

the reduction process corresponds to an electron being located at the LUMO level. This means that, the HOMO/LUMO can be determined on the value of first oxidation and on the value of the first reduction electrochemical potentials. The mathematic equation according to the HOMO/LUMO energy level and electrochemical potential (for Ag/AgCl reference electrode) is:

$$E_{\mathrm{HOMO,LUMO}} = -(E_{\mathrm{OX/RED}} + 4.4)\ \mathrm{eV} \quad (5)$$

where $E_{\mathrm{OX}}$ and $E_{\mathrm{RED}}$ are the onset potentials of oxidation and reduction, respectively. The onset potentials of oxidation and reduction were specified from tangents being intersected between the peak and the baseline.[56–60]

Fig. 10 shows the results of cyclic voltammetry measurements. The onset potentials of the oxidation of corroles were observed at about 1.1–1.2 V, while the reduction potentials were −0.8 and −1.0 V for corroles **1** and **2**, respectively. Based on eqn (5), the HOMO/LUMO energy levels were calculated and summarized in Table 3. It can be concluded that corrole **1** is characterized by a lower LUMO energy value. It means that corrole **2** is a better electron acceptor than corrole **1**.[58] The TD-DFT calculated values of the HOMO and LUMO levels (Table 2) are in quite good agreement with the values obtained from the electrochemical studies. All the energy levels are slightly overestimated and the difference is bigger for the LUMO levels. However, the relation between the results obtained for corrole **1** and **2** from both methods (TD-DFT and cyclic voltammetry) is preserved, it can be seen in the mutual positions of HOMO and LUMO levels in both corroles, and in the size of the HOMO–LUMO energy gap (smaller for corrole **1**).

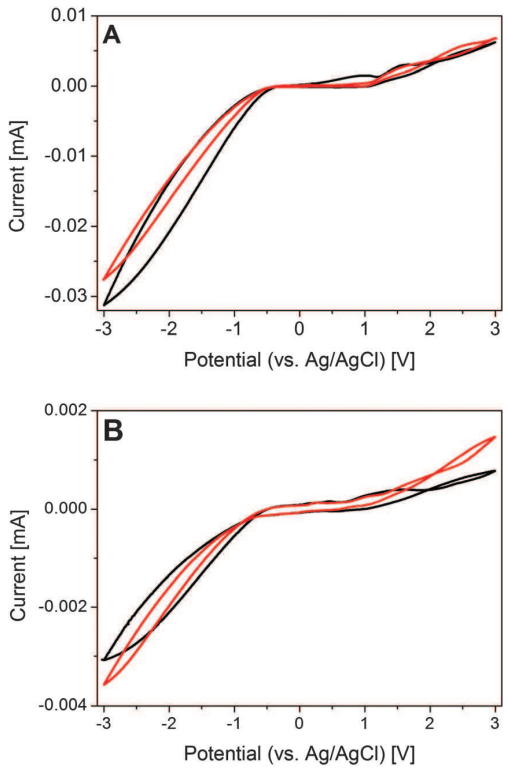


Fig. 10 Cyclic voltammetry of corrole **1** (A) and corrole **2** (B) in TL, in the dark (black lines) and under illumination (red lines).

Table 3 The potential of oxidation and reduction and HOMO and LUMO energies (in eV) of the tested corroles calculated from cyclic voltammetry measurements

| Sample | $E_{\mathrm{ox}}$ [V] | $E_{\mathrm{red}}$ [V] | HOMO [eV] | LUMO [eV] | $\Delta_{\mathrm{H-L}}$ [eV] |
|---|---|---|---|---|---|
| TL 1 | 1.1 | −0.8 | −5.50 | −3.6 | 1.90 |
| TL 1 light | 1.1 | −0.9 | −5.60 | −3.5 | 2.10 |
| TL 2 | 1.1 | −1.0 | −5.50 | −3.4 | 2.10 |
| TL 2 light | 1.25 | −1.2 | −5.65 | −3.2 | 2.45 |

It is worth mentioning that during illumination, the energy gap increases in the case of corroles **1** and **2**. However, a clearer enlargement of the energy gap after illumination using a xenon lamp was observed for corrole **2**. Under lighting an electron can be excited from the HOMO to the LUMO level only if the ionization potential difference between the donor and the acceptor affinity is larger than the binding energy of the exciton (electron–electron hole system). Moreover, under illumination the HOMO energy level decreases, but the LUMO energy level increases. Therefore, the energy gap increases after lighting.[27]

The functionalization of corroles strongly influences the properties of the macrocycle; therefore, a detailed analysis is essential due to a practical point of view. From cyclic voltammetry measurements, it can be seen that the reduction potential is equal to −0.8 V and −1.0 V for corrole **1** and corrole **2**, respectively. It can be stated that $-NO_2$ groups are electron-withdrawing species, which provide the reduction processes to a more positive value of potential. Corrole rings because of high electron density can operate as a donor, on the other hand $-NO_2$ substituents can act as an acceptor, resulting in a lower energy of the LUMO level.[61–63]

### 3.5. Laser induced optoacoustic spectroscopy (LIOAS) experiments – triplet state studies

The activation and deactivation of the triplet state of corroles **1** and **2** were investigated by LIOAS experiments. LIOAS was used

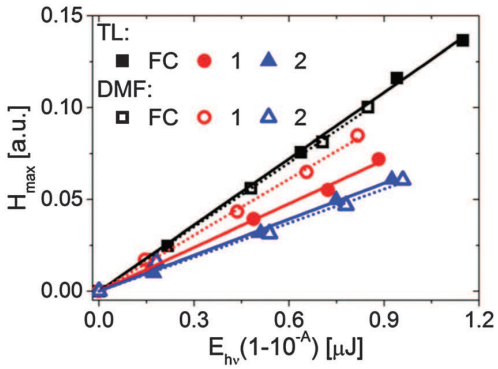


Fig. 11 LIOAS signal $H_{\mathrm{max}}$ of sample **1** (red), **2** (blue) and ferrocene (black) in TL (closed symbols) and in DMF (opened symbols) as a function of the laser energy $E_{h\nu}$; $\lambda_{\mathrm{exc}}$ = 405 nm; $R^2 \geq 0.99$.

Table 4 LIOAS parameters for sample **1** and **2** in solvents. $E_T\Phi_T$ and $\Phi_\Delta$ are calculated based on eqn (3) and (4)

| | $\alpha^{Ar}$ (±0.05) | | $E_T\Phi_T$ [kJ mol$^{-1}$] (±6 kJ mol$^{-1}$) | | $\alpha^{air}$ (±0.05) excited at 405 nm/614 nm | | $\Phi_\Delta$ (±0.05) excited at 405 nm/614 nm | |
|---|---|---|---|---|---|---|---|---|
| Solvent | **1** | **2** | **1** | **2** | **1** | **2** | **1** | **2** |
| DMSO | 0.77 | 0.48 | 65 | 60 | 0.86 | 0.56 | 0.41 | 0.41 |
| DMF | 0.82 | 0.47 | 51 | 88 | 0.86/0.60 | 0.53/0.41 | 0.41/0.81 | 0.75/0.49 |
| CL | 0.76 | 0.55 | 64 | 115 | 0.85 | 0.61 | 0.42 | 1.03 |
| TL | 0.65 | 0.52 | 86 | 124 | 0.66/0.52 | 0.61/0.50 | 0.86/0.84 | 1.02/0.88 |

for the first time to evaluate the triplet state population and determine $\Phi_\Delta$ in corroles **1** and **2**. Fig. 11 illustrates the relation between the $H_{max}$ of sample **1** and **2** in TL and DMF as a function of energy ($E_{h\nu}$) applied by a 405 nm laser.

The LIOAS results of corroles **1** and **2** in TL, CL, DMF and DMSO are collected in Table 4. $\alpha^{air}$ and $\alpha^{Ar}$ present the part of energy exchanged to heat promptly in the time shorter than the time resolution of the used device. The $\alpha^{air}$ and $\alpha^{Ar}$ values for samples **1** and **2** were dependent on the solvents used in the experiments. The $\alpha^{air}$ values were about 0.66–0.86 (sample **1**) and 0.53–0.61 (sample **2**) in TL, CL, DMF and DMSO when excited at 405 nm. When excitation was at 614 nm, their values were lower, ranging from 0.41 to 0.61. The variations in $\alpha^{air}$ can originate from the different contributions of tautomers T2 and T1 in energy deactivation. The 405 nm laser beam excites mostly tautomer T2, resulting in T2 participation in thermal deactivation. In contrast, when 614 nm light was used in the experiment, tautomer T1 was mostly excited and it contributed to light energy conversion. The yield of the triplet population, expressed as the $E_T\Phi_T$ values, was also dependent on the type of solvent used: they ranged from 51 to 86 kJ mol$^{-1}$ for sample **1** and 60–124 kJ mol$^{-1}$ for sample **2** in all used solvents.

An evaluation of the LIOAS data in the context of the fluorescence results can provide insights into the thermal deactivation processes in which the singlet and triplet states of the corroles are involved. The observed intensity of corrole emission competes with the processes of the internal conversion $S_1$–$S_0$ (IC). The emission of corroles in the present study was affected by DMF and DMSO – sample **1** fluorescence was strongly quenched while that of sample **2** was not. Moreover, $\alpha^{Ar}$ is higher for sample **1** in comparison to sample **2**, thus, we cannot suppose higher intersystem crossing quantum yields in **1** *i.e.* population of the triplet state.

The $\Phi_\Delta$ values were also evaluated (Table 4). The process that is responsible for singlet oxygen formation is the interaction between the excited triplet and the oxygen. $\Phi_\Delta$ was in the range of 0.41 to almost 1.00, depending on the solvent. These results indicate the efficient generation of singlet oxygen by the corroles studied in this paper. Similar values (0.51–0.77) were determined by Ventura *et al.* by investigations of free-based corroles in TL by singlet oxygen luminescence experiments.[8]

## 4. Conclusions

We have investigated the relationship between the strength of electron-withdrawing substituents and their photophysical properties as well as the deprotonation of free base corroles in non-polar and polar solvents. The replacement of a moderately electron-withdrawing $C_6F_5$ group with a strongly electron-withdrawing 4-$NO_2C_6H_4$ substituent led to significant changes of optical properties due to the formation of a strong donor–acceptor system. The changes in absorption spectra indicated that in the presence of polar solvents (DMF, DMSO), a mesomeric form of a corrole possessing $NO_2$ group and deprotonated forms of both corroles are present. Our hypothesis concerning different ratios of various tautomers for these two corroles is supported for the $NO_2$-corrole by fluorescence quenching. We also demonstrated that an increase of DMF in the DMF/TL mixture leads to a hypsochromic shift of the wavelength of the fluorescence emission maximum of the tris(pentafluorophenyl)corrole (TPFC), which confirms the formation of the $H_2AB^-$ form.[14]

The TD-DFT calculations explain the different behaviors of samples $NO_2$-corrole and TPFC in solution. They show that the changes in the UV-vis spectra of the $NO_2$-corrole in solutions are related to the localization of the LUMO on the nitro group, which is quite distinct from that of TPFC. Our results also show that energies of the frontier orbitals of both corroles are sensitive to the solvent permittivity while the HOMO–LUMO gap is influenced by the solvent only in the case of $NO_2$-corrole.

The onset potentials of oxidation of the corroles were observed at about 1.1–1.2 V, while the reduction potentials were −0.8 and −1.0 V for corroles **1** and **2**, respectively. The HOMO and LUMO results evaluated by TD-DFT are consistent with cyclic voltammetry measurements.

Tautomerization and deprotonation of the samples are very important because of their influence on the behavior of $NO_2$-corrole and TPFC in non-polar and/or polar solvents. The changes in the absorption band shapes confirm the effect of simple manipulation of the protonation/deprotonation states with appropriately selected polarity of solvents. It is worth noting that only some tautomers were obtained by the simple manipulation of solvent polarity. This result reflects the asymmetry of the tetrapyrrole ring; such that the two tautomeric forms are distinct and are structurally quite different.[64] The laser induced optoacoustics studies show a high quantum efficiency of the triplet state population and high singlet oxygen generation both of samples $NO_2$-corrole and TPFC. Moreover, for the aprotic solvents DMSO and DMF, similar photophysical parameters were observed.

On the basis of our experimental and chemical calculations, the optical properties of corroles open the pathway for their applications such as the construction of polarity-probes and in dye-sensitized solar cells.

 

## Abbreviations

| | |
|---|---|
| TL | Toluene |
| CL | Chloroform |
| DMF | Dimethylformamide |
| DMSO | Dimethyl sulfoxide |
| LIOAS | Laser induced optoacoustic spectroscopy |
| TD-DFT | Time-dependent density functional theory |
| Chl | Chlorophyll |
| Pheo | Pheophytin |
| IC | Internal conversion |
| ISC | Intersystem crossing |
| HOMO | Highest occupied molecular orbital |
| LUMO | Lowest unoccupied molecular orbital |
| TPFC | tris(pentafluorophenyl)corrole |

## Acknowledgements

This work was supported by Poznan University of Technology (grant No. 06/62/DSPB/0216, BB, DW, MK) and Polish National Centre for Research and Development (grant OLAE+). We thank Eli M. Espinoza (UC Riverside) for amending the manuscript.

## References

1 D. Holten, D. F. Bocian and J. S. Lindsey, *Acc. Chem. Res.*, 2002, **35**, 57–69.
2 A. W. Johnson and I. T. Kay, *J. Chem. Soc.*, 1965, 1620–1629.
3 Z. Gross, N. Galili and I. Saltsman, *Angew. Chem., Int. Ed.*, 1999, **38**, 1427–1429.
4 F. DSouza, R. Chitta, K. Ohkubo and S. Fukuzumi, *J. Am. Chem. Soc.*, 2008, **130**, 14263–14272.
5 R. Voloshchuk, D. T. Gryko, M. Chotkowski, A. I. Ciuciu and L. Flamigni, *Chem. – Eur. J.*, 2012, **18**, 14845–14859.
6 B. Koszarna and D. T. Gryko, *J. Org. Chem.*, 2006, **71**, 3707–3717.
7 D. T. Gryko and K. E. Piechota, *J. Porphyrins Phthalocyanines*, 2002, **6**, 81–97.
8 B. Ventura, A. Degli Esposti, B. Koszarna, D. T. Gryko and L. Flamigni, *New J. Chem.*, 2005, **29**, 1559–1566.
9 T. Ding, E. A. Alemán, D. A. Modarelli and C. J. Ziegler, *J. Phys. Chem. A*, 2005, **109**, 7411–7417.
10 J. F. B. Barata, M. G. P. M. S. Neves, A. C. Tomé, M. A. F. Faustino, A. M. S. Silva and J. A. S. Cavaleiro, *Tetrahedron Lett.*, 2010, **51**, 1537–1540.
11 W. Beenken, M. Presselt, T. H. Ngo, W. Dehaen, W. Maes and M. Kruk, *J. Phys. Chem. A*, 2014, **118**, 862–871.
12 A. L. Ward, H. L. Buckley, W. W. Lukens and J. Arnold, *J. Am. Chem. Soc.*, 2013, **135**, 13965–13971.
13 Y. B. Ivanova, V. A. Savva, N. Z. Mamardashvili, A. S. Starukhin, T. H. Ngo, W. Dehaen, W. Maes and M. M. Kruk, *J. Phys. Chem. A*, 2012, **116**, 10683–10694.
14 M. Kruk, T. H. Ngo, V. Savva, A. Starukhin, W. Dehaen and W. Maes, *J. Phys. Chem. A*, 2012, **116**, 10704–10711.
15 C. L. He, F. L. Ren, X. B. Zhang and Z. X. Han, *Talanta*, 2006, **70**, 364–369.
16 S. Yamauchi, M. Tanabe, Y. Ohba, K. Sugisaki, K. Toyota, K. Sato, T. Takui and I. Saltsman, *Chem. Phys. Lett.*, 2012, **521**, 64–68.
17 L. Tortora, G. Pomarico, S. Nardis, E. Martinelli, A. Catini, A. D'Amico, C. Di Natale and R. Paolesse, *Sens. Actuators, B*, 2013, **187**, 72–77.
18 C. Chen, Y. Z. Zhu, Q. J. Fan, H. Bin Song and J. Y. Zheng, *Tetrahedron Lett.*, 2013, **54**, 4143–4147.
19 J. H. Palmer, A. C. Durrell, Z. Gross, J. R. Winkler and H. B. Gray, *J. Am. Chem. Soc.*, 2010, **132**, 9230–9231.
20 M. Kruk, T. H. Ngo, V. Savva, A. Starukhin, W. Dehaen and W. Maes, *J. Phys. Chem. A*, 2012, **116**, 10704–10711.
21 B. Bursa, B. Barszcz, W. Bednarski, J. P. Lewtak, D. Koszelewski, O. Vakuliuk, D. T. Gryko and D. Wróbel, *Phys. Chem. Chem. Phys.*, 2015, **17**, 7411–7423.
22 K. Lewandowska, B. Barszcz, J. Wolak, A. Graja, M. Grzybowski and D. T. Gryko, *Dyes Pigm.*, 2013, **96**, 249–255.
23 B. Bursa, D. Wrobel, K. Lewandowska, A. Graja, M. Grzybowski and D. T. Gryko, *Synth. Met.*, 2013, **176**, 18–25.
24 A. Graja, *Mol. Cryst. Liq. Cryst.*, 2012, **554**, 31–42.
25 K. Lewandowska, B. Barszcz, A. Graja, B. Bursa, A. Biadasz, D. Wróbel, W. Bednarski, S. Waplak, M. Grzybowski and D. T. Gryko, *Synth. Met.*, 2013, **166**, 70–76.
26 S. E. Braslavsky and G. E. Heibel, *Chem. Rev.*, 1992, **92**, 1381–1410.
27 A. Shafiee, M. M. Salleh and M. Yahaya, *Sains Malays.*, 2011, **40**, 173–176.
28 D. T. Gryko and B. Koszarna, *Synthesis*, 2004, 2205–2209.
29 D. T. Gryko and B. Koszarna, *Org. Biomol. Chem.*, 2003, **1**, 350–357.
30 H. Scheer, *Chlorophylls*, CRC Press, Boca Raton Ann Arbor Boston London, 1991.
31 M. J. Frisch, G. W. Trucks, H. B. Schlegel, G. E. Scuseria, M. A. Robb, J. R. Cheeseman, J. A. Montgomery, T. Vreven, K. N. Kudin, J. C. Burant, J. M. Millam, S. S. Yengar, J. Tomasi, V. Barone, B. Mennucci, M. Cossi, G. Scalmani, N. Rega, G. A. Petersson, H. Nakatsuji, M. Hada, M. Ehara, K. Toyota, R. Fukuda, J. Hasegawa, M. Ishida, T. Nakajima, Y. Honda, O. Kitao, H. Nakai, M. Klene, X. Li, J. E. Knox, H. P. Hratchian, J. B. Cross, V. Bakken, C. Adamo, J. Jaramillo, R. Gomperts, R. E. Stratmann, O. Yazyev, A. J. Austin, R. Cammi, C. Pomelli, J. W. Ochterski, P. Y. Ayala, K. Morokuma, G. A. Voth, P. Salvador, J. J. Dannenberg, V. G. Zakrzewski, S. Dapprich, A. D. Daniels, M. C. Strain, O. Farkas, D. K. Malick, A. D. Rabuck, K. Raghavachari, J. B. Foresman, J. V Ortiz, Q. Cui, A. G. Baboul, S. Clifford, J. Cioslowski, B. B. Stefanov, G. Liu, A. Liashenko, P. Piskorz, I. Komaromi, R. L. Martin, D. J. Fox, T. Keith, M. A. Al-Laham, C. Y. Peng, A. Nanayakkara, M. Challacombe, P. M. W. Gill, B. Johnson, W. Chen, M. W. Wong, C. Gonzalez and J. A. Pople, *Gaussian 03, Revision D.01*, Gaussian, Inc., Wallingford CT, 2004.
32 N. M. O'Boyle, A. L. Tenderholt and K. M. Langner, *J. Comput. Chem.*, 2008, **29**, 839–845.
33 D. Wróbel, A. Biadasz and B. Bursa, *Int. J. Thermophys.*, 2012, **33**, 716–732.

34 A. Rosencwaig, *Photoacoustics and Photoacoustic Spectroscopy*, Wiley, New York, 1980.
35 M. Pilch, A. Dudkowiak, B. Jurzyk, J. Łukasiewicz, A. Susz, G. Stochel and L. Fiedor, *Biochim. Biophys. Acta, Bioenerg.*, 2013, **1827**, 30–37.
36 C. Marti, O. Jürgens, O. Cuenca, M. Casals and S. Nonell, *J. Photochem. Photobiol., A*, 1996, **97**, 11–18.
37 M. Kotkowiak, J. Łukasiewicz and A. Dudkowiak, *Int. J. Thermophys.*, 2013, **34**, 588–596.
38 M. Kasha, *Radiat. Res.*, 1963, **20**, 55–70.
39 F. Tantussi, F. Fuso, M. Allegrini, N. Micali, I. G. Occhiuto and L. Mons, *Nanoscale*, 2014, **6**, 10874–10878.
40 T. Zhuang, S. Sasaki, T. Ikeuchi, J. Kido and X.-F. Wang, *RSC Adv.*, 2015, **5**, 45755–45759.
41 T. Doane, A. Chomas, S. Srinivasan and C. Burda, *Chem. – Eur. J.*, 2014, **20**, 8030–8039.
42 J. R. Weinkauf, S. W. Cooper, A. Schweiger and C. C. Wamser, *J. Phys. Chem. A*, 2003, **107**, 3486–3496.
43 P. Bhyrappa and P. Bhavana, *Chem. Phys. Lett.*, 2001, **342**, 39–44.
44 D. Ding, J. D. Harvey and C. J. Ziegler, *J. Porphyrins Phthalocyanines*, 2005, **9**, 22–27.
45 A. Siejak, D. Wróbel and R. M. Ion, *J. Photochem. Photobiol., A*, 2006, **181**, 180–187.
46 Y. B. Ivanova, V. A. Savva, N. Z. Mamardashvili, A. S. Starukhin, T. H. Ngo, W. Dehaen, W. Maes and M. M. Kruk, *J. Phys. Chem. A*, 2012, **116**, 10683–10694.
47 M. Kruk, T. H. Ngo, P. Verstappen, A. Starukhin, J. Hofkens, W. Dehaen and W. Maes, *J. Phys. Chem. A*, 2012, **116**, 10695–10703.
48 A. Ghosh, T. Wondimagegn and A. B. J. Parusel, *J. Am. Chem. Soc.*, 2000, **122**, 5100–5104.
49 R. S. Becker, *Theory and Interpretation of Fluorescence and Phosphorescence*, New York, Wiley Inte., 1969.
50 B. Valeur, *Molecular Fluorescence Principles and Applications*, Wiley-VCH Verlag, 2002.
51 M. K. Panda, G. D. Sharma, K. R. Justin Thomas and A. G. Coutsolelos, *J. Mater. Chem.*, 2012, **22**, 8092–8102.
52 S. Hachiya, K. Asai and G. Konishi, *Tetrahedron Lett.*, 2013, **54**, 1839–1841.
53 T. Ueno, Y. Urano, H. Kojima and T. Nagano, *J. Am. Chem. Soc.*, 2006, **128**, 10640–10641.
54 A. Bolduc, Y. Dong, A. Guérin and W. G. Skene, *Phys. Chem. Chem. Phys.*, 2012, **14**, 6946–6956.
55 B. Carlotti, F. Elisei, U. Mazzucato and A. Spalletti, *Phys. Chem. Chem. Phys.*, 2015, **17**, 14740–14749.
56 B. W. D'Andrade, S. Datta, S. R. Forrest, P. Djurovich, E. Polikarpov and M. E. Thompson, *Org. Electron.*, 2005, **6**, 11–20.
57 P. I. Djurovich, E. I. Mayo, S. R. Forrest and M. E. Thompson, *Org. Electron.*, 2009, **10**, 515–520.
58 A. Misra, P. Kumar, R. Srivastava, S. K. Dhawan, M. N. Kamalasanan and S. Chandra, *Indian J. Pure Appl. Phys.*, 2005, **43**, 921–925.
59 C. Ye, M. Li, J. Luo, L. Chen, Z. Tang, J. Pei, L. Jiang, Y. Song and D. Zhu, *J. Mater. Chem.*, 2012, **22**, 4299–4305.
60 P. Petrova, P. Ivanov, Y. Marcheva and R. Tomova, *Bulg. Chem. Commun.*, 2013, **45**, 159–164.
61 M. Stefanelli, G. Pomarico, L. Tortora, S. Nardis, F. R. Fronczek, G. T. McCandless, K. M. Smith, M. Manowong, Y. Fang, P. Chen, K. M. Kadish, A. Rosa, G. Ricciardi and R. Paolesse, *Inorg. Chem.*, 2012, **51**, 6928–6942.
62 S. Nardis, M. Stefanelli, P. Mohite, G. Pomarico, L. Tortora, M. Manowong, P. Chen, K. M. Kadish, F. R. Fronczek, G. T. McCandless, K. M. Smith and R. Paolesse, *Inorg. Chem.*, 2012, **51**, 3910–3920.
63 M. Stefanelli, F. Mandoj, M. Mastroianni, S. Nardis, P. Mohite, F. R. Fronczek, K. M. Smith, K. M. Kadish, X. Xiao, Z. Ou, P. Chen and R. Paolesse, *Inorg. Chem.*, 2011, **50**, 8281–8292.
64 S. Szymański, P. Paluch, D. T. Gryko, A. Nowak-Król, W. Bocian, J. Sitkowski, B. Koszarna and J. Śniechowska, *Chem. – Eur. J.*, 2014, **20**, 1720–1730.

 

**Praca nr 5**

**[Lewandowska, SM 2013]** K. Lewandowska, B. Barszcz, A. Graja, B. Bursa, A. Biadasz. D. Wróbel, W. Bednarski, S. Waplak, M. Grzybowski, D.T. Gryko, *Absorption and emission properties of the corrole-fullerene dyad*, Synthetic Metals, **166** (2013) 70-76

Synthetic Metals 166 (2013) 70–76

Contents lists available at SciVerse ScienceDirect

Synthetic Metals

journal homepage: www.elsevier.com/locate/synmet

# Absorption and emission properties of the corrole–fullerene dyad

Kornelia Lewandowska[a], Bolesław Barszcz[a], Andrzej Graja[a,*,1], Bartosz Bursa[b], Andrzej Biadasz[b], Danuta Wróbel[b,*,2], Waldemar Bednarski[a], Stefan Waplak[a], Marek Grzybowski[c], Daniel T. Gryko[c,*,3]

[a] Institute of Molecular Physics, Polish Academy of Sciences, 60-179 Poznań, Poland
[b] Faculty of Technical Physics, Institute of Physics, Poznan University of Technology, 60-965 Poznań, Poland
[c] Institute of Organic Chemistry, Polish Academy of Sciences, 01-224 Warsaw, Poland

ARTICLE INFO

*Article history:*
Received 30 November 2012
Received in revised form 23 January 2013
Accepted 23 January 2013

*Keywords:*
Corrole–fullerene dyad
Electronic absorption and fluorescence spectra
Fluorescence quantum yield and lifetime
Charge localization and distribution
Electron magnetic resonance

ABSTRACT

The bichromophoric systems comprising of corrole and fullerene units and representing one of the rare cases of elaborate structures based on corrole have been studied with the use of photophysical methods. The dyad displays spectroscopic properties which are the superposition of the component spectra, indicating a very weak electronic coupling. Excitation of the corrole unit leads to charge redistribution. The results of UV–vis absorption and fluorescence and also fluorescence kinetics suggest the presence of charge separation. It was shown that light absorption of the corrole–fullerene dyad is better fitted to the sunlight spectrum than porphyrin. Electron paramagnetic resonance investigations suggest partial spin density redistribution at low temperature between corrole and fullerene in the dyad. Quantum chemical calculations support experimental results.



## 1. Introduction

Due to the excellent properties and availability of porphyrins, they have constituted for several decades the most used components of models for light energy collection and conversion [1,2]. However, the need of the performance improvement and increase the variety of such molecular systems encouraged the use of other porphyrinoids. Solving the energy problems requires searching for novel molecular materials, which should be characterized by a large absorption coefficient, fast process of charge separation and much slower process of charge recombination [3–5]. Among various materials fulfilled these requirements there are organic donor–acceptor systems containing fullerene $C_{60}$ as an electron acceptor and an organic dye as electron donor. The excellent electron-accepting capability of fullerenes makes them appropriate building blocks for designing various photovoltaic devices [6,7].

Corroles are one-carbon-shorter analogs of porphyrins possessing the skeleton of corrin with three *meso*-carbons between the four pyrrole rings. They were found to be suitable replacement for porphyrins in these electron-donor/electron-acceptor systems [8]. When compared with porphyrins, these tribasic aromatic macrocycles exhibit lower oxidation potentials, higher fluorescence quantum yields, larger Stokes shifts, and more intense absorption of red light [9,10]. Free-base corroles reveal the Soret-type absorption in the 400–440 nm region and Q band transitions between 500 and 700 nm. Spectral properties of corroles, similarly as of porphyrins can be tuned *via*: introducing various central metals, putting suitable substituents on the periphery of conjugated ring systems, or solvent conditions [8–11]. It is necessary to add, that the effect of substitution on the optical properties of corroles is significantly larger than in porphyrins. Finally, corroles can be very emissive, with high quantum yields of fluorescence [8–11]. The corroles are, in general, less stable than porphyrins, but the stability of their dyads is better than that of the corresponding component corroles [12]. In the last decade, *meso*-substituted corroles are among the most widely investigated compounds as potential materials for application in photovoltaic systems [8,9,12–14].

Recently, we have described synthesis and vibrational properties of a new corrole-based-fullerene dyad (named **3**) and its components: modified corrole (**2**) and a suitable spacer (pentafluorophenyl **1**) [15] shown in Fig. 1. In the paper [15] our systematic spectral studies of the dyad and its components were presented for the first time. The infrared absorption and Raman scattering spectra were supported by the quantum chemical calculations of the equilibrium geometry and normal mode vibrations of the investigated molecules. It was found that the strongest excitations in the dyad are mainly related to the excitations of the modified corrole part with some influence of the spacer and fullerene parts [15].

* Corresponding authors.
*E-mail addresses:* graja@ifmpan.poznan.pl (A. Graja), danuta.wrobel@put.poznan.pl (D. Wróbel), danieltgryko@gmail.com, daniel@icho.edu.pl (D.T. Gryko).
[1] Tel. +48 61 86 95 275.
[2] Tel. +48 61 66 53 179.
[3] Tel. +48 22 34 33 063.

0379-6779/$ – see front matter © 2013 Published by Elsevier B.V.
http://dx.doi.org/10.1016/j.synthmet.2013.01.014

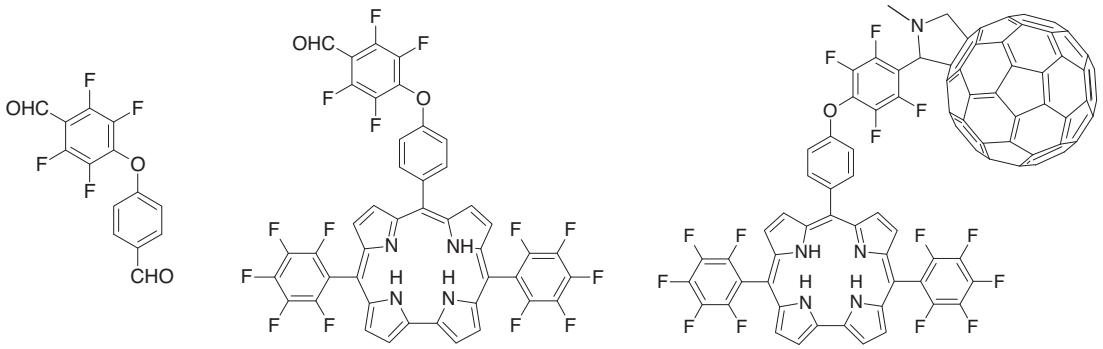


**Fig. 1.** Molecular structure of the corrole-based-fullerene dyad **3** and its components **1** and **2**.

The aim of present paper is to evaluate optical and photophysical properties of the dyad **3** and explain its electronic spectra, including fluorescence and spin effects.

## 2. Experimental

Molecular structures of the corrole-based-fullerene dyad **3** and its main components **1**, **2** are shown in Fig. 1. Details about synthesis and configuration of the investigated corrole **2** and its dyad with fullerene **3** was reported in our previous paper [15].

The electronic absorption spectra of the samples **1**–**3** were recorded with a spectrophotometer Carry 4000 in the range 250–800 nm but fluorescence measurements were made with a HITACHI F-4500 fluorescence spectrophotometer and fluorescence was excited at the wide wavelength range (250–613 nm). Fluorescence intensity decays were followed with the use of a time-correlated single photon counting system (EasyLife V—Photon Technology Instruments). Fluorescence signals were obtained with a 1.5 ns pulse of LED (405 nm) as an excitation source, and a sample response was collected in the full fluorescence range. Fluorescence lifetimes were estimated by fitting the decay data using a deconvolution procedure based on the Program EasyLife II.

The relative fluorescence quantum yield ($\Phi_F$) of the samples were evaluated on the basis of the absorption and fluorescence spectra according to the methods described elsewhere [16,17]:

$$\Phi_F = \Phi_R \frac{I}{I_R} \frac{A_R}{A} \frac{n^2}{n_{R^2}}, \quad (1)$$

where $\Phi_R$ is the fluorescence quantum yield of a reference sample (chlorophyll *a*; $\Phi_R = 32\%$ [18]), $I$ and $I_R$ are the integrated fluorescence of the sample and reference, respectively, $A$ and $A_R$ are the absorbance of the sample and reference, respectively and $n$ and $n_R$ are the refractive indices of the sample and reference, respectively. Corrections for re-absorption of the fluorescence light and secondary fluorescence effects were taken into account.

All the samples were dissolved in chloroform and their concentrations were: $10^{-4}$, $10^{-5}$, and $10^{-6}$ M depending on a type of measurements; the spectroscopic measurements in the UV–vis range were performed in 1 mm and 1 cm quartz cells, at room temperature.

For deeper interpretation of the experimental UV–vis spectra we have calculated the transition energies by means of a time-dependent density functional theory (TD-DFT) method with hybrid B3LYP functional (Becke 3-parameter exchange functional combined with Lee–Yang–Parr correlational functional) and 6-31G basis set for samples **2** and **3**. Calculations were performed with a help of the Gaussian 03 package [19] and using the equilibrium geometries of the molecules obtained in our previous investigations [15]. Part of the results analysis was made with the use of the Gauss Sum program [20].

Electron paramagnetic resonance studies were performed by means of an X-band Bruker ElexSys spectrometer in the temperature range 5–300 K. The EPR spectra were recorded as a first derivative of the absorption signal. Sample temperature was controlled and stabilized with an OXFORD ESR900 cryostat. Concentration of the EPR centers was obtained after double integration of the EPR lines and next by comparing with a suitable standard.

## 3. Results and discussion

The electronic absorption spectra of the corrole-based-fullerene dyad **3** and its components **1** and **2** in chloroform are shown in Fig. 2. A strong and complex Soret-like absorption band of **2** and **3** appears around 410 nm and weak Q bands are recorded in the wavelength range 500–650 nm. The origin of the Soret-like and the Q bands of corroles is the same as of porphyrins [21] but the absorption in the visible region of corroles is more intense than that of porphyrins [22]. Deconvolution of the Soret-like band at **2** shows that it contains two components centered at 410 nm and 429 nm. Similarly, there are four components of the Q band which are localized at 517, 565, 613 and 639 nm. According to our quantum chemical calculations the electron transitions with the energy of 3.11 eV

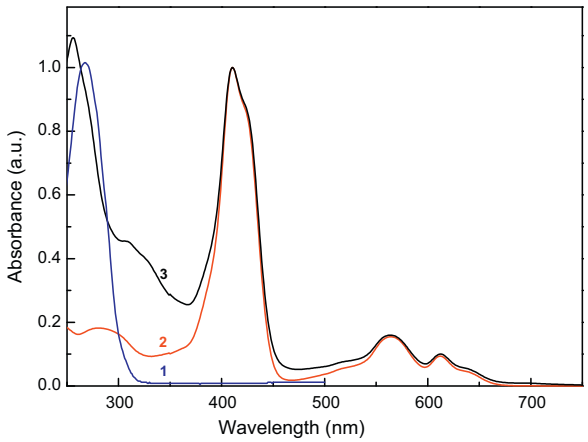


**Fig. 2.** Electron absorption spectra of the corrole-based-fullerene dyad **3** and its components **1** and **2** recorded in chloroform ($10^{-5}$ M) at room temperature.

**Table 1**
Absorption parameters of corrole (**2**) and corrole–fullerene (**3**) in chloroform.

| Band position (nm) | | FWHM ($cm^{-1}$) | | $\varepsilon \times 10^4$ ($M\,cm^{-1}$) | |
|---|---|---|---|---|---|
| **2** | **3** | **2** | **3** | **2** | **3** |
| 290 | 255 | 1903 | 2250 | | |
| | 309 | | 1038 | | |
| | 329 | | 2163 | | |
| 410 | 410 | 2683 | 2596 | | |
| 429 | 427 | 1644 | 1557 | 1.49 | 1.05 |
| 517 | 519 | 2723 | 2769 | | |
| 565 | 564 | 3751 | 3634 | | |
| 613 | 613 | 1885 | 1817 | | |
| 639 | 638 | 2296 | 2336 | | |

FWHM—full width at half maximum; $\varepsilon$—molar absorption coefficient.

(399 nm) are allowed for the corrole **2**; it corresponds quite good to the observed components of the Soret-like band (see Fig. 2). On the other hand, our calculations do not contradict with two or more components of the Soret band. The absorption parameters of the compounds **2**–**3** are gathered in Table 1.

The theory "four-track model" for tetraphenylporphyrin, which describes the electron spectra of porphyrins is also applicable for corroles [11]. By analogy to regular symmetric porphyrins, the absorption bands of corroles are generated by $\pi$–$\pi^*$ electron transitions [9,23]. However, the reduced symmetry of the corrole is expected to induce a splitting of the lowest-unoccupied molecular orbitals. Therefore, in the absorption spectrum of the corrole we have observed a blue-shift in the Soret band in comparison to porphyrins. Some splitting of this band is also observed. Likewise, the same effects were observed elsewhere [9]. It is noteworthy to add that we can exclude formation of corrole dimers containing two differently oriented corrole molecules as a reason of the Soret band splitting because the doublet appears independently of the solution concentration from $10^{-6}$ to $10^{-4}$ M (not shown). The study of the system's absorption done for the different concentrations of dye show no major changes in the shape of the spectra and positions of the maxima as well as of half widths. This evidences domination of monomeric forms of both **2** and **3** as well as their weak tendency to create aggregates. According to the Kasha exciton model [24] the presence of some aggregated molecular structures is usually manifested by modifications of the absorption spectra by the appearance of the band shifts, band splitting and changes in the band widths [25–27]. However, it is not the case in our absorption experiments—we do not observe the changes neither upon concentration increasing nor at different excitation wavelengths.

The absorption spectrum of the dyad **3** shows inconsiderable differences in the shapes and position of the bands with regard to **2** (Fig. 2). These data provide the direct evidence that components of the dyad are electronically disconnected in the ground state. The Soret band region of the dyad **3** is dominated by the strong band typical for **2**, centered at about 410 nm. The deconvolution of this band reveals two components located at 411 and 429 nm. There are also the Q bands composed of four weak bands at 519, 565, 613, and 638 nm; some of these components show very small shifts in comparison to the non-bonded corrole **2**. These changes are caused by the bonding of the fullerene to the corrole **2**, which extorts charge transfer from the electron donor (corrole) to an acceptor (fullerene) and adequate changes in the electron density distribution. The spectrum of the dyad **3** contains also the bands typical for fullerene at about 255 nm and another one located between 300 and 350 nm; the later absorption correspond to the fullerene band at 343 nm.

For better understanding of the dyad absorption in the UV–vis range we performed the quantum chemical calculations using TD-DFT methods. The well-known B3LYP hybrid functional with the 6-31G basis set was used for this purpose. The main electronic transitions (those with oscillator strength higher than 0.1) of the corrole **2** and dyad **3** are collected in Tables 2 and 3, respectively. In Figs. 3 and 4 the appropriate frontier molecular orbitals are presented. On the basis of these results we can say that the Soret band in both corrole **2** and dyad **3** is related to the transitions which involve the central core of the corrole (see the description in the tables and molecular orbitals in Figs. 3 and 4). Similar description fits to the Q band. The only exception is partial contribution of the

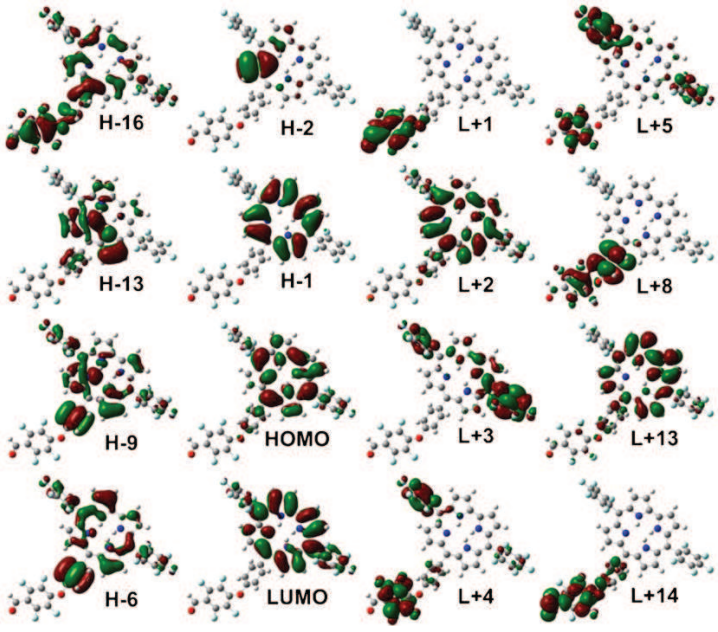


**Fig. 3.** The B3LYP/6-31G generated frontier molecular orbitals of the corrole **2**.

**Table 2**
Main transitions for **2** (with oscillator strength above 0.1).

| Wavelength (nm) | Oscillator strength | Major contributions |
|---|---|---|
| 559 | 0.1780 | H-1 → LUMO (17%), H-1 → L+2 (16%), HOMO → LUMO (48%), HOMO → L+2 (12%) |
| 540 | 0.1042 | H-1 → LUMO (32%), HOMO → LUMO (19%), HOMO → L+1 (17%), HOMO → L+2 (22%) |
| 399 | 0.8106 | H-1 → LUMO (19%), HOMO → L+2 (38%) |
| 385 | 0.5739 | H-2 → LUMO (31%), H-1 → L+2 (36%) |
| 371 | 0.4451 | H-2 → LUMO (59%), H-1 → L+2 (18%) |
| 348 | 0.1635 | HOMO → L+3 (72%) |
| 320 | 0.2061 | H-2 → L+2 (23%), H-1 → L+3 (38%) |
| 316 | 0.2374 | H-1 → L+4 (24%), H-1 → L+5 (53%) |
| 243 | 0.2008 | H-16 → L+1 (63%), HOMO → L+14 (12%) |
| 209 | 0.1436 | H-6 → L+5 (13%), H-2 → L+13 (15%), HOMO → L+16 (23%) |
| 191 | 0.1085 | H-13 → L+8 (16%), H-9 → L+8 (12%) |

**Table 3**
Main transitions for **3** (with oscillator strength above 0.1).

| Wavelength (nm) | Oscillator strength | Major contributions |
|---|---|---|
| 560 | 0.1965 | H-1 → L+2 (15%), H-1 → L+4 (17%), HOMO → L+2 (51%), HOMO → L+4 (11%) |
| 538 | 0.1035 | H-1 → L+2 (42%), HOMO → L+2 (17%), HOMO → L+4 (31%) |
| 400 | 0.8978 | H-1 → L+2 (19%), HOMO → L+4 (38%) |
| 386 | 0.5382 | H-8 → L+2 (31%), H-1 → L+4 (36%) |
| 373 | 0.4077 | H-8 → L+2 (60%), H-1 → L+4 (18%) |
| 348 | 0.1829 | HOMO → L+10 (55%) |
| 322 | 0.2249 | H-8 → L+4 (27%), H-1 → L+10 (36%) |
| 318 | 0.3222 | H-1 → L+11 (65%) |
| 289 | 0.1049 | H-7 → L+7 (14%), H-5 → L+9 (32%) |

transition at 540 nm in **2** (HOMO or H → L+1, see Table 2), where the location of the molecular orbital changes significantly during transition. Nevertheless, this is the only component of the band. In fact, the main transitions of both compounds (**2** and **3**) look quite similarly to each other (see Fig. 5). The main difference is found in the region below 350 nm, where the transitions observed in **3** are stronger. However, the nature of these transitions is similar for both molecules—for example the dominant part of the transition at 348 nm in **2** is H → L+3. The location of molecular orbital changes upon this transition from the core of corrole to the $C_6F_5$ rings. The transition at 348 nm in **3** has very similar characteristics (see Figs. 2 and 5). Of course, in the spectrum of **3** the transitions which involve the fullerene part also appear (*e.g.* 289 nm). The higher oscillator strength of the corrole-related transitions and the

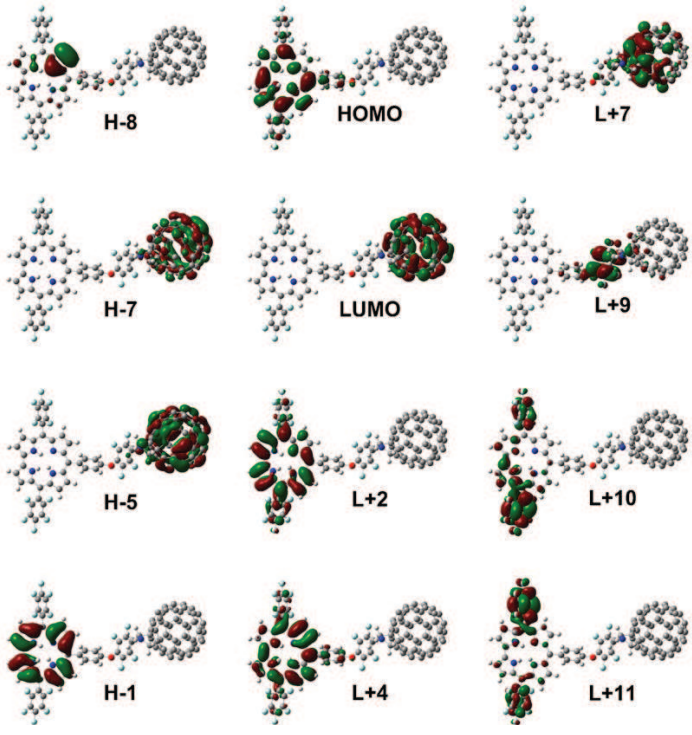


**Fig. 4.** The B3LYP/6-31G generated frontier molecular orbitals of the dyad **3**.

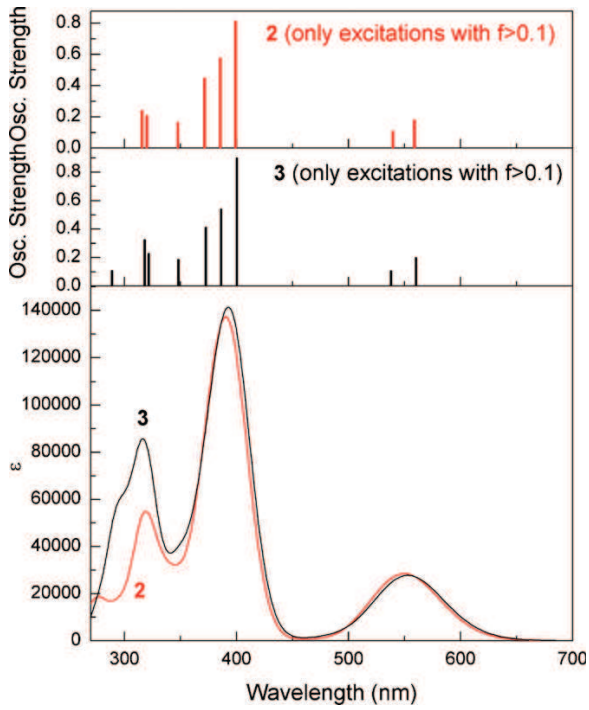


**Fig. 5.** Main electronic transitions (oscillator strength higher than 0.1) of the corrole **2** (a) and dyad **3** (b) together with the generated UV–vis spectra of them (c). Theory level: B3LYP/6-31G.

presence of the excitations related to the fullerene part causes that the simulated spectrum of **3** is more intense than that of **2** in the region below 350 nm (see Fig. 5 bottom). This follows quite well the experimental spectra of compounds **2** and **3** shown in Fig. 2. Moreover, the calculation results indicate that location of the H and L levels of the dyad is similar to that described by D'Souza et al. [8] for different corrole–fullerene system. They found that the H levels were located on the corrole $\pi$-system, while the L level was located on the fullerene. In our case we observe similar behavior (see Fig. 4). It suggests that photoinduced electron transfer occurs in our system. It is necessary to notice that lower and higher molecular orbitals are located on different parts of the dyad (Fig. 4). For example, the H level is placed at the corrole part (as it was mentioned above), while the H-7 orbital is located at the fullerene part. Similarly, the L level is localized at the fullerene part, L + 2 orbital—at the corrole, but L + 11—at the pentafluorophenyl substituents.

Solutions of compounds **2** and **3** (at different concentrations—$10^{-4}$, $10^{-5}$, $10^{-6}$ M) were excited at the wavelength matching the proper Soret (250–422 nm) and Q bands (563 and 613 nm) maxima. The exemplary fluorescence spectra of the corrole-based-fullerene dyad **3** and its main component **2** in chloroform (**1** does not fluoresce) are shown in Fig. 6a; the spectra shapes and location of the band maxima are independent of the excitation wavelengths and dye concentrations. The corresponding fluorescence parameters (fluorescence maxima, fluorescence quantum yields and fluorescence lifetimes) are summarized in Table 4. Usually, the fluorescence spectra of corroles are characterized by strong emission bands between 620 and 680 nm with fluorescence quantum yield 2–30% depending on substituents and solvents [8–11]. The luminescence lifetime is of the order of a few nanoseconds. The fluorescence quantum yields of the substituted corroles are in general higher than those of the analogous porphyrins [11].

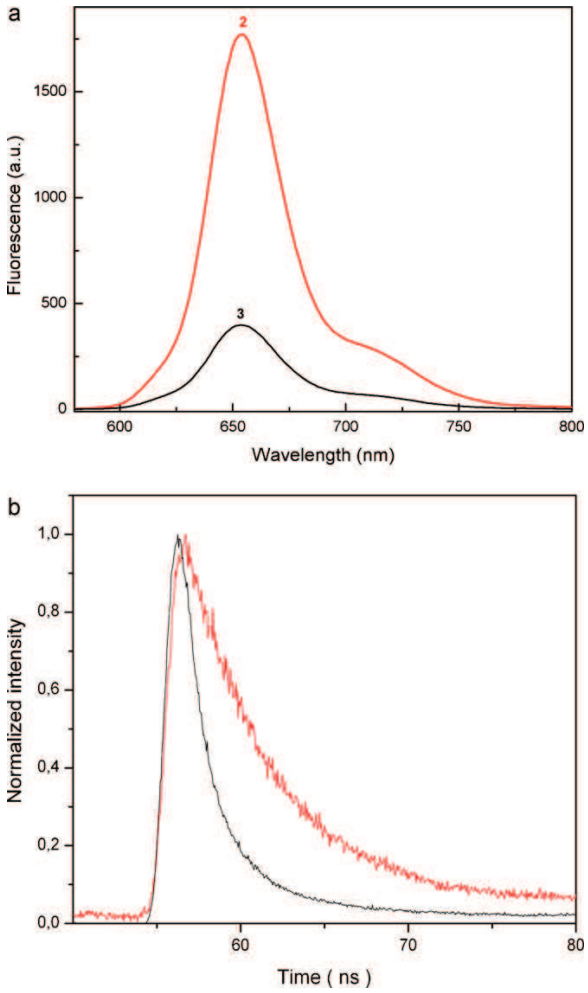


**Fig. 6.** Fluorescence spectra of the corrole **2** (red lines) and the corrole-based-fullerene dyad **3** (black lines) recorded in $10^{-5}$ M chloroform solution at room temperature; excitation = 410 nm—(a), room temperature fluorescence decays of the corrole **2** and the corrole-based-fullerene dyad **3**; excitation 405 nm; concentration $10^{-4}$ M—(b). (For interpretation of the references to color in this figure legend, the reader is referred to the web version of the article.)

According to our experimental investigations the fluorescence spectrum of the corrole **2** is characterized by a strong emission band and a long wavelength hump. The fluorescence intensity of the sample **3** (the corrole–fullerene dyad) is much lower than that of the sample 2 (the fluorescence experiments were done exactly under the same conditions) and evidently indicates strong interaction of the corrole with fullerene. The band and the hump are located at 665 and 715 nm for the corrole **2** and are shifted to 660 and 720 nm for the dyad **3**. The emission peaks of the fluorescence spectra of both samples could be ascribed to the radiative transitions from $S_1$ to $S_0$ after the corrole molecule excitation. The luminescence bands detected for corrole can be attributed to a vibrational progression of the lowest singlet excited state. For the dyad **3** we observe a quenching of corrole fluorescence; the lower value of the fluorescence quantum yield of corrole fluorescence is attributed to charge-transfer transitions from the corrole macrocycle to the fullerene. It is worth to underline that no changes in shape and band maxima positions in the fluorescence spectra recorded for different concentrations of species are observed.

**Table 4**
Fluorescence parameters of the investigated compounds.

| Sample | Fluorescence life time $\tau$ (ns) | Weight parameter (%) | Residuum[a] | Fluorescence quantum yield $\Phi_F$ (%) |
|---|---|---|---|---|
| **1** | – | – | – | – |
| **2** | $\tau 1 = 3.80 \pm 0.03$ | $100 \pm 0.35$ | 2.036 | 10 |
| **3** | $\tau 2 = 6.54 \pm 0.51$ | $6.02 \pm 0.22$ | | |
| | $\tau 3 = 1.00 \pm 0.01$ | $94.04 \pm 0.01$ | 1.155 | 5 |

[a] Estimated on the basis of the Marquardt algorithm [28].

Similarly, we do not observe concentration dependent fluorescence quenching. These results confirm our statement from the electronic absorption spectra—the investigated materials occur predominantly in the monomeric forms. It is also necessary to notice that the fluorescence maximum position does not change with the excitation wavelength. Only the changes in the intensity of the fluorescence bands are observed; the most intense bands are observed for excitation at $\lambda_{exc}$ = 410–422 nm, as expected. To reaffirm our supposition as to corrole fluorescence quenching in the dyad **3** upon covalent linkage of the corrole to the fullerene luminescence kinetics were also performed. Fig. 6b shows the results of the fluorescence decay measurements done in the corrole fluorescence range. As seen, the time decay of the corrole emission changes significantly in the presence of fullerene. To evaluate the values of decay times we have fitted the decay curves assuming the presence of one or two exponential components. The evaluated fluorescence life times are as follows: one lifetime—$\tau_1$ = 3.80 ns for the corrole **2** and two lifetimes—$\tau_2$ = 6.54 ns and $\tau_3$ = 1.00 ns for the dyad **3**. The detailed parameters of the evaluated lifetimes are gathered in Table 4. The lifetime of 3.80 ns comes from the unlinked corrole **2**. In the case of the sample **3** two evaluated lifetimes can be assigned to two species and the results can be explained as follows: (i) in the sample **3** the emission decay time of the corrole–fullerene sample decreased of about 4 times with respect to that of the corrole sample **2** ($\tau_3$ *versus* $\tau_1$) indicates the efficient deactivating process; (ii) domination of $\tau_3$ (94%) *versus* $\tau_2$ (6%) surely confirms an efficient electron transfer from the corrole core to the fullerene part. This conclusion is strongly supported by our quantum calculation: the H level is located on the corrole $\pi$-system, while the L level is located on the fullerene. After bonding to the fullerene part, the distribution of electron density is markedly changed in the corrole species in **3**. This conclusion is coherent with that presented in Figs. 3 and 4. Most probably, the origin of the lifetime $\tau_2$ is the corrole species which are linked by the pentafluorophenyl substituents (**1**) to the fullerene in **3** and can also interact by space with the other corrole–fullerene dyads in the vicinity. Thus, the differences between the values of $\tau_2$ and $\tau_1$ could be explained as coming from the corrole species which are not involved in the electron transfer to the fullerene but interact with the corrole–fullerene dyads which are in the quite close vicinity and do not participate in the process of fluorescence quenching. The species which are involved in the electron transfer process to the fullerene exhibit much shorter time ($\tau_3$). Finally, we want to establish also influence of the fullerene presence in **3** on the fluorescence quantum yields $\Phi_F$ (the $\Phi_F$ values were evaluated with the use of Eq. (1)). The fluorescence quantum yield results also reveal distinct behavior of the samples; the values of 10% and 5% for the samples **2** and **3**, respectively, evidently corroborate the occurring of fluorescence quenching by the electron transfer transition.

Electron paramagnetic resonance studies of powdered samples show that only **2** and **3** compounds reveal EPR signals. EPR spectra at room temperature (RT) consist of single lines characterized by the linewidth of about 6.5 G and the *g*-factor 2.0029. The large EPR linewidth point out the non split superhyperfine structure resulting from electron spin interaction with ligands nuclear spin. In Fig. 7 the temperature dependencies of *g*-values for corrole **2** and **3** corrole-based-fullerene dyad are presented. In accord with

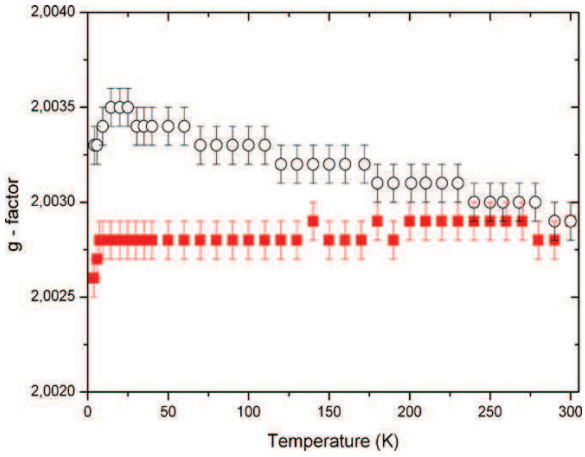


**Fig. 7.** Temperature dependence of *g*-values for the corrole **2** (red squares) and the corrole-based-fullerene dyad **3** (circles). (For interpretation of the references to color in this figure legend, the reader is referred to the web version of the article.)

conclusions drawn for fullerene-molecule-derived *g*-values [28] the shift $\Delta g = g - 2.0023$ is a measure of the spin–orbit interaction depending on the orbital hybridization on which the unpaired electron resides. EPR data (Fig. 7) shows that for both samples $g > g_0$ like as for $C_{60}^+$ centers [28] but with different amount of charge transferred.

In Fig. 8 susceptibility $\chi_{EPR}$ data (measured as integrated intensity of EPR line) *versus* temperature of **2** and **3** powdered samples are shown. The temperature behavior of $\chi_{EPR}$ (spin concentration $4.96 \times 10^{17}$ and $4.19 \times 10^{17}$ spin/g at RT) in the components **2** and

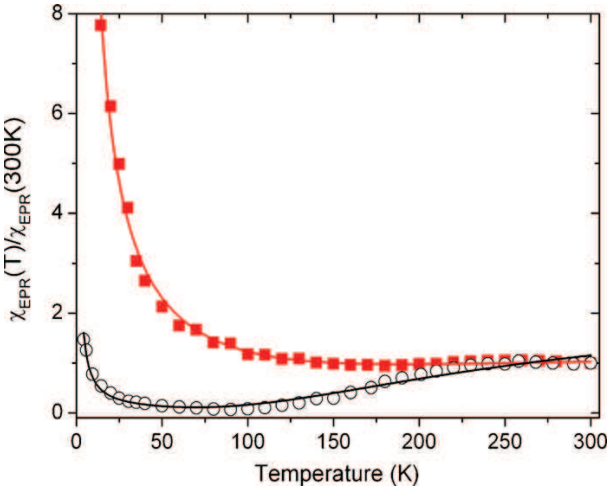


**Fig. 8.** EPR susceptibility scaled to the value measured at 300 K *versus* temperature: symbols—experimental data, smooth curves—fitted in accord with Eq. (2).

**3** were fit with the Troyer expression [29] for a two leg spin ladder system with the energy gap of $T_0$:

$$\chi_{EPR} = \frac{C}{T} + \alpha T^{-1/2} \exp\left(-\frac{T_0}{T}\right) \quad (2)$$

where $C$ is the Curie constant, $\alpha$ is the constant, $T_0$ is the energy gap and $T$ is the temperature. These parameters are equal $C = 115 \pm 1$ K, $\alpha = 43 \pm 14$ K$^{0.5}$, $T_0 = 402 \pm 77$ K for sample **2** and $C = 6.74 \pm 0.24$ K, $\alpha = 89 \pm 10$ K$^{0.5}$, $T_0 = 453 \pm 27$ K for sample **3**.

Magnetic susceptibilities $\chi_{EPR}$ tend to become smaller at lower temperature than those expected from Curie-law. That may indicate partial single covalent bond formation of electron pair with antiparallel (antiferromagnetic) coupling. Such coupling is very strong in corrole-based-fullerene dyad **3** with about 17 times lower Curie value $C = N\mu^2/3k$, where $\mu$—magnetic moment, $k$—Boltzmann constant, and $N$—number of localized spins.

The $g$-values (Fig. 7) are equivalent for both **2** and **3** samples at RT and confirm unpaired electron localization on corrole. This $g$-value of the corrole **2** is almost temperature independent. In opposite in the compound **3** it grows up to about 2.0035 at 20 K and suggests the paths of spin density transfer corrole–fullerene [30]

## 4. Conclusions

For the first time the detailed spectroscopic investigations of new corrole–fullerene dyad were performed. It was shown that fine-tuning of the spacer linking both photoactive units of the dyad significantly modifies its spectroscopic properties. This and other our observations provide new insight into factors influencing the electron transfer efficiency in the organic chromophore-fullerene dyads.

It was stated that the H molecular orbital of the dyad is located on the corrole $\pi$-system, while L—on the fullerene. The Soret-like band in both corrole and its dyad with fullerene is related to the transitions which involve the central core of the corrole. The fluorescence of the corrole moiety in the dyad is only partially quenched but the decay time of the corrole–fullerene dyad indicates the efficient deactivation process. The denomination of $\tau_3$ *vs.* $\tau_2$ confirms electron transfer from the corrole species to the fullerene part.

The charge transfer from the corrole to the fullerene permitted us to observe the EPR spectra. At room temperature the spectrum consists of single, relatively broad line with $g$-factor of 2.0029. The large EPR linewidth points out the non split superhyperfine structure resulting from the electron spin interaction with nuclear spins of ligands. The $g$-values equality for the corrole and the dyad samples at room temperature suggests unpaired electron localization on the corrole. In the dyad it grows up with the temperature decreasing suggesting partial spin density redistribution between the corrole and fullerene moieties at low temperature. Our EPR studies show that antiferromagnetic coupling is mainly realized at low temperature due to dimerization. This statement is drown from susceptibility $c_{EPR}$ data and does not contradict with optical measurements at room temperature.

## Acknowledgements

The paper was partially supported by the National Science Center of Poland (Post-doctoral internship No. 2012/04/S/ST5/00071; K. L.) and by Poznan University of Technology, Poznan, Poland—DS 62-176 (D.W., A.B., B.B.).

## References

[1] D. Dolphin (Ed.), The Porphyrins, vol. 3, Academic Press, New York, 1978.
[2] H. Imahori, Journal of Physical Chemistry B 108 (2004) 6130–6143.
[3] H. Imahori, Y. Mori, Y. Matano, Journal of Photochemistry and Photobiology C: Photochemistry Review 4 (2003) 51–83.
[4] M.E. El-Khouly, O. Ito, P.M. Smith, F. D'Souza, Journal of Photochemistry and Photobiology C: Photochemistry Review 5 (2004) 79–104.
[5] D. Wróbel, A. Graja, Coordination Chemistry Reviews 255 (2011) 2555–2577.
[6] M.S. Dresselhaus, G. Dresselhaus, P.C. Eklund, Science of Fullerenes and Carbon Nanotubes, Academic Press, San Diego/Boston/New York/London/Sydney/Tokyo/Toronto, 1996.
[7] F. Diederich, M. Gómez-López, Chemical Society Reviews 28 (1999) 263–277.
[8] F. D'Souza, R. Chitta, K. Ohkubo, M. Tasior, N.K. Subbaiyan, M.E. Zandler, M.K. Rogacki, D.T. Gryko, S. Fukuzumi, Journal of the American Chemical Society 130 (2008) 14263–14272.
[9] B. Ventura, A. Degli Esposti, B. Koszerna, D.T. Gryko, L. Flamigni, New Journal of Chemistry 29 (2005) 1559–1566.
[10] J. Poulin, C. Stern, R. Guilard, D. Harvey, Photochemistry and Photobiology 82 (2006) 171–176.
[11] T. Ding, E.A. Alemán, D.A. Modarelli, C.J. Ziegler, Journal of Physical Chemistry A 109 (2005) 7411–7417.
[12] L. Flamigni, D.T. Gryko, Chemical Society Reviews 38 (2009) 1635–1646.
[13] L. Flamigni, B. Ventura, M. Tasior, T. Becherer, H. Langhals, D.T. Gryko, Chemistry: A European Journal 14 (2008) 169–183.
[14] I. Aviv, Z. Gross, Chemical Communications (2007) 1987–1999.
[15] K. Lewandowska, B. Barszcz, J. Wolak, A. Graja, M. Grzybowski, D.T. Gryko, Dyes and Pigments 96 (2013) 249–255.
[16] M.A.M.J. van Zandvoort, D. Wróbel, P. Lettinga, G. Van Ginkel, Y.K. Levine, Photochemistry and Photobiology A: Chemistry 62 (1995) 279–289.
[17] J.R. Lakowicz, Principles of Fluorescence Spectroscopy, third ed., Springer, New York, 2006.
[18] H. Scheer (Ed.), Chlorophylls, CRC Press, Boca Raton/Ann Arbor/Boston/London, 1991.
[19] M.J. Frisch, G.W. Trucks, H.B. Schlegel, G.E. Scuseria, M.A. Robb, J.R. Cheeseman, J.A. Montgomery, Jr., T. Vreven, K.N. Kudin, J.C. Burant, J.M. Millam, S.S. Iyengar, J. Tomasi, V. Barone, B. Mennucci, M. Cossi, G. Scalmani, N. Rega, G.A. Petersson, H. Nakatsuji, M. Hada, M. Ehara, K. Toyota, R. Fukuda, J. Hasegawa, M. Ishida, T. Nakajima, Y. Honda, O. Kitao, H. Nakai, M. Klene, X. Li, J.E. Knox, H.P. Hratchian, J.B. Cross, C. Adamo, J. Jaramillo, R. Gomperts, R.E. Stratmann, O. Yazyev, A.J. Austin, R. Cammi, C. Pomelli, J.W. Ochterski, P.Y. Ayala, K. Morokuma, G.A. Voth, P. Salvador, J.J. Dannenberg, V.G. Zakrzewski, S. Dapprich, A.D. Daniels, M.C. Strain, O. Farkas, D.K. Malick, A.D. Rabuck, K. Raghavachari, J.B. Foresman, J.V. Ortiz, Q. Cui, A.G. Baboul, S. Clifford, J. Cioslowski, B.B. Stefanov, G. Liu, A. Liashenko, P. Piskorz, I. Komaromi, R.L. Martin, D.J. Fox, T. Keith, M.A. Al-Laham, C.Y. Peng, A. Nanayakkara, M. Challacombe, P.M.W. Gill, B. Johnson, W. Chen, M.W. Wong, C. Gonzalez, J.A. Pople. Gaussian 03, Revision D.01. Gaussian, Inc., Pittsburgh, PA, 2003.
[20] N.M. O'Boyle, A.L. Tenderholt, K.M. Langner, Journal of Combinatorial Chemistry 29 (2008) 839–845.
[21] M. Guterman, L. Stryer, Journal of Chemical Physics 37 (1962) 2260–2266.
[22] M. Tasior, D.T. Gryko, M. Cembor, J.S. Jaworski, B. Ventura, L. Flamigni, New Journal of Chemistry 31 (2007) 247–259.
[23] A. Ghosh, T. Wondimagegn, A.B.J. Parusel, Journal of the American Chemical Society 122 (2000) 5100–5104.
[24] M. Kasha, H.R. Rawls, M.A. El-Bayoumi, Pure and Applied Chemistry 11 (1965) 371–392.
[25] N.C. Maiti, S. Mazumdar, N. Periasamy, Journal of Physical Chemistry B 102 (1998) 1528–1538.
[26] M. Ghadamgahi, D. Ajloo, Journal of Porphyrins and Phthalocyanines 15 (2011) 240–256.
[27] S.M. Andrade, R. Teixeira, S.M.B. Costa, A.J.F.N. Sobral, Biophysical Chemistry 133 (2008) 1–10.
[28] J. Stankowski, L. Piekara-Sady, W. Kempiński, Applied Magnetic Resonance 19 (2000) 539–546.
[29] M. Troyer, H. Tsunetsugu, D. Würtz, Physical Review B 50 (1994) 13515–13527.
[30] K. Lewandowska, W. Bednarski, G. Milczarek, S. Waplak, A. Graja, E.Y. Park, T.D. Kim, K.S. Lee, Synthetic Metals 161 (2011) 1640–1645.

**Praca nr 6**

**[Bursa, SM 2013]** B. Bursa, D. Wróbel, K. Lewandowska, A. Graja, M. Grzybowski, D.T. Gryko, *Spectral studies of molecular orientation in corrole-fullerene thin films*, Synthetic Metals, **176** (2013) 18-25

Synthetic Metals 176 (2013) 18–25

Contents lists available at SciVerse ScienceDirect

Synthetic Metals

journal homepage: www.elsevier.com/locate/synmet

# Spectral studies of molecular orientation in corrole-fullerene thin films☆

B. Bursa[a], D. Wróbel[a,*], K. Lewandowska[b], A. Graja[b,**], M. Grzybowski[c], D.T. Gryko[c,***]

[a] Faculty of Technical Physics, Institute of Physics, Poznan University of Technology, 60-965 Poznań, Poland
[b] Institute of Molecular Physics, Polish Academy of Sciences, 60-179 Poznań, Poland
[c] Institute of Organic Chemistry, Polish Academy of Sciences, 01-224 Warsaw, Poland

ARTICLE INFO

*Article history:*
Received 5 March 2013
Received in revised form 29 April 2013
Accepted 7 May 2013
Available online 15 June 2013

*Keywords:*
Corrole-fullerene dyad
Langmuir–Blodgett dyad layers
Molecular orientation

ABSTRACT

The paper deals with the studies of Langmuir–Blodgett (LB) corrole and corrole-fullerene dyad layers with the use of electronic and vibrational absorption and reflection–absorption spectroscopies. UV–vis and IR spectra were recorded with polarized and unpolarized light to evaluate orientation of the molecules with respect to a solid substrate and to describe interaction of the corrole and corrole-fullerene dyad with various substrates. The electronic spectra of the corrole and its dyad with a fullerene in solutions were also recorded and discussed. Gathered new data can potentially be useful for practical tailoring of molecular devices.



## 1. Introduction

The perfect agents for molecular photovoltaics should be organic dyes with the π-electron systems as electron donors that could generate photocurrent [1–3]. On the other side one of the best electron donating materials are organics covalently linked to fullerene as shown in several papers [4–9]. Thus, a lot attention has been put on the basic photophysical properties of some organic dyes-fullerene dyads both in solution and in a form of ultra-thin films on solid substrates [6,7,10,11]. Such investigations are needed in searching for good organic dyes that could be used in a new generation dye-fullerene photodevice based on covalent donor–acceptor systems. A corrole dye and corrole-fullerene dyad could be some of them.

Corroles are synthetic aromatic macrocycles of the tetrapyrrolic family, that includes also porphyrins and phthalocyanines. Corroles [12,13] considered as intermediates between corrins and porphyrins are currently one of the most intriguing research targets among porphyrinoids. The main advantages of these macrocycles are large delocalized π-electron conjugation and their stability under ambient conditions required for many applications in several fields [14,15]. The photophysical properties of corroles make them promising candidates as building units of solar cells and various photo-, opto-, and electro-active devices. In particular, they could be used as efficient components of arrays for light energy collection and conversion due to excellent properties and availability of corroles as well as their best matching to the sunlight spectrum [8,16–18]. In recent years, the use of a thin film of corrole compounds has also attracted considerable interest due to their potential applications as photoconductors, electronic devices, and gas sensors [19,20].

The spectroscopic properties of selected corroles and corrole-fullerene dyads have been previously studied by us with infrared absorption, Raman scattering, electron paramagnetic resonance, and UV–vis spectroscopies [21,22]. Our experimental methods were supported by the quantum chemical calculations. Taking into account the results of experimental and theoretical studies, full spectral characterization of the investigated materials was given [21,22]. The knowledge of their structural and electronic behavior as molecular adsorbents on solid substrates is of genuine interest. This is a reason why we have now performed the investigations of the corrole and corrole-fullerene dyad in a form of Langmuir–Blodgett films.

The aim of these investigations is to provide information on electronic properties and molecular organization of thin films of corrole and its dyad with fullerene deposited on gold and quartz substrates. It is necessary to notice that the investigated corrole and corrole-fullerene dyad are characterized with UV–vis spectroscopy for the first time in this paper. Our attempts to evaluate orientation of the corrole-derived dyad are also unique. Spectral studies are done with the use of UV–vis and infrared methods as a basis for evaluation of the molecular orientation in LB films of the



* Corresponding author. Tel.: +48 61 66 53 179; fax: +48 616653178.
** Corresponding author. Tel.: +48 61 86 95 275.
*** Corresponding author. Tel.: +48 22 34 33 063.
*E-mail addresses:* danuta.wrobel@put.poznan.pl (D. Wróbel), graja@ifmpan.poznan.pl (A. Graja), danieltgryko@gmail.com (D.T. Gryko).

0379-6779/$ – see front matter © 2013 Elsevier B.V. All rights reserved.
http://dx.doi.org/10.1016/j.synthmet.2013.05.015

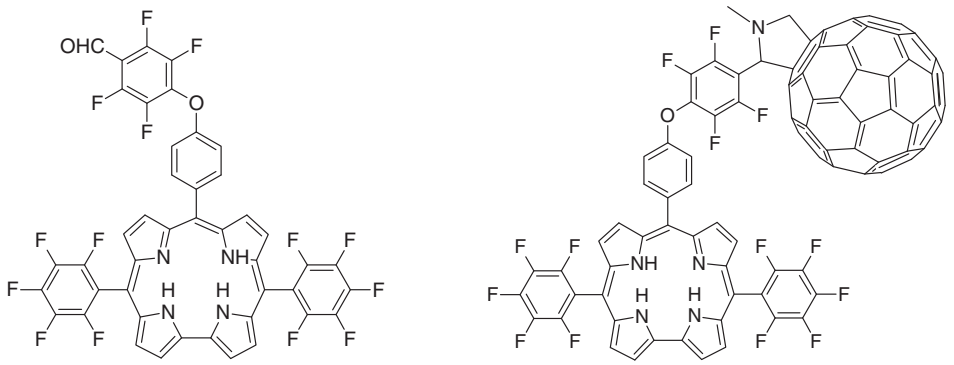

**Fig. 1.** Molecular structure of the functionalized corrole **1** and its dyad with the fullerene **2**.

systems. The applied methods are also suitable for watching changes in intermolecular interaction after molecular layer formation and molecular orientation since both are very essential in effective energy/electron transport in organic photovoltaic systems.

## 2. Materials and experiment

In these studies we present investigations of the Langmuir–Blodgett layers of corrole **1** and corrole-fullerene ($C_{60}$) dyad **2** shown in Fig. 1. Detailed description of the synthesis of **1** and **2** as well as full characterization of these materials was given in our previous paper [21].

Thin layers of the investigated dyads are prepared with a KSV 2000 minitrough equipped with a temperature control system. The temperature of subphase (deionized water with resistivity 18.2 MΩ cm) was achieved and kept constant (22 °C). The samples were dissolved in chloroform and $10^{-4}$ M solution was spread onto the subphase and let chloroform to be evaporated (about 15 min). The floating film of a Langmuir (L) layer was compressed symmetrically from both sides with motion barrier speed of 5 mm/min (from 10 to 40 mN/m). The transfer of the Langmuir–Blodgett onto the substrates (gold and quartz plates) was performed at surface pressure of 20 mN/m and with speed of 2 mm/min during an upstroke and downstroke.

A Varian spectrophotometer Cary 4000 in the range 300–800 nm, in non-polarized and polarized light with the use of a suitable Glan prism was applied for recording of the electronic spectra. We have also done *in situ* absorption study of the dye Langmuir layer to get some information about closely packed dyes in a compressed ultra-thin layer.

The same Cary 4000 spectrophotometer was also used for recording of the electronic absorption of **1** in selected solvents. As standard samples of the corrole in non-polar and polar solvents were used: toluene ($\varepsilon = 2.38$), chloroform ($\varepsilon = 4.80$) and dimethylsulfoxide (DMSO; $\varepsilon = 46.70$). Absorption spectra in solution were done for $10^{-6}$, $10^{-5}$ and $10^{-4}$ M concentrations.

### 2.1. Applied methods for molecular orientation determination

Absorption measurements in polarized light were performed for the LB thin layer sample for the parallel and perpendicular directions of the incident beam *E* vector with respect to the *Y*-axis (*Y*-axis is the sample upstroke direction) in order to evaluate molecular arrangement. The incidence angle $\alpha$ was selected from 0 to 60°; $\alpha$ is the angle that a direction of the incident beam makes with the normal to the LB layer, and $(90^\circ - \theta)$ is the angle that $Z'$-axis makes with the *Y*-axis, and $\varphi$ is the angle that a projection of $Z'$ makes with the *X*-axis (for the space coordination system see [23]).

Using the model proposed by Yoneyama et al. [23] under supposition of the flat $\pi$–$\pi^*$ molecular structure of the organic chromophore and that the layer is illuminated with the polarized light at the angle $\alpha$, dichroic ratio, $D_\alpha$ of the film can be expressed as:

$$D_\alpha = \frac{A_1}{A_2} \tag{1}$$

where $A_1$ and $A_2$ are the film absorbance for the polarized light with the electrical vectors parallel and perpendicular to the film dipping direction (*Y*-axis), respectively. The values of dichroic ratio is a function of $\varphi$, $\theta$, and $\alpha$ angles determining an orientation of the flat molecule in the Cartesian space. The parameter *F* corresponds to the fraction of molecules with the center axis $Z'$ projections parallel to the Cartesian *X* axis

$$F = \frac{\langle \sin^2\theta \cdot \cos^2\varphi \rangle}{\langle 1 - < \cos^2\theta \rangle} \tag{2}$$

where $\langle\rangle$ denotes a statistical average and

$$\langle \sin^2\theta \cos^2\varphi \rangle = \frac{D_0 - \langle \cos^2\theta \rangle}{1 + D_0} \tag{3}$$

$$\langle \cos^2\theta \rangle = \frac{D_0 - (1 + D_0 \sin^2\alpha) D_\alpha}{(1 - 2\sin^2\alpha) D_\alpha - (1 + D_\alpha \sin^2\alpha) D_0} \tag{4}$$

The spectral studies and evaluated values of the dichroic ratios $D_\alpha$ and *F* parameters allow to define orientation of the molecules on solid substrates (according to Yoneyama et al. [23]). The *F* parameter is limited to $0 < F < 1$. It means that when $F > 0.5$ a ring face is oriented preferably to the *X* axis, and to the *Y* axis when $F < 0.5$. Previously, this method was successfully used by us for study the molecular arrangement of selected porphyrin and phthalocyanine dyes [24].

Infrared reflection–absorption spectroscopy (IRRA) was applied for vibrational analysis of the LB films. In this experiment the sample to be analyzed was placed on a gold mirror so that absorption of the sample reduced reflectance, and a sort of transmission spectrum of the sample results. IRRA spectra for unpolarized and polarized light, with the electric vector of the light wave parallel (*p*-polarization) and perpendicular (*s*-polarization) to the plane of incidence were recorded with a FT IR Bruker Equinox 55

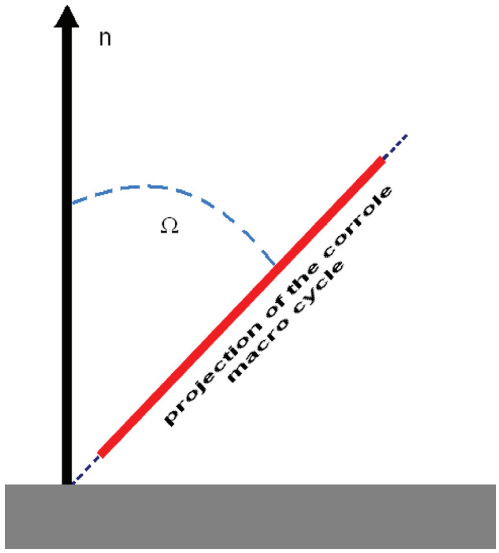


**Fig. 2.** Scheme of orientation of the macrocycle plane projection on the light incidence plane.

spectrometer in the range 400–4000 $cm^{-1}$. The spectra were obtained at various angles of incidence, from 20 to 80°.

As it was mentioned in our previous papers [25,26] the orientation of organic molecules grafted to a metal surface can be determined with the use of IRRA spectroscopy. In orientation evaluations we have applied the simplified method proposed by Arnold et al. [27]. A tilt angle $\Omega$ (Fig. 2) between the transition moment $M_i$ and normal to the samples surface can be estimated using the following equation:

$$\tan^2 \Omega = I_i^{\text{bulk}} \cdot \leq I_j^{\text{LB}} / I_j^{\text{bulk}} \cdot I_i^{\text{LB}} \quad (5)$$

where $I_i^{\text{bulk}}$ and $I_j^{\text{bulk}}$ are intensities of the measured ($i$) and reference ($j$) bands, respectively, recorded in KBr pellets and $I_i^{\text{LB}}$ and $I_j^{\text{LB}}$ are intensities of the adequate bands of the LB films.

## 3. Results and discussion

We have started our investigations with measurements of some basic spectroscopic features of the dye **1**, namely the electronic absorption in various solvents. Fig. 3A shows the absorption spectra of the sample **1** in DMSO solutions ($10^{-6}$, $10^{-5}$ and $10^{-4}$ M); the spectra are normalized to 1 at the Soret-like band between 410 and 500 nm. In Fig. 3B the collection of the normalized spectra of **1** ($10^{-4}$ M) in chloroform, toluene and DMSO are presented. As seen, location of the bands and full widths at half maximum (*FWHM*) depend on solvent used in the experiment. From the data collected in Table 1 one can see that the band intensity ratios are also solvent dependent. The shapes of the absorption spectra of the sample in toluene, their band position and intensity ratios are independent of dye concentration (from $10^{-6}$ M to $10^{-4}$ M); the same remark relates to the dye in chloroform. This observation indicates the domination of a monomeric form of the dye in the wide range of dye concentration in these non-polar solvents even that the solvents of weak polarity are used. Otherwise, DMSO (strongly polar solvent) provides some changes in the dye absorption behavior. It is particularly seen in shifting of the bands with respect to those in non-polar solvents (chloroform and toluene) as well as in the differences in their *FWHM* parameters. This conclusion is also suggested from an analysis of the second derivative absorption spectra of **1** in chloroform, toluene *versus* those in DMSO (Fig. 3C). The absorption feature of the corrole in DMSO *versus* those in chloroform and toluene changes–the band intensity ratios differ in DMSO (1.1–1.2) from those in chloroform and toluene (5.6 and 5.4, respectively). Nevertheless, we have to note that the band ratios are not changed with increasing dye concentration. Thus we can believe in domination of monomeric forms over tiny amount of some aggregates in **1** in DMSO. However, we have also to take into consideration the "blue" band shifts of about 10–16 nm observed in DMSO *versus* chloroform and toluene. It occurs as a result of interaction of the dyes molecules with DMSO species and can be explained by decreasing energy of the dye molecule states in vicinity of strongly polar DMSO.

The solvent-dependent absorption of corroles could also result from other various contributing factors [28–30]. Firstly, the changes in the electronic spectra of corroles can be due to the solvent hydrogen bonding with the internal N—H group [28] or other external groups. On the other hand, the deprotonation of the macrocycle

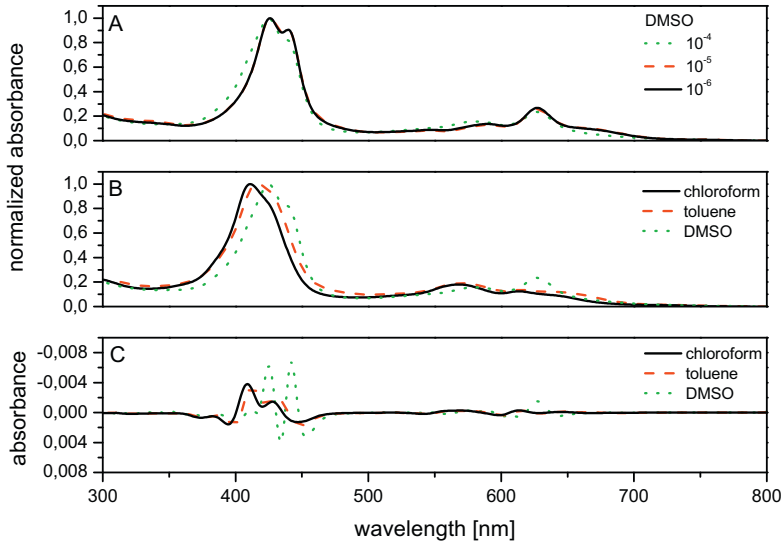


**Fig. 3.** Electronic absorption spectra of corrole **1** in DMSO solutions (A), the spectra of **1**. in selected solvents (B) and exemplary second derivative spectra in three solvents (C). Dyes concentrations in (B) and (C) are $10^{-4}$ M.

**Table 1**
UV–vis absorption parameters for selected bands of corrole **1** in chloroform, toluene, DMSO solutions and also in L and LB layers.

| Solvent | Concentration [M] | Band intensity ratio | | | FWHM [$cm^{-1}$] | |
|---|---|---|---|---|---|---|
| | | 411/568 nm | 411/614 nm | 568/614 nm | 411 nm | 429 nm |
| Chloroform | $10^{-4}$ | 5.6 | 8.0 | 1.5 | 1092 | 339 |
| | $10^{-5}$ | 5.6 | 8.0 | 1.5 | 1092 | 339 |
| | $10^{-6}$ | 5.6 | 8.0 | 1.5 | 1092 | 339 |

| Solvent | Concentration [M] | Band intensity ratio | | | | FWHM [$cm^{-1}$] | |
|---|---|---|---|---|---|---|---|
| | | 416/570 | 416/616 | 416/644 | 570/616 | 409 nm | 414 nm |
| Toluene | $10^{-4}$ | 5.4 | 7.37 | 8.47 | 1.4 | 984 | 1487 |
| | $10^{-5}$ | 5.4 | 7.37 | 8.47 | 1.4 | 984 | 1487 |
| | $10^{-6}$ | 5.4 | 7.37 | 8.47 | 1.4 | 984 | 1487 |

| Solvent | Concentration [M] | Band intensity ratio | | | | | | FWHM [$cm^{-1}$] | |
|---|---|---|---|---|---|---|---|---|---|
| | | 426/440 | 426/579 | 426/589 | 426/627 | 579/627 | 589/627 | 424 nm | 443 nm |
| DMSO | $10^{-4}$ | 1.2 | 6.6 | | 4.3 | 0.7 | | 1241 | 231 |
| | $10^{-5}$ | 1.1 | 7.37 | 8.1 | 3.8 | | 0.5 | 661 | 374 |
| | $10^{-6}$ | 1.1 | 7.37 | 8.1 | 3.7 | | 0.5 | 661 | 374 |

| Layer | Band intensity ratio | | | FWHM [$cm^{-1}$] | |
|---|---|---|---|---|---|
| | 427/570 | 427/618 | 570/618 | 400 nm | 432 nm |
| Langmuir | 4.5 | 6.0 | 1.3 | 1156 | 1189 |

| Layer | Band intensity ratio | | | FWHM [$cm^{-1}$] | |
|---|---|---|---|---|---|
| | 418/583 | 418/625 | 586/625 | 390 nm | 441 nm |
| Langmuir-Blodgett | 3.8 | 3.9 | 1.0 | 2348 | 2384 |

is possible in polar solvents – it could affect also the electronic spectra of the corroles. Similarly, because of the asymmetry of the tetrapyrrole ring of the corrole the inner NH protons can migrate around the ring. There are two tautomeric forms which have similar energies [31] – the electronic spectra show two components (well seen in **1** in DMSO) – this is why a contribution of tautomeric forms to the solvent-dependent absorption properties is possible but rather not dominant. Thus, on the basis of our results and discussion as well as the results presented in [28,30] we can suppose that the solvent dependence results from hydrogen-bonding interactions rather than from aggregation, deprotonation or tautomerization effects. We have also done the *in situ* absorption study of the dye Langmuir (L) layer to get some information about closely packed dyes in a compressed ultra-thin layer and to follow interaction between dye molecules. To confirm inclination of the corrole dye to create (or not) some aggregates we have done an experiment with the Langmuir monolayer on the water subphase. The result is shown in Fig. 4A which presents the electronic absorption spectra of **1** in the L layer at different surface pressure. As one can easily see the shapes of the spectra are changed when

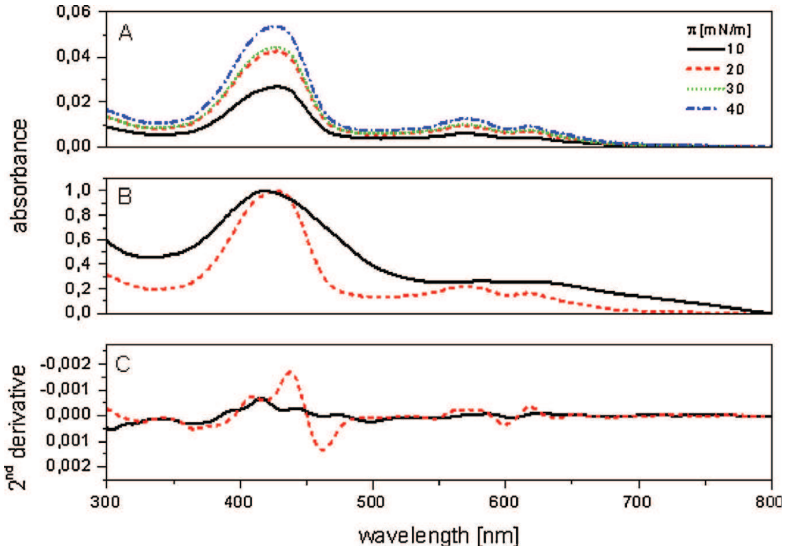


**Fig. 4.** Electronic absorption spectra of **1** in Langmuir monolayer at different surface. pressure (A), in Langmuir–Blodgett films containing 10 dye layers deposited on the quartz substrate (solid line) and Langmuir monolayer at pressure 20 mN/m (dashed line) (B) and second derivative of the spectra shown in (B) and (C). (For interpretation of the references to color in figure legend, the reader is referred to the web version of the article.)

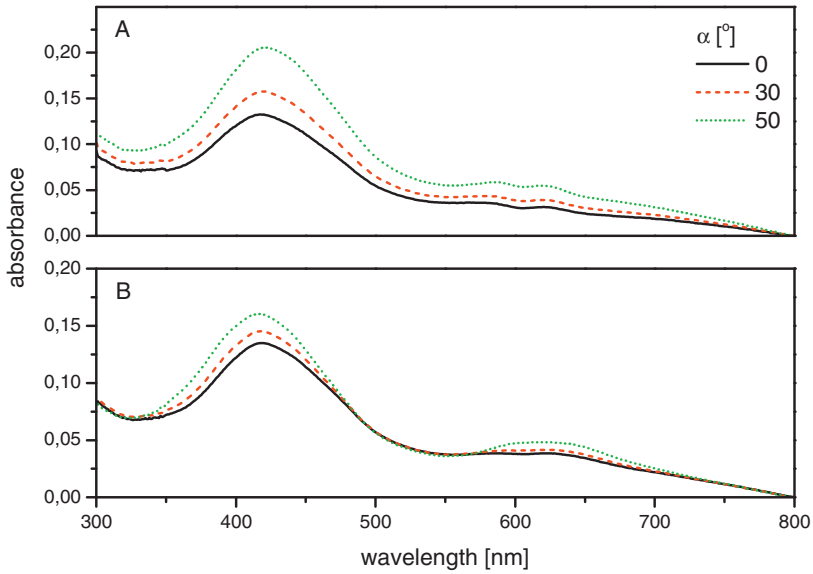


**Fig. 5.** Polarized UV–vis absorption spectra of **1** in the LB layer on the quartz substrate for various $\alpha$ angles, recorded for parallel (A) and perpendicular (B) light polarizations.

compared to those in solutions and indicate formation of molecular aggregates under pressure. Significant changes were observed both in the Soret-like region (350–500 nm) and in the Q-bands (550–650 nm) – the location of the bands, their intensity ratios and the *FWHM* parameters are significantly changed (see Fig. 4A and B); the parameters evaluated for the L (and LB) layers are also gathered in Table 1. These conclusions are convincingly shown in Fig. 4C. The similar behavior was also observed for other porphyrin-like dyes in strongly packed dye monolayers [32]. Of course we realized that much stronger interaction between the dyes takes place when they form the closely packed L layer, what is evidenced by comparison of the changes in *FWHM* of the absorption spectra in solution *versus* those of the L layer.

Absorption measurements in polarized light were done for the LB thin layer sample at the different incident angle $\alpha$ in order to evaluate molecular arrangement The exemplary results of the electronic absorption spectra done for two different light polarizations (parallel and perpendicular to the sample *Y*-axis) at $\alpha = 0$, 30, 50° are shown in Fig. 5A and B. On the basis of the Yoneyama parameters [23] (Eqs. (1)–(4)), collected in Table 2, we can discuss how the molecules are oriented with respect to the sample "director". The *F* parameters are 0.19–0.26 in the range of the transition moment responsible for the Q-bands and 0.48 for the Soret band. It means that the $\theta$ angles calculated according to Eq. (4) are about 34° and 39° for the *Q* and Soret bands, respectively. The 0.19–0.26 values strongly indicate that the long wavelength *Q* transition moment is oriented preferably to the *Y*-axis ($F < 0.5$). Nevertheless, if we take into account the *F* values of nearly 0.5 (0.48 in the range of the Soret region) it is rather difficult to judge univocally the molecular arrangement of the dye molecules in the LB layer. Thus, in our discussion we have to take into consideration: (i) our spectral results, (ii) the supposition of the flat $\pi$–$\pi^*$ molecular structure of corrole [33] and (iii) the Yoneyama model [23]. On the assumption of the Yoneyama model [23] we can deduce that the transition moment responsible for the Soret transition in the macrocyclic ring plane is preferably oriented to the *X*-axis (although the *F* values is nearly 0.5). In our previous papers [24,32] we discussed orientation of porphyrin and phthalocyanine dyes on solid substrates and we determined molecular orientation of the L and LB layers with the use of the Yoneyama model. The orientation angles in [24] were different than those evaluated for corrole in this paper. Thus, to find explanation of the difference in the dye's molecular arrangement (porphyrin *versus* corrole) we have also to take into consideration the molecular symmetry of both dye families. The porphyrins are characterized by the $D_{2h}$ or $D_{4h}$ symmetry, whereas the corrole is much less symmetric (its symmetry is $C_{2v}$). Nevertheless, the four-orbital model refers also to corrole systems [34,35]. The reduced symmetry can affect the oscillator strengths [34,35] and can provide their different orientations. Thus, in consequence the two different *F* values were evaluated in our polarized experiments.

**Table 2**
Linear dichroic parameters of corrole **1** in LB film.

| Band [nm] | $\alpha$[°] | $D_a$ | $\cos^2(\theta)$ | $\theta$>[°] | $\sin^2(\theta)\cos^2((\phi)$ | $F(\pm 0.02)$ |
|---|---|---|---|---|---|---|
| Soret band | 0 | 0.98 | | | | |
| 418 | 30 | 1.08 | 0.60 | 39 | 0.19 | 0.48 |
| | 50 | 1.28 | 0.61 | 39 | 0.19 | 0.48 |
| Qband | 0 | 0.82 | | | | |
| 625 | 30 | 0.94 | 0.72 | 32 | 0.05 | 0.19 |
| | 50 | 1.14 | 0.66 | 36 | 0.09 | 0.26 |

Fig. 6 shows the FT-IR reflection–absorption spectra in polarized light, recorded at the angle of incidence $\alpha = 80°$, in the range from 400 to 1800 $cm^{-1}$ for the 5-layer LB films of corrole **1** and corrole-fullerene dyad **2** on the gold substrate; these spectra are presented together with the absorption spectra of powdered compounds dispersed in the KBr pellet. Generally, for both samples the spectra of thin films are very similar to those in the bulk. However, comparing carefully the IRRA spectra with the spectra of the adequate substance in KBr one can notice some differences. We observed changes in the positions, shapes and intensities of bands. These modifications can be assigned to an intermolecular interaction between metallic substrate and the first molecular layer, *i.e.* to a small charge transfer at the substrate-layer interface. The most spectacular changes are noticed in the range of 750 to 1800 $cm^{-1}$, where the normal mode vibrations of the corrole, benzene ring, and $C_6F_4$, $C_6F_5$ rings are located. In order to interpret the experimental results of IR absorption and to realize an optimal structure of the compounds quantum chemical calculations were performed [21]. The molecular geometry was optimized using the Density

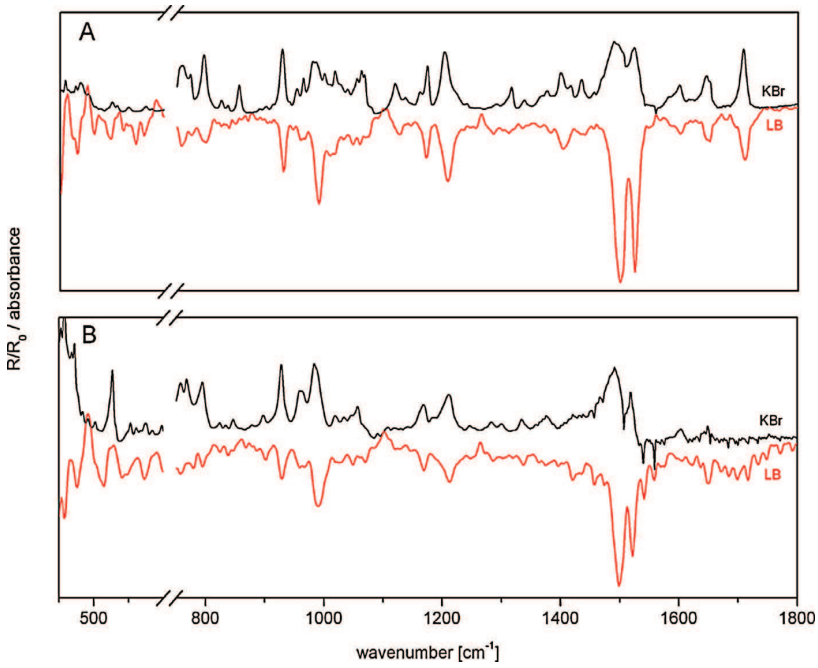


**Fig. 6.** The FT-IR reflection–absorption spectra in *p*-polarized light, recorded at the angle of incidence 80° for 5 layers films of corrole **1** (A) and corrole-fullerene dyad **2** (B) on the gold substrate. For comparison the spectra of **1** and **2** in KBr matrix are given.

Functional Theory (DFT) method with B3LYP hybrid functional and 6-31G and 6-31G(d) basis sets. The calculations of normal mode frequencies and intensities were also performed. All calculations were made using Gaussian 03 package [36]. The GaussView program was used to propose an initial geometry of investigated molecules and for visual inspection of the normal modes [21]. IR wavenumbers and band assignment of selected bands of LB film and KBr pellet are collected in Table 3.

Significant changes in band position are observed for the bands related to the stretching of C—F bond in $C_6F_4$ ring, they are shifted at about 6 $cm^{-1}$. Similarly, relatively large shifts are recorded for the bands related to in-plane stretching of C—C and C=C bonds, bending vibrations of C—C—H bonds in phenyl ring and stretching of C—F bond in $C_6F_5$ ring. Inconsiderable bands position shifts are observed for the bands associated with vibrations of corrole. In particular, the bands observed in the bulk at 795/794, 928/927, 983/984 $cm^{-1}$ (for the sample **1** and **2**, respectively) are observed in the film sample at 796/796, 930/930 and 990/991 $cm^{-1}$ (for sample **1** and **2,** respectively).

**Table 3**
IR wavenumbers and band assignment of selected bands in KBr pellets and LB layers of corrole **1** and the dyad corrole-fullerene **2** as well as the tilt angle $\Omega$ between the transition moment $M_i$ and the normal to sample surface.

| Sample 1 | | | Sample 2 | | | Band assignment |
|---|---|---|---|---|---|---|
| Wavenumber of IRRA bands [$cm^{-1}$] | | Angle $\Omega$ [°] | Wavenumber of IRRA bands [$cm^{-1}$] | | Angle $\Omega$ [°] | |
| KBr pellet | LB layers | | KBr pellet | LB layers | | |
| 758 | 758 | | | | | Def. corrole ring |
| 795 | 796 | 32 | 794 | 796 | 31 | C—C—H b op corrole |
| 856 | | | | | | C—C—H b op benzene ring |
| | | | 897 | 902 | | C—N s pyrrole ring |
| 928 | 930 | 42 | 927 | 930 | 36 | Def corrole rings |
| | | | 960 | 964 | | C—F in $C_6F_5$ ring |
| 983 | 990 | | 984 | 991 | | Def corrole rings |
| 1016 | 1013 | 46 | 1019 | 1025 | 52 | C—F sin $C_6F_4$ ring |
| 1062 | 1059 | | 1057 | 1058 | | C—H s in benzene ring + def corrole ring |
| 1119 | 1123 | | | | | C—O s |
| 1173 | 1171 | | 1167 | 1168 | | C—O s + C—C—H b ip benzen ring |
| 1202 | 1307 | | 1208 | 1213 | | C—C—H b ip benzen ring |
| 1314 | 1313 | | | | | C—C—H b in corrole ring |
| | | | 1334 | 1338 | 52 | C—F s in C6F4 ring |
| 1398 | 1398 | | | | | C—F s + C—C s in $C_6F_4$ ring |
| 1433 | 1436 | 42 | | | | C—F s in $C_6F_4$ ring |
| 1488 | 1500 | 54 | 1492 | 1498 | 52 | C—O s |
| 1521 | 1524 | 56 | 1519 | 1522 | 52 | C—F s in $C_6F_4$ |
| 1600 | 1602 | | 1602 | 1603 | | C=C s ip in benzene ring |
| 1645 | 1647 | 39 | 1648 | 1652 | 49 | C=C s ip in benzene ring |
| 1707 | 1709 | | | | | C=O s |

When we compare the spectra of **1** with the spectra of **2** for the LB layers we see also some characteristic changes. Some band shift in the experimental error limits but some others shift distinctly, especially those corresponding the vibrations of bonds in the phenyl and $C_6F_4$ rings. These changes are related to modification of the molecular geometry of the dyads, which are caused by fullerene linking to **1**. The changes could be also related to the modification of the electron density on molecules as a result of deposition of the dyes on a solid substrate, due to an interaction with the solid Au. The electron density changes are related to possibility of electron transfer between the solid substrate and the molecules in the LB layers. These changes are not only the result of intermolecular interactions between the molecules and gold substrate but also are related to the orientation of molecules on the solid. The possibility of existence of a small permanent polarization at the substrate/layers interface and its influence on IR spectra should be also taken into account. The measurements of IRRA spectra of the thin films in polarized light have been carried out to prove this hypothesis.

The IRRA spectra for *p*-polarization of the LB layers of the corrole and corrole-fullerene dyad are shown in Fig. 6. The most important and characteristic bands related to the stretching, in-plane and out-of-plane bending vibrations of corrole, phenyl ring and $C_6F_4$ and $C_6F_5$ rings could give information on the aromatic rings orientation. Thus, using the simplified method of evaluation of the tilt angle $\Omega$ between the transition moment $M_i$ and the normal to sample surface [27] we can determine orientation of selected bonds and indirectly the plane of rings in the corrole. According to our estimations the band at 1173/1167 $cm^{-1}$ (**1**/**2**) related to the in-plane bending of C—C—H bond in the phenyl ring was assumed as a reference band. We calculate the values of the angle $\Omega$ for the corrole and its dyad using the bands located at: 796, 930, 1013, 1025, 1338, 1436, 1498, 1500, 1522, 1524, 1647 and 1652 $cm^{-1}$(the data on the molecules orientation are collected in Table 3). The first two bands are associated with the out-of-plane bending of C—C—H and stretching of C—C bonds in the corrole ring. The values of the tilt angle for the band 790 $cm^{-1}$ are 32° for **1** and 31° for **2**, respectively. For the band related to the stretching of C—C bond in the corrole ring the value of the angle $\Omega$ varies depending on the sample, and so, for **1** it is 42° and for **2**–36°. This result indicates the change in the orientation of the corrole ring after the dyad formation. We observe an increase in value of the angle $\Omega$ from 46° to 42° for **1** to 52° for **2** for the bands related to the stretching of C—F bonds in $C_6F_4$ ring located at 1013, 1025, 1338 and 1436 $cm^{-1}$. For the band at about 1490 $cm^{-1}$, corresponding with the stretching of C—O bond between the benzene and $C_6F_4$ rings no major changes of the angle $\Omega$ are observed. This suggests that $C_{60}$ attached to the corrole ring does not determine orientation of this bond. Because, the band at about 1490 $cm^{-1}$ is related to the stretching vibration of the link between the benzene ring and $C_6F_4$ ring, therefore the orientation of the $C_6F_4$ ring also will not undergo major changes and more or less the average angle $\Omega$ of this ring is about 50°. While the orientation of the $C_6F_4$ rings does not change, the orientation of the phenyl ring (in the linker) strongly depends on the presence of fullerene. Incorporation of the fullerene molecule to the corrole gives occasion to increase the angle between the transition moment and the normal to the sample surface of about 10°. It shows that the fullerene linked to the corrole influences the orientation not only of the corrole central ring but also the orientation of the remaining rings in this structure.

Thanks to the infrared measurements in polarized light we can determine not only orientation of the molecules but also evaluate which part of the molecules links to the solid substrate. From these studies we can assume that the corrole and corrole-fullerene dyad are deposited on the Au substrate *via* the $C_6F_5$ rings. The corrole is also deployed from the substrate, and probably these molecules form the bonds with the substrate which is proved by the presence of the bands located at about 3000 $cm^{-1}$ and related to the vibration of C—H bonds in the corrole ring.

## 4. Conclusions

Two complementary methods of evaluation of the molecular orientation of the corrole-fullerene dyad in LB layers were applied. The first method based on the electron absorption of the polarized light gives information on orientation of the electron transition moment. On the contrary, the second method (IRRA spectra) informs us on the orientation of the vibrational transition moments of selected intramolecular bonds. Under assumption that these transition moments approximate the plane of the corrole ring, we obtain information on the ring orientation.

For the LB layers of the corrole the average angle $\Omega$ is about 44° but for the LB layers of the corrole-fullerene dyad – it is about 46°. It confirms our expectation that the presence of the large spherical $C_{60}$ molecule in the multilayer significantly changes the corrole ring orientation. This conclusion is confirmed by evaluation of the ring orientation from the UV–vis spectral method. The small values of the *F* parameter (0.19–0.26) suggest that transition moment is oriented preferably to the *Y*-axis. Thus, the average $\theta$ value for the corrole sample, determined in the range of the Soret band, is about 39° but in the Q band it is 34°. It is necessary to notice, that the orientation of the electronic or vibrational transition moments does not lie exactly in the same plane.

The next conclusion from analysis of the principal spectral parameters describing the Soret band determined in non-polar toluene or chloroform solutions indicates the domination of the monomeric spectral form of the dye in the wide range of dye concentration, even that the solvents of weak polarity were used. The "blue" band shifts observed in DMSO *versus* chloroform and toluene occurs as a result of interaction of the dyes molecules with DMSO species and can be explained by decreasing energy of the dye molecule states in vicinity of strongly polar DMSO. These conclusions are strongly supported by the absorption and its second derivative spectra in chloroform, toluene and DMSO. On the basis of our absorption results we can suppose that the solvent dependence results from hydrogen-bonding interactions rather than from aggregation, deprotonation or tautomerization effects.

The reflection–absorption IR spectra of the thin film suggest redistribution of charges in the LB layers containing the dyads with respect to that in the corrole molecule. The studies in polarized light evidence the strong influence of the fullerene on orientation of some parts of the corrole molecule in the dyad. From this observation we can also assume that the corrole and corrole-fullerene dyad are deposited on the Au substrate *via* the $C_6F_5$ rings. The corrole is also deployed from the substrate, and probably these molecules form the bonds with the substrate, which is proved by the presence of the band located at about 3000 $cm^{-1}$ related to the vibration of C—H bonds in the corrole ring.

## Acknowledgements

The paper was partially supported by Poznan University of Technology (grant DS 62-176/2013; D.W. and B.B.) and by the National Science Center of Poland (Post-doctoral internship No. 2012/04/S/ST5/00071; K.L.).

## References

[1] B. O'Regan, M. Grätzel, Nature 335 (1991) 7377–7385.
[2] C.C. Lesnoff, A.B.P. Lever, Photocyanines: Properties and Applications, VCH, New York, 1996.
[3] D. Wróbel, Comptes Rendus Chimie 6 (2003) 417–429.

[4] H. Imahori, Y. Mori, Y. Matano, Journal of Photochemistry and Photobiology C: Photochemistry Review 4 (2003) 51–83.
[5] H. Imahori, Organic and Biomolecular Chemistry 2 (2004) 1425–1433.
[6] F.G. Brunetti, R. Kumar, F. Wudl, Journal of Materials Chemistry 20 (2010) 2934–2948.
[7] D. Wróbel, A. Graja, Coordination Chemistry Reviews 255 (2011) 2555–2577.
[8] L. Flamigni, D.T. Gryko, Chemical Society Reviews 38 (2009) 1635.
[9] O. Ito, F. D'Souza, Molecules 17 (2012) 5816–5835.
[10] B. Barszcz, A. Bogucki, A. Biadasz, B. Bursa, D. Wróbel, A. Graja, Journal of Photochemistry and Photobiology A: Chemistry 218 (2011) 48–57.
[11] K. Lewandowska, D. Wróbel, A. Graja, Optical Materials 34 (2012) 1729–1734.
[12] D.T. Gryko, J.P. Fox, D.P. Goldberg, Journal of Porphyrins and Phthalocyanines 8 (2004) 1091–1105.
[13] C.J. Lemon, P.J. Brothers, Journal of Porphyrins and Phthalocyanines 15 (2011) 809–834.
[14] I. Aviv, Z. Gross, Chemical Communications (2007) 1987–1999.
[15] L. You, H. Shen, L. Shi, G. Zhang, H. Li, H. Wang, L. Ji, Science China Physics, Mechanics and Astronomy 53 (2010) 1491–1496.
[16] M. Kruk, T.H. Ngo, P. Verstappen, A. Starukhin, J. Hofkens, W. Dehaen, W. Maes, Journal of Physical Chemistry A 116 (2012) 10695–10703.
[17] M. Kruk, T.H. Ngo, V. Savva, A. Starukhin, W. Dehaen, W. Maes, Journal of Physical Chemistry A 116 (2012) 10704–10711.
[18] Y.B. Ivanova, V. Savva, N.Z. Marmardashvili, A. Starukhin, T.H. Ngo, W. Dehaen, W. Maes, M. Kruk, Journal of Physical Chemistry A 116 (2012) 10683–10694.
[19] J.M. Barbe, G. Canard, S. Brandés, R. Guilard, European Journal of Organic Chemistry 21 (2005) 4601–4611.
[20] J.M. Barbe, G. Canard, S. Brandés, R. Guilard, Angewandte Chemie International Edition 44 (2005) 3103–3106.
[21] K. Lewandowska, B. Barszcz, J. Wolak, A. Graja, M. Grzybowski, D.T. Gryko, Dyes and Pigments 96 (2013) 249–255.
[22] K. Lewandowska, B. Barszcz, A. Graja, B. Bursa, D. Wróbel, W. Bednarski, S. Waplak, M. Grzybowski, D.T. Gryko, Synthetic Metals 166 (2013) 70–76.
[23] M. Yoneyama, M. Sugi, M. Saito, K. Ikegami, S. Kuroda, S. Iizima, Japanese Journal of Applied Physics 25 (1986) 961–965.
[24] K. Lewandowska, D. Wróbel, A. Biadasz, R. Świetlik, Journal of Photochemistry and Photobiology A: Chemistry 200 (2008) 225–231.
[25] A. Graja, K. Lewandowska, B. Laskowska, A. Łapiński, D. Wróbel, Chemical Physics 352 (2008) 339–344.
[26] K. Lewandowska, A. Graja, B. Barszcz, A. Biadasz, D. Wróbel, New Journal of Chemistry 35 (2011) 1291–1295.
[27] R. Arnold, A. Terfort, Ch Wöll, Langmuir 17 (2001) 4980–4989.
[28] T. Ding, E.A. Alemán, D.A. Moderelli, C.J. Ziegler, Journal of Physical Chemistry 109 (2005) 7411–7417.
[29] R.S. Czernuszewicz, V. Mody, A.A. Zareba, M.B. Zaczek, M. Gałęzowski, V. Sashuk, K. Grela, D.T. Gryko, Inorganic Chemistry 46 (2007) 5616–5624.
[30] C.J. Zieger, J.R. Sabin, G.R. Geiger III, V.N. Nemykin, Chemical Communications 48 (2012) 4743–4745.
[31] D. Ding, J.D. Harvey, C.J. Ziegler, Journal of Porphyrins and Phthalocyanines 9 (2005) 22–27.
[32] A. Biadasz, B. Bursa, B. Barszcz, A. Bogucki, B. Laskowska, A. Graja, D. Wróbel, Dyes and Pigments 89 (2011) 86–92.
[33] J.B. Birks, Organic Molecular Photophysics, vol. 1, J. Wiley, New York, 1973.
[34] N.S. Hush, J.M. Dyke, M.L. Williams, I.S. Woolsey, Journal of the Chemical Society, Dalton Transactions 39 (1974) 5–39, 9.
[35] A. Ghosh, T. Wondimagegn, A.B.J. Parusel, Journal of the American Chemical Society 122 (2000) 5100–5104.
[36] M.J. Frisch, G.W. Trucks, H.B. Schlegel, G.E. Scuseria, M.A. Robb, J.R. Cheeseman, J.A. Montgomery Jr., T. Vreven, K.N. Kudin, J.C. Burant, J.M. Millam, S.S. Iyengar, J. Tomasi, V. Barone, B. Mennucci, M. Cossi, G. Scalmani, N. Rega, G.A. Petersson, H. Nakatsuji, M. Hada, M. Ehara, K. Toyota, R. Fukuda, J. Hasegawa, M. Ishida, T. Nakajima, Y. Honda, O. Kitao, H. Nakai, M. Klene, X. Li, J.E. Knox, H.P. Hratchian, J.B. Cross, C. Adamo, J. Jaramillo, R. Gomperts, R.E. Stratmann, O. Yazyev, A.J. Austin, R. Cammi, C. Pomelli, J.W. Ochterski, P.Y. Ayala, K. Morokuma, G.A. Voth, P. Salvador, J.J. Dannenberg, V.G. Zakrzewski, S. Dapprich, A.D. Daniels, M.C. Strain, O. Farkas, D.K. Malick, A.D. Rabuck, K. Raghavachari, J.B. Foresman, J.V. Ortiz, Q. Cui, A.G. Baboul, S. Clifford, J. Cioslowski, B.B. Stefanov, G. Liu, A. Liashenko, P. Piskorz, I. Komaromi, R.L. Martin, D.J. Fox, T. Keith, M.A. Al-Laham, C.Y. Peng, A. Nanayakkara, M. Challacombe, P.M.W. Gill, B. Johnson, W. Chen, M.W. Wong, C. Gonzalez, J.A. Pople, Gaussian Inc., Wallingford CT, 2004.